



Durham E-Theses

Extended defects in curved spacetimes

Bonjour, Filipe

How to cite:

Bonjour, Filipe (1999) *Extended defects in curved spacetimes*, Durham theses, Durham University.
Available at Durham E-Theses Online: <http://etheses.dur.ac.uk/4966/>

Use policy

The full-text may be used and/or reproduced, and given to third parties in any format or medium, without prior permission or charge, for personal research or study, educational, or not-for-profit purposes provided that:

- a full bibliographic reference is made to the original source
- a [link](#) is made to the metadata record in Durham E-Theses
- the full-text is not changed in any way

The full-text must not be sold in any format or medium without the formal permission of the copyright holders.

Please consult the [full Durham E-Theses policy](#) for further details.

Extended Defects in Curved Spacetimes

Filipe Bonjour

The copyright of this thesis rests with the author. No quotation from it should be published without the written consent of the author and information derived from it should be acknowledged.

A Thesis submitted in partial fulfilment for the
degree of Doctor of Philosophy
of the University of Durham



Department of Mathematical Sciences
University of Durham
England



— September 1999 —

17 JAN 2000

Cette Thèse est dédiée à ma Mère et à ma Soeur

Extended Defects in Curved Spacetimes

Filipe Bonjour

Ph.D. Thesis, September 1999

Abstract

This Thesis is concerned with three particular aspects of extended cosmic strings and domain walls in cosmology: their dynamics, gravitation and interaction with a black hole.

In Chapter 3, we study the dynamics of an abelian–Higgs cosmic string. We find its equations of motion from an effective action and compare, for three test trajectories, the resulting motion with that observed in the Nambu–Gotō approximation. We also present a general argument showing that the corrected motion of any string is generically antirigid. We pursue the investigation of the dynamics of topological defects in Chapter 5, where we find (from integrability conditions rather than an effective action) the effective equations governing the motion of a gravitating curved domain wall.

In Chapter 4 we investigate the spacetime of a gravitating domain wall in a theory with a general potential $V(\Phi)$. We show that, depending on the gravitational coupling ϵ of the scalar Φ , all nontrivial solutions fall into two categories interpretable as describing respectively domain wall and false vacuum–de Sitter solutions. Wall solutions cannot exist beyond a value $\frac{4}{3}\epsilon_{\max}$, and vacuum–de Sitter solutions are unstable to decaying into wall solutions below ϵ_{\max} ; at ϵ_{\max} we observe a phase transition between the two types of solution. We finally specialize for the Goldstone and sine-Gordon potentials.

In Chapter 6 we consider a Nielsen–Olesen vortex whose axis passes through the centre of an extremal Reissner–Nordström black hole. We examine in particular the existence of piercing and expelled solutions (where the string respectively does and does not penetrate the black hole’s horizon) and determine that while thin strings penetrate the horizon — and therefore can be genuinely called hair — thick strings are expelled; the two kinds of solution are separated by a phase transition.

Table of Contents

| | |
|--|-------------|
| Declaration and Statement | x |
| Conventions and Notations | xiii |
| I Topological Defects | 1 |
| 1 Extended Defects | 2 |
| 1.1 Extended Defects in Cosmology | 2 |
| 1.2 The Goldstone Model: Global Strings and Domain Walls | 4 |
| 1.3 The Abelian–Higgs Model: Local Strings | 8 |
| 1.4 More Complicated Models: Superconducting Strings | 12 |
| II The Dynamics of Topological Defects | 17 |
| 2 The Gauß–Codazzi Formalism for Topological Defects | 18 |
| 3 Effective Motion of a Cosmic String | 23 |
| 3.1 Introduction and Chronology | 23 |
| 3.2 The Expansion of the Equations of Motion | 26 |
| 3.2.1 The Zeroth Order and the Nambu Action | 28 |
| 3.2.2 The First Order | 29 |
| 3.2.3 The Second Order | 31 |
| 3.3 The Effective Action and Equations of Motion | 32 |
| 3.3.1 The Effective Action | 32 |

| | | |
|----------|--|-----------|
| 3.3.2 | The Effective Equations of Motion | 33 |
| 3.4 | Three Illustrative Trajectories | 37 |
| 3.4.1 | The Collapsing Loop | 38 |
| 3.4.2 | The Travelling Wave | 40 |
| 3.4.3 | The Helical Breather | 41 |
| 3.5 | The Worldsheet Rigidity from the Action | 44 |
| 3.6 | Outlook | 47 |
| 4 | Gravitating Plane-Symmetric Domain Walls | 49 |
| 4.1 | Introduction | 49 |
| 4.2 | Plane-Symmetric Spacetimes | 51 |
| 4.3 | Analytical Predictions | 55 |
| 4.3.1 | Existence of a Wall Solution | 56 |
| 4.3.2 | Stability of the Vacuum-de Sitter Solution | 56 |
| 4.3.3 | A More General Perturbation | 57 |
| 4.4 | Weak Gravity | 59 |
| 4.4.1 | The Goldstone Model | 60 |
| 4.4.2 | The Sine-Gordon Model | 60 |
| 4.5 | Strong Gravity | 61 |
| 4.6 | Domain Walls in a de Sitter or Anti-de Sitter Background | 63 |
| 4.7 | Discussion and Conclusion | 68 |
| 5 | The Dynamics of Curved Gravitating Domain Walls | 72 |
| 5.1 | Introduction | 72 |
| 5.2 | The Equations of Motion | 73 |
| 5.3 | The Gravity-Dominated Case ($\epsilon > \varsigma$) | 75 |
| 5.3.1 | The Zeroth Order | 76 |
| 5.3.2 | The First Order | 77 |
| 5.3.3 | The Second and Third Orders | 78 |
| 5.4 | The Curvature-Dominated Case ($\varsigma > \epsilon$) | 79 |
| 5.5 | An Example: Bending the Gravitating Wall | 82 |

| | | |
|------------|--|------------|
| A | An Exact Solution to the Perturbed Equations of Motion for the Helical Breather | 85 |
| B | Numerical Tables | 87 |
| | B.1 Effective Motion of a Cosmic String | 87 |
| | B.2 Gravitating Plane-Symmetric Domain Walls | 88 |
| III | Cosmic Strings and Black Holes | 90 |
| 6 | Abelian–Higgs Hair for Extreme Reissner–Nordstrøm Black Holes | 91 |
| | 6.1 Introduction and Chronology | 91 |
| | 6.2 Abelian–Higgs Strings in a Reissner–Nordstrøm Background | 94 |
| | 6.3 Numerical Method and Results | 95 |
| | 6.4 String Ending on a Black Hole | 104 |
| | 6.5 Analytical Considerations | 106 |
| | 6.5.1 Proof of Flux Expulsion for Thick Strings | 108 |
| | 6.5.2 Proof of Penetration for Thin Strings | 110 |
| | 6.5.3 String Ending on a Black Hole | 111 |
| | 6.6 Discussion and Outlook | 112 |
| C | Numerical Tables | 116 |
| IV | Conclusion | 118 |
| | Conclusion | 119 |
| | Bibliography | 121 |

List of Figures

| | | |
|-----|--|----|
| 1.1 | The potentials for the real and complex Goldstone models | 5 |
| 1.2 | The global string | 7 |
| 1.3 | The static kink or domain wall | 8 |
| 1.4 | The Nielsen–Olesen vortex | 12 |
| 1.5 | The straight superconducting string | 16 |
| 2.1 | Origin of the normal fundamental form | 21 |
| 3.1 | The Nielsen–Olesen solution | 30 |
| 3.2 | The second order solution | 33 |
| 3.3 | The parameters $\mu(\beta^{-1})$ and $\alpha_1(\beta^{-1})$ | 34 |
| 3.4 | The parameters $\alpha_2(\beta^{-1})$ and $\alpha_3(\beta^{-1})$ | 34 |
| 3.5 | The corrected collapsing loop | 40 |
| 3.6 | The corrected helical breather | 44 |
| 3.7 | The Polyakov argument | 45 |
| 3.8 | Rigidity zones for the helical breather | 47 |
| 4.1 | The two possible evolutions of $X_h(\epsilon)$ | 56 |
| 4.2 | The flat spacetime kink solution | 60 |
| 4.3 | Comparison between the numerical and perturbative solutions | 61 |
| 4.4 | Numerical wall solution for $\epsilon = 0.9$ | 62 |
| 4.5 | The phase transition from domain wall to false vacuum-de Sitter | 63 |
| 4.6 | Evolution of X_h as a function of ϵ and Λ | 65 |
| 4.7 | Distance to the wall’s horizon as a function of ϵ and Λ | 65 |
| 4.8 | Wall solutions in an anti-de Sitter background | 66 |

| | | |
|------|--|-----|
| 4.9 | Parameter space (Λ, ϵ) and the types of solutions found | 67 |
| 4.10 | Bifurcation diagram for the gravitating domain wall | 68 |
| 4.11 | The de Sitter hyperboloid and its spherical section | 68 |
| 4.12 | The spatial section of the sine-Gordon domain wall | 70 |
| 5.1 | Bending a plane-symmetric wall | 83 |
| 6.1 | Diagram of a cosmic string threading a black hole | 93 |
| 6.2 | Thin cosmic string threading a Schwarzschild black hole. | 97 |
| 6.3 | Thick cosmic string threading a Schwarzschild black hole. | 98 |
| 6.4 | Contours of X and P for a core and vacuum/sine guesses | 101 |
| 6.5 | Field X for a core and vacuum/sine guesses | 102 |
| 6.6 | Solution on the horizon for $\beta = N = 1$ | 102 |
| 6.7 | Evolution of X_m and P_m for $N = 1$ | 103 |
| 6.8 | Expelled solution for $M = Q = 1.8$ and $\beta = N = 1$ | 104 |
| 6.9 | Critical mass M_c as a function of β and of N | 105 |
| 6.10 | Solution on the horizon for a single string for $\beta = N = 1$ | 106 |
| 6.11 | Solution on the grid for a single string for $\beta = N = 1$ | 107 |
| 6.12 | “Monopole” configuration for a string ending on a black hole | 107 |

List of Tables

| | | |
|-----|--|-----|
| B.1 | Numerical coefficients of the effective action for a cosmic string | 87 |
| B.2 | Distance to the horizon and Higgs field at the horizon for a $\lambda\Phi^4$ wall | 88 |
| B.3 | Value of ϵ at which the $\lambda\Phi^4$ wall develops a horizon | 89 |
| B.4 | Value of ϵ at which the sine-Gordon wall develops a horizon | 89 |
| C.1 | Value of $X(\pi/2)$ and $P(\pi/2)$ on the horizon | 116 |
| C.2 | Value of $X(\pi)$ on the horizon for a string ending on a black hole . . . | 117 |

Declaration and Statement

This thesis describes research carried out by the author at the Department of Mathematical Sciences of the University of Durham from October 1996 to August 1999. No part of it has been submitted for any other degree in this or any other University, with the exception of part of Chapter 3 as detailed below. Some of the material presented in this thesis has been published in several journals.

Chapters 1 and **2** are composed of background material, for which no claim of originality is made. **Chapter 3** is based on *Effective action and motion of a cosmic string* [4]. Part of the work described in this chapter has been submitted in the author's M.Sc. dissertation, *Cosmic strings and their dynamics* [17]; these are sections 3.1, 3.2, and subsection 3.3.1. **Chapter 4** is based on *Thick domain wall universes* [18] and *Thick self-gravitating plane-symmetric domain walls* [19]. **Chapter 5** is based on research still to be submitted. **Chapter 6** is based on *Comment on "Absence of abelian Higgs hair for extreme black holes"* [21] and *Vortices and extreme black holes: The question of flux expulsion* [20].

Copyright © 1999 by Filipe Bonjour.

"The copyright of this thesis rests with the author. No quotation from it should be published without their prior written consent and information derived from it should be acknowledged."

Acknowledgements

It is a pleasure to acknowledge here the help of so many people without whom this thesis and the work it describes would never have been possible.

I am first and foremost thankful to my supervisor, Dr. Ruth Gregory, for all her help and support during the four years that I have spent in Durham. So many things about a thesis are determined by the choice of its supervisor that I can only be glad that I chose to write my M.Sc. dissertation on cosmology three years ago.

I am also indebted for their help to many members of the department, especially those with whom I have had the pleasure to work — Christos Charmousis and Roberto Emparan — and Bernard Piette for continuous help with numerical aspects of my work. I am also very grateful to our head of Department, Professor Ed Corrigan, for his support throughout my stay in Durham.

I would also like to thank here all the people I have known and befriended in Durham during these four years. This includes everyone already mentioned, as well as my housemates (Amanda and Rick; Lisa, Matt and Dave; Theodora, Alejandra, Stephen and Diego); my fellow rowers (Neil, John C, Aude and Tom; Delia, Lucy, Jens, John M and Michael; Helen, Matt, Anja and John O; Jo, Prash, Rومان, Richard and Steve; Rachel, Ola, Maria and Jane; Mandy, Elena and Aline); and the other postgraduates in Maths (Medina, Tom, and all the others). As my housemate for two years, and tireless pool player, Matt deserves my special thanks.

These acknowledgements would not be complete without my thanking also the many people who have helped me from far away. I am most grateful to Professor André Châtelain, from the Swiss Federal Institute of Technology at Lausanne, for his help and support during this thesis. I would like to thank specially my Mother

and my Sister Danièle, Joël and Dirck in Geneva; and Loira, Luiz, Tera, Tita, Tó and everyone from my family in Brazil.

Finally, I am also thankful to the following organizations, whose financial help was essential in completing this thesis: the Council of the Swiss Federal Institutes of Technology, for a “Sunburst” scholarship; the Swiss National Science Foundation, for a “Bourse de Relève;” the Committee of Vice-Chancellors and Principals of the Universities of the United Kingdom (CVCP), for an “Overseas Research Students Awards Scheme” (ORS) scholarship; and the University of Durham — especially the Department of Mathematical Sciences — for generously waiving my home fees during my last year, for helping me so many times to travel to attend conferences and for awarding me the “Nick Brown Memorial Fund,” the “Euan Squires Memorial Prize” and the “Quayle Postgraduate Bursary.”

Conventions and Notations

We use the following conventions:

- **Sets and groups**

The sets of the integer, real and complex numbers are denoted by \mathbb{Z} , \mathbb{R} and \mathbb{C} respectively. Groups are noted in a sans serif font [e.g. $U(1)$] and \mathbb{S}^n denotes the n -dimensional unit-radius sphere.

- **Coordinates**

All spacetimes are four-dimensional, and we use the following coordinates:

- Cartesian coordinates: $\{t, x^1, x^2, x^3\}$;
- Cylindrical coordinates: $\{t, \varrho, \vartheta, z\}$;
- Spherical coordinates: $\{t, r, \theta, \varphi\}$.

- **Metric signature**

We use a “mostly minus” signature $(+, -, -, -)$.

- **Manifolds and Embeddings**

The spacetime manifold is denoted by \mathcal{M} and has dimension $d = 4$. A general submanifold is denoted by \mathcal{S} and has dimension n ; its orthogonal complement in \mathcal{M} will be written ${}^\perp\mathcal{S}$ and have dimension n' , so that $d = n + n'$. In the case of a string’s worldsheet or a wall’s worldvolume, the submanifold will be noted \mathcal{W} . The vacuum manifold of a field theory will be written \mathcal{V} , and a black hole’s (outer) horizon, \mathcal{H} .

- **Tensor Indices**

We use the following conventions when indexing a tensor in the Gauß–Codazzi formalism:

- Spacetime indices are denoted with lowercase Latin letters: a, b, c, \dots
- Worldsheet indices are denoted by uppercase Latin letters: A, B, C, \dots
- Directions perpendicular to the worldsheet are denoted by Greek letters from the middle of the alphabet: λ, μ, ν, \dots

- **Miscellaneous notations**

- When an equation defines its left-hand side, we shall replace the equal sign by “ $\stackrel{\text{def}}{=}$ ”.
- When an equation introduces a new notation, we shall replace the equal sign by “ $\stackrel{\text{notn}}{=}$ ”.
- In chapters 3 and 5, we denote quantities evaluated at the defect’s core by underlining them. For instance, $\underline{\kappa}_{ab} \stackrel{\text{notn}}{=} \kappa_{ab}|_{\mathcal{W}} \equiv \kappa_{ab}|_{\text{defect}}$.

Part I

Topological Defects



Extended Defects

1.1 Extended Defects in Cosmology

Over the past few decades, topological defects have become a familiar class of objects in many areas of physics. In solid state physics, for instance, defects are an important topic in the study of crystals and their properties; in high energy physics, topological solutions, such as solitons or instantons, are nonperturbative solutions to the field equations, and therefore have much to contribute to the understanding of particle physics beyond the perturbative level.

In cosmology — the context that interests us — topological defects (domain walls, cosmic strings, monopoles and textures) are believed to have formed generically during phase transitions in the very early Universe, at times well beyond the reach of any traditional particle physics experiment, via the Kibble mechanism [63]. Perhaps most notably, the gravitational properties of strings have been invoked to account for the existence of cosmic structure (galaxies and galaxy clusters) in the Universe [59,89]. Whether strings would really have been able to seed structures compatible with the ones we observe today or not is still an open question (see the discussion on pages 49*ff*); in any case, there is no denying that the idea of topological defects is a beautiful and powerful one, and that its study may have a great deal to teach physicists.

In the past, topological defects have often been considered in the so-called thin limit, where they have no thickness. Such pioneering works as Israel's "thin wall formalism" [61] to study the dynamics of membranes, Vilenkin's [87] and Ipser & Sikivie's [60] efforts to determine the gravitational field of walls, and Aryal, Ford &

Vilenkin's metric [7] describing a cosmic string piercing a black hole are all important precursors of the work described in this thesis which assume that the defects have zero thickness. At first sight, this approximation seems perfectly reasonable, since the defects of cosmological interest are likely to have formed at the Grand Unified Theory (GUT) scale $\eta \sim 10^{16}$ GeV, and that — even for finite-sized defects such as wall bubbles of string loops — their thickness is typically many orders of magnitude smaller than their size. In fact, most efforts to understand extended defects followed the proposition by Hill, Schramm and Fry [58] of a late time phase transition producing thick walls (see the discussion at the beginning of chapter 4) and, more recently, the idea of topological inflation [88,69,70].

There are, however, other well-recognised reasons for studying thick defects. For instance, it is cosmologically important to study the collapse of bubbles and loops, because this tells us interesting things, such as the lifespan of these defects (which in turn constraints their cosmological impact) or whether this collapse forms a black hole. Presumably, at the end of the collapse (where most of the physical interest resides) the string's thickness may become comparable to its size, and the thin defect formalism breaks down.

For these reasons, and others discussed on page 24, it is important to consider the effect of the defects' thickness on the results obtained in the infinitesimally thin limit. In this thesis we contribute to the effort made over the past decade or so to understand these effects.

In Chapter 3, we study the dynamics of thick abelian-Higgs cosmic strings in a flat spacetime, focusing on three illustrative trajectories, then discuss more generally the implications of the thickness of the defects for their rigidity. Chapter 4 describes the plane-symmetric gravitating solutions of the Goldstone and sine-Gordon models; it was originally intended as a preliminary to the study of the dynamics of thick gravitating walls (which is the topic of Chapter 5), but has spanned some interesting results in its own right. Chapter 6 presents an investigation of the system consisting of a Nielsen-Olesen cosmic string and an extreme Reissner-Nordström black hole, with the axis of the string passing through the centre of the black hole. In particular, we investigate whether or not the previously observed phenomenon of “flux expulsion” does indeed occur. Somewhat unexpectedly, we find similarities between

our results and those of chapter 4.

1.2 The Goldstone Model: Global Strings and Domain Walls

The Goldstone model [49, section 4] is given by the action

$$S = \int d^4x \sqrt{-g} \mathcal{L}, \quad (1.1)$$

where \mathcal{L} is the Lagrangian density

$$\begin{aligned} \mathcal{L} &= \frac{1}{2} (\nabla_a \Phi) (\nabla^a \Phi)^\dagger - V(\Phi), \\ V(\Phi) &= \lambda (\Phi \Phi^\dagger - \eta^2)^2. \end{aligned} \quad (1.2)$$

This theory of a single (real or complex) scalar ‘‘Higgs’’ field $\Phi(x^a)$ depends on two real parameters: the coupling constant λ , which gives the strength of the self-interaction of Φ , and the vacuum expectation value (VEV) η of Φ , which is the value of $|\Phi|$ for which the potential reaches its global minimum. The Higgs vacuum (i.e. the configuration devoid of Higgs particles) is therefore given by $|\Phi| = \eta$.¹

Here we consider the range of parameters $\lambda, \eta > 0$. If $\Phi \in \mathbb{R}$, the potential $V(\Phi)$ is the ‘‘double well potential’’ shown on figure 1.1a, which admits two degenerate minima at $\{\pm\eta\}$; if $\Phi \in \mathbb{C}$, the potential is the well-known ‘‘Mexican hat’’ (or ‘‘wine bottle’’) potential displayed on figure 1.1b, for which the degenerate vacua form a circle of radius η in the complex plane.

The Lagrangian (1.2) is clearly invariant under global $U(1)$ gauge transformations defined by

$$\Phi \rightarrow U(\Phi) \stackrel{\text{def}}{=} e^{i\alpha} \Phi, \quad (1.3)$$

where α is a constant. Because of the form of (1.3), the polar decomposition of the complex Higgs field

$$\Phi = \eta X(x^a) e^{i\chi(x^a)} \quad (1.4)$$

is particularly useful, since a gauge transformation then only affects χ , shifting it uniformly by a factor α . The real functions X and χ are called respectively the

¹In this thesis we are interested only in solutions which tend to the vacuum at spatial infinity, and therefore represent ‘‘finite’’ objects. This condition is necessary, but not sufficient, for the solution to be local.

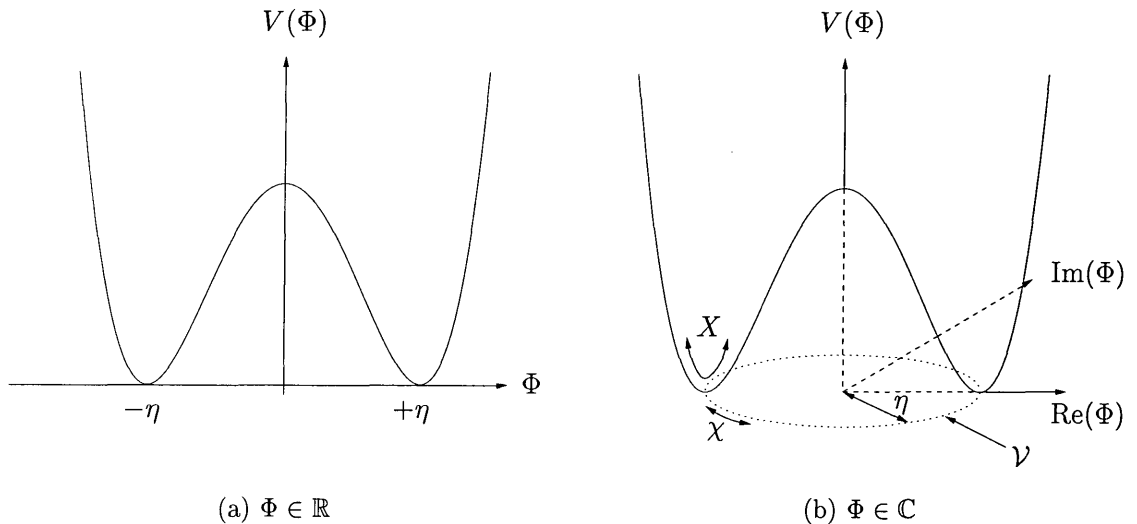


Figure 1.1: (a) The double well potential of the real Goldstone model. (b) The Mexican hat potential of the complex Goldstone model.

Higgs and the Goldstone fields. If Φ is real, the above remains trivially true, with $\chi \equiv 0$, and α can only take the values $\{0, \pm\pi\}$.

Replacing this decomposition into (1.2), we obtain

$$\mathcal{L} = \eta^2 \left[(\nabla_a X) (\nabla^a X) + X^2 (\nabla_a \chi) (\nabla^a \chi) - \frac{1}{w_H^2} (X^2 - 1)^2 \right], \quad (1.5)$$

where

$$w_H \stackrel{\text{def}}{=} \frac{1}{\sqrt{\lambda\eta}}. \quad (1.6)$$

An important consequence of the $U(1)$ -invariance of the potential is that it has degenerate minima. The vacuum manifold \mathcal{V} of this theory, defined as the set of all Φ that minimize the potential, is the circle $|\Phi| = \eta$. The $U(1)$ symmetry can therefore be spontaneously broken by an explicit choice of vacuum at each point of spacetime. The Higgs mechanism and the Goldstone theorem then tell us that the Higgs field acquires a mass,

$$m_H \stackrel{\text{def}}{=} \sqrt{\lambda}\eta, \quad (1.7)$$

whereas the Goldstone field remains massless. The reason for this is that X describes fluctuations of Φ in a radial direction, for which the potential is curved (at $\Phi = \eta$, $V'' = 4\lambda\eta^2 = 4m_H^2$) while χ describes angular fluctuations of Φ , for which the potential remains flat (see figure 1.1b). Note that the quantity w_H is defined as the inverse of the Higgs mass, and therefore characterizes the fall-off of this field towards

its vacuum value. In other words, when we have a localized solution (a defect), w_H is its characteristic size: width of a domain wall, thickness of a cosmic string or radius of a monopole.

The Euler-Lagrange equations derived from Lagrangian (1.5) are

$$\square X - X [(\nabla_a \chi)(\nabla^a \chi) - 2(X^2 - 1)] = 0, \quad (1.8a)$$

$$\square \chi + 2X^{-1}(\nabla_a X)(\nabla^a \chi) = 0 \quad (1.8b)$$

(where we have rescaled the coordinates x^a so that $w_H \equiv 1$). A static cosmic string solution along the z -direction in flat spacetime can be found by making the Ansatz $X = X(\varrho)$, $\chi = N\vartheta$; the constant $N \in \mathbb{Z}$ is then the string's winding number. This form clearly solves (1.8b), leaving an equation for X ,

$$X'' + \frac{X'}{\varrho} - X \left[\frac{N^2}{\varrho^2} + (X^2 - 1) \right] = 0, \quad (1.9)$$

whose solution can be shown to satisfy asymptotically:

$$X = \begin{cases} x_N \varrho^{|N|} \left[1 - \frac{1}{4(N+1)} \varrho^2 + \mathcal{O}(\varrho^4) \right] & \text{for } \varrho \rightarrow 0, \\ 1 - \frac{N^2}{2\varrho^2} + \mathcal{O}(\varrho^{-4}) & \text{for } \varrho \rightarrow \infty. \end{cases} \quad (1.10)$$

Eq. (1.9) can be solved numerically using the routine SOLVDE from Ref. [82], which yields the parameter x_N . The profiles $X(\varrho)$ for $N = 1, 2, 3$ and 4 are presented in figure 1.2; the energy densities plotted are the tt components of the rescaled version \hat{T}_{ab} of the energy-momentum tensor T_{ab} , which is conventionally defined by

$$\delta S[\Phi, g_{ab}] \Big|_{\delta \Phi=0} = \frac{1}{2} \int d^4x \sqrt{-g} T_{ab} \delta g^{ab}. \quad (1.11)$$

For our model (1.2) we obtain, in terms of the Higgs and Goldstone fields,

$$\begin{aligned} \hat{T}_{ab} \stackrel{\text{def}}{=} \frac{w_H^2}{\eta^2} T_{ab} &= (\nabla_a X)(\nabla_b X) + X^2 (\nabla_a \chi)(\nabla_b \chi) \\ &- \frac{1}{2} g_{ab} \left[(\nabla_a X)(\nabla^a X) + X^2 (\nabla_a \chi)(\nabla^a \chi) - \frac{1}{2} (X^2 - 1)^2 \right]. \end{aligned} \quad (1.12)$$

The solutions of figure 1.2 describe linear objects called global (abelian) strings. By ‘‘linear’’ it is understood that these objects are much longer than they are thick; however, the string's width w_H is set to 1 and they are not one-dimensional. Also, although the solutions that we have found are straight, cosmic strings come in all shapes, including loops; we shall deal abundantly with curved strings in this thesis.

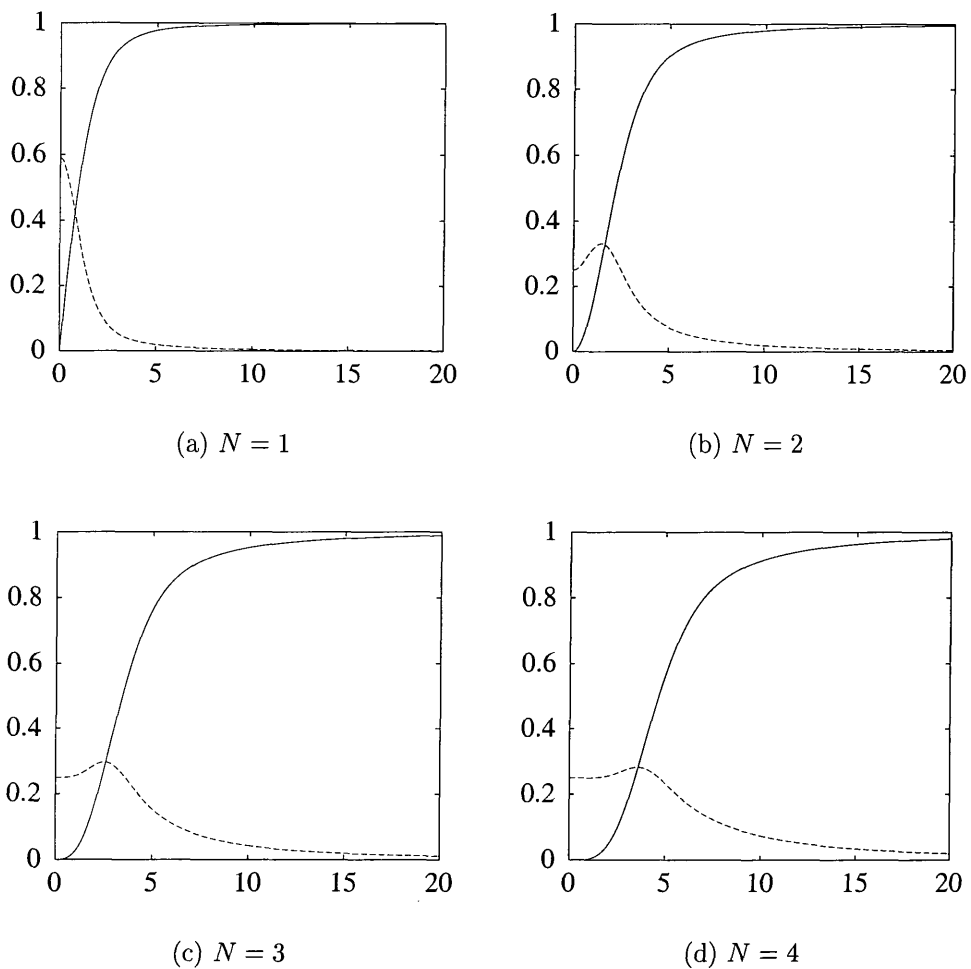


Figure 1.2: Profiles $X(\varrho)$ (solid) and energy density profiles for global strings with (a) $N = 1, \dots$, (d) $N = 4$.

Note in particular that the total energy per unit length of global strings, which is given by $\int d^2x \sqrt{|{}^{(3)}g|} T^0_0$, diverges logarithmically at infinity:

$$\lim_{\varrho \rightarrow \infty} E \sim \lim_{\Lambda \rightarrow \infty} \int_{w_H}^{\Lambda} \varrho d\varrho \varrho^{-2} \sim \lim_{\Lambda \rightarrow \infty} \ln \left(\frac{\Lambda}{w_H} \right). \quad (1.13)$$

However, in a cosmological setting, cosmic strings are never alone but form a network. Then, Λ is not allowed to tend to infinity, but only to a cutoff value ξ which is the typical distance between global strings in the network.

If $\Phi \in \mathbb{R}$, equation (1.8) becomes simply

$$\square X + 2X(X^2 - 1) = 0; \quad (1.14)$$

this time we can solve this equation if we make the Ansatz $X = X(z)$, and find the flat spacetime kink solution (see figure 1.3)

$$X(z) = \tanh(z). \quad (1.15)$$

This solution describes a domain wall separating two regions with different vacua: for negative z , the vacuum is $X = -1$ and for positive z , the vacuum is $X = +1$. Again, although this particular solution describes a flat wall, curved walls can exist, and we shall encounter some examples later on.

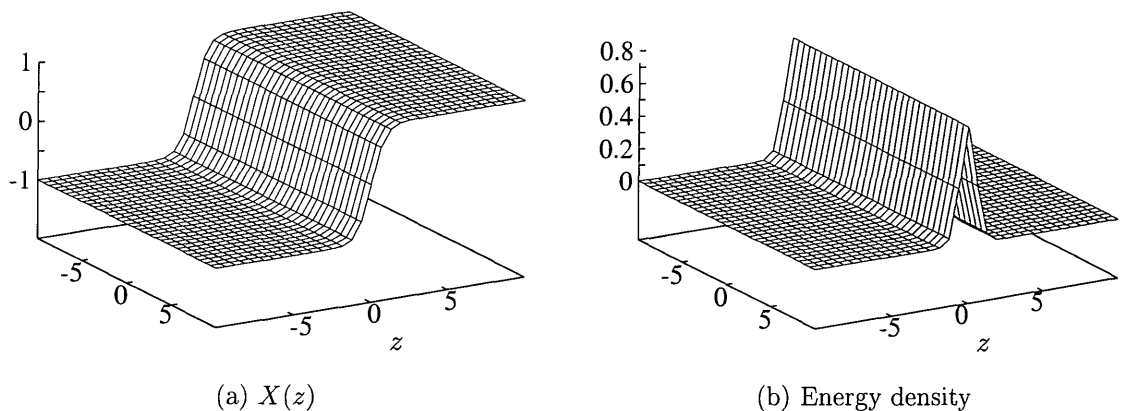


Figure 1.3: The static kink solution. (a) The field solution $X = \tanh(z)$. (b) The energy density associated with this solution.

1.3 The Abelian–Higgs Model: Local Strings

The second model in which we are going to consider topological defects is the local version of the Goldstone model, called the abelian–Higgs model. This is given by

the action (1.1), this time with

$$\mathcal{L} = (D_a \Phi) (D^a \Phi)^\dagger - \frac{1}{4} \tilde{F}_{ab} \tilde{F}^{ab} - V(\Phi), \quad (1.16a)$$

$$V(\Phi) = \frac{\lambda}{4} (\Phi^\dagger \Phi - \eta^2)^2. \quad (1.16b)$$

The parameters λ and η have the same meaning as in the Goldstone model (and are still strictly positive) and the potential for Φ ($\in \mathbb{C}$) is still the usual Mexican hat potential. This model can be obtained from the Goldstone model by requiring that the abelian–Higgs Lagrangian be invariant under local $U(1)$ transformations, which are defined by

$$\Phi \rightarrow U(\Phi) \stackrel{\text{def}}{=} e^{ie\alpha(x^a)} \Phi. \quad (1.17a)$$

(The factor e , which is the charge associated with the group $U(1)$, is conventional.) To maintain the invariance of the Lagrangian, this forces us to introduce new terms to cancel those appearing, from the spatial dependence of α , in the kinetic part of \mathcal{L} . This implies the introduction of a gauge field A_a which must transform as

$$A_a \rightarrow A_a + e^{-1} \nabla_a \alpha. \quad (1.17b)$$

These new terms can be incorporated in the gauge covariant derivative

$$D_a \stackrel{\text{def}}{=} \nabla_a + ieA_a, \quad (1.18)$$

and one must also introduce in the Lagrangian a kinetic term for the new particle, which we take to be quadratic in \tilde{F}_{ab} , where

$$\tilde{F}_{ab} \stackrel{\text{def}}{=} 2 \partial_{[a} A_{b]}. \quad (1.19)$$

Contrary to the global case, the possibility of choosing a space-dependent phase $\alpha(x^a)$ allows us to get rid of the phase of Φ , and it is conventional to rewrite the field content of this theory in terms of two new fields X and P_a defined by

$$\begin{aligned} \Phi &= \eta X, \\ A_a &= \frac{1}{e} (P_a - \nabla_a \alpha). \end{aligned} \quad (1.20)$$

Moreover, although the parameters λ , η and e appearing in the Lagrangian are well-adapted to the description of the properties of the particle solutions of the

theory before the symmetry breakdown, we shall use another set of parameters which are more natural to discuss the topological solutions after the breaking. These parameters are the string's Higgs and gauge widths w_H and w_g , and the Bogomol'nyi parameter β [15], and are defined by

$$\begin{aligned} w_H &\stackrel{\text{def}}{=} m_H^{-1} \equiv \frac{1}{\sqrt{\lambda\eta}}, \\ w_g &\stackrel{\text{def}}{=} m_g^{-1} \equiv \frac{1}{\sqrt{2e\eta}}, \\ \beta &\stackrel{\text{def}}{=} \frac{m_H^2}{m_g^2} \equiv \frac{\lambda}{2e^2}. \end{aligned} \tag{1.21}$$

The Bogomol'nyi parameter is sometimes defined as the inverse of β above.²

The coordinate rescaling to make $w_H = 1$ must this time be accompanied by a rescaling of the gauge field,

$$\begin{aligned} x^a &\rightarrow w_H x^a, \\ P_a &\rightarrow w_H^{-1} P_a, \end{aligned} \tag{1.22}$$

which allows us to get completely rid of the width w_H in the equations of motion (w_g does not appear there, as it can be written in terms of w_H and β); this corresponds simply to choosing units in which the string has a Higgs width of order unity.

In the new variables, and calling F_{ab} the strength field associated with P_a , the Lagrangian and equations of motion become

$$\mathcal{L} = \eta^2 \left[(\nabla_a X) (\nabla^a X) + X^2 P_a P^a - \frac{\beta}{2} F_{ab} F^{ab} - \frac{1}{4} (X^2 - 1)^2 \right]. \tag{1.23}$$

and

$$\begin{aligned} \square X - X P_a P^a + \frac{1}{2} X (X^2 - 1) &= 0, \\ \nabla_a F^{ab} + \frac{X^2 P^b}{\beta} &= 0. \end{aligned} \tag{1.24}$$

The prototypical solution for this theory is found by assuming that the string is static, straight and along the z -axis in flat spacetime; that is, by writing the Ansatz

$$\begin{aligned} X &= X(\varrho), \\ P_a &= N P(\varrho) \nabla_a \vartheta. \end{aligned} \tag{1.25}$$

²This is the case for instance in our paper [4], and therefore some care is necessary when comparing that paper to the chapter derived from it in this thesis, chapter 3.

This leaves us two coupled ordinary differential equations (ODEs):

$$\begin{aligned} X'' + \frac{X'}{\varrho} - \frac{N^2 P^2 X}{\varrho^2} - \frac{1}{2} X (X^2 - 1) &= 0, \\ P'' - \frac{P'}{\varrho} - \frac{X^2 P}{\beta} &= 0. \end{aligned} \quad (1.26)$$

The functions which solve these equations (for $N = 1$) will be written X_{NO} and P_{NO} and called the Nielsen–Olesen (NO) solution [76]. They admit the following asymptotic behaviour [80]:

$$\begin{aligned} X_{\text{NO}} &= \begin{cases} x_N \varrho^{|N|} \left[1 + \frac{2N^2 p_2 - \frac{1}{2}}{4(N+1)} \varrho^2 + O(\varrho^4) \right] & \text{for } \varrho \rightarrow 0, \\ 1 - x_\infty \frac{e^{-\varrho}}{\sqrt{\varrho}} & \text{for } \varrho \rightarrow \infty, \beta < 4, \\ 1 - \frac{N^2 p_\infty^2 \beta}{(\beta - 4)\varrho} e^{-2\varrho/\sqrt{\beta}} & \text{for } \varrho \rightarrow \infty, \beta > 4; \end{cases} \\ P_{\text{NO}} &= \begin{cases} 1 - p_2 \varrho^2 & \text{for } \varrho \rightarrow 0, \\ p_\infty \sqrt{\varrho} e^{-\varrho/\sqrt{\beta}} & \text{for } \varrho \rightarrow \infty. \end{cases} \end{aligned} \quad (1.27)$$

Note that we obtain a global string in the limit $\beta \rightarrow \infty$ by setting $P \equiv 1$, i.e. choosing the gauge vacuum, in Eq. (1.26).³

The Nielsen–Olesen functions are plotted on figure 1.4 for $\beta = 1$ and a few values of N . This solution, unlike the global string, has a finite energy per unit length; this is due to the presence of the gauge field: for very large ϱ , it aligns itself so as to cancel the gauge covariant derivative term in the energy density.

The special case $\beta = 1$ is called the critical case. Assume that $\beta = 1$, and consider the energy per unit length E_ℓ obtained by varying the action (1.1) with the Lagrangian (1.16). We can then find a Bogomol’nyi argument for the system by writing E_ℓ in the following way:

$$\begin{aligned} E_\ell &= \int d^2x \sqrt{-g} \left\{ [\varepsilon^a{}_b \nabla_a X + X P_b]^2 + \left[F_{ab} - \frac{1}{2} \varepsilon_{ab} (X^2 - 1) \right]^2 \right\} \\ &\quad - \int d^2x \sqrt{-g} \varepsilon^{ab} [2P_a \nabla_b X - F_{ab} (X^2 - 1)] \end{aligned} \quad (1.28)$$

(where ε_{ab} is the totally antisymmetric tensor of two indices). Noting that the integrand in the last term is $\nabla_a [\varepsilon^{ab} P_b (X^2 - 1)]$, we can use Gauß’s theorem to

³In fact, this is not exactly the global string of the previous section, because of the factor $1/4$ by which we multiplied the potential. However, we will never deal with global strings in this thesis, only domain walls, and the extra factor in the potential will never cause any problem.

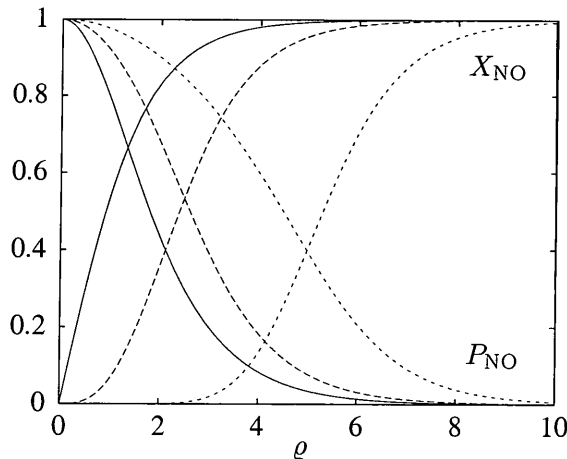


Figure 1.4: Profiles $X_{\text{NO}}(\varrho)$ and $P_{\text{NO}}(\varrho)$ for $\beta = 1$ and $N = 1$ (solid), $N = 3$ (long-dashed) and $N = 10$.

express it in terms of the string's winding number N :

$$E_\ell = 2\pi|N| + \int d^2x \sqrt{-g} \left\{ [\varepsilon^a_b \nabla_a X + X P_b]^2 + \left[F_{ab} - \frac{1}{2} \varepsilon_{ab} (X^2 - 1) \right]^2 \right\} \geq 2\pi|N|. \quad (1.29)$$

Therefore, we see that the energy will be minimized — by $2\pi|N|$ — if the following “Bogomol’nyi equations” are satisfied:

$$\begin{aligned} \varepsilon^a_b \nabla_a X &= -X P_b, \\ F_{ab} &= \frac{1}{2} \varepsilon_{ab} (X^2 - 1). \end{aligned} \quad (1.30)$$

These equations are first order ODEs, as opposed to the second order equations (1.24) to which they are equivalent. If $\beta \neq 1$, we cannot write the energy as a topological term plus a positive contribution as above and the system does not admit Bogomol’nyi equations.

1.4 More Complicated Models: Superconducting Strings

There are several ways to generalize the Goldstone and abelian–Higgs models of the previous sections. The first generalization is (just as we modified the Goldstone model by demanding that it be locally invariant) to impose a non-abelian symmetry to the theory — this corresponds to considering vector Higgs fields rather than scalar ones. A second generalization consists in including new, different fields. In

this section, we will see how this may lead to the strings becoming superconducting. (More precisely, we will consider the case of the bosonic superconducting string.)

Enlarge the abelian–Higgs theory to contain the two fields Φ and A_a plus two new fields σ and B_a , with Lagrangian density

$$\begin{aligned} \mathcal{L} = & (D_a \Phi) (D^a \Phi)^\dagger - \frac{1}{4} \tilde{F}_{ab} \tilde{F}^{ab} + \\ & (D_a \sigma) (D^a \sigma)^\dagger - \frac{1}{4} \tilde{G}_{ab} \tilde{G}^{ab} - V(\Phi, \sigma), \end{aligned} \quad (1.31a)$$

$$V(\Phi, \sigma) = \frac{\lambda}{4} (\Phi \Phi^\dagger - \eta^2)^2 + \frac{\tilde{\lambda}}{4} |\sigma|^4 - m^2 |\sigma|^2 + f |\Phi|^2 |\sigma|^2. \quad (1.31b)$$

This Lagrangian is invariant under transformations of $U(1) \times U(1)_{\text{EM}}$. The first $U(1)$ group is associated with the Higgs field Φ and the gauge field A_a , which interact with each other through the gauge-covariant derivative $D_a \Phi \stackrel{\text{def}}{=} (\nabla_a + ieA_a) \Phi$. As before, this symmetry is spontaneously broken and the Higgs acquires a mass; this breakdown is responsible for the existence of the topological defect. The second group, $U(1)_{\text{EM}}$, is associated with the new scalar σ which interacts with a gauge field B_a via the derivative $D_a \sigma = (\nabla_a + igB_a) \sigma$; this group will not be broken outside the string, and therefore the gauge particle associated with the B -field will remain asymptotically massless. For this reason, it is commonly referred to as the photon and $U(1)_{\text{EM}}$ is called electromagnetism.

As before, \tilde{F}_{ab} is the strength field of A_a , and now \tilde{G}_{ab} is that of B_a . The parameters λ, η and e retain their previous physical meaning; the new parameters are $\tilde{\lambda}$ (which gives the strength of the self-interaction of the σ), m (which is the mass of the σ), f (which characterizes the Φ - σ interaction) and g , the electromagnetic charge.

This time we make the following Ansätze for the fields:

$$\begin{aligned} \Phi &= \eta X(x^a), & \sigma &= \frac{\sqrt{2}m^2}{\sqrt{\tilde{\lambda}}} s(x^a) e^{i\chi(x^a)}, \\ A_a &= \frac{1}{e} (P_a - \nabla_a \alpha), & B_a &= \frac{1}{g} (C_a - \nabla_a \chi), \end{aligned} \quad (1.32)$$

with which the Lagrangian becomes

$$\begin{aligned} \frac{\mathcal{L}}{\lambda \eta^4} = & (\nabla_a X) (\nabla^a X) + P_a P^a X^2 + \alpha_1 [(\nabla_a s) (\nabla^a s) + C_a C^a s^2] \\ & - \frac{\beta}{2} F_{ab} F^{ab} - \frac{\tilde{\beta}}{2} G_{ab} G^{ab} - V(X, s), \end{aligned} \quad (1.33a)$$

$$V(X, s) = \frac{1}{4} (X^2 - 1)^2 + \alpha_2 X^2 s^2 + \alpha_3 s^2 (s^2 - 2). \quad (1.33b)$$

Here, we have defined the following (positive) parameters:

$$\begin{aligned} \alpha_1 &= \frac{2m^2}{\tilde{\lambda}\eta^2}, & \alpha_2 &= \frac{2fm^2}{\lambda\tilde{\lambda}\eta^2}, & \alpha_3 &= \frac{m^4}{\lambda\tilde{\lambda}\eta^4}, \\ \beta &= \frac{\lambda}{2e^2}, & \tilde{\beta} &= \frac{\lambda}{2g^2}. \end{aligned} \quad (1.34)$$

β is the usual Bogomol'nyi parameter, and $\tilde{\beta}$ plays a similar rôle for electromagnetism. We shall determine the respective ranges for the parameters shortly. As usual, we have also redefined the coordinates, so that the string has a Higgs width of order unity, and rescaled the gauge fields P_a and C_a by w_H .

The idea behind superconducting strings [93] is to choose the parameters in such a way that electromagnetism is broken inside the string; the photon then acquires a mass there, and the string carries a current

$$j_a \stackrel{\text{def}}{=} ig \left[\sigma^\dagger D_a \sigma - \sigma (D_a \sigma)^\dagger \right] = 4 \frac{m^2 g}{\tilde{\lambda}} s^2 C_a. \quad (1.35)$$

Babul *et al.* [9] have argued that in order to have a superconducting string with a current along it, the following conditions must be met:

1. A string must be present:

This can be achieved by imposing the usual boundary conditions $X(0) = P(\infty) = 0, X(\infty) = P(0) = 1$.

2. The vacuum must be non-conducting:

$V(s = 0, X = 1) < V(s \neq 0, X = 0)$, which implies:

$$\alpha_3 < \frac{1}{4}. \quad (1.36)$$

Note that this condition is not very strict: it was obtained by minimizing $s(s^2 - 1)$ by -1 . If s never reaches 1, e.g. if $s(s^2 - 1) > -1 + \kappa$ (for positive, small κ) then the condition becomes

$$\alpha_3 < \frac{1}{4} (1 + \kappa). \quad (1.37)$$

3. The vacuum must be a global minimum:

In other words, $(\delta^2/\delta s^2) V(s = 0, X = 1) > 0$, i.e.:

$$\alpha_2 - 2\alpha_3 > 0. \quad (1.38)$$

4. **It must be energetically favourable for the string to conduct electromagnetism:**

This is only true if the contribution to the system's energy due to the fact that “ $s(\text{inside string}) \neq 0$ ” is negative. This implies

$$U < 0 \quad (1.39)$$

where

$$U = \int \varrho d\varrho \left[s'^2 + s^2 C^2 + \frac{\alpha_2}{\alpha_1} s^2 X_{\text{NO}}^2 + \frac{\alpha_3}{\alpha_1} s^2 (s^2 - 2) \right]. \quad (1.40)$$

(Here we have simplified the real expression; see [9, Eq. (9)] for a fuller expression. In particular, we have assumed that C does not change significantly when one switches on s .)

More constraints apply if one considers quantum effects [55].

A prototypical solution can again be found numerically for a static straight string (say at $x = y = 0$) with a current along it, that is

$$\begin{aligned} X &= X(\varrho), \\ s &= s(\varrho), \\ P_a &= NP(\varrho) \nabla_a \vartheta, \\ C_a &= C(\varrho) \nabla_a z. \end{aligned} \quad (1.41)$$

The equations of motion from (1.1, 1.33) then become

$$\begin{aligned} X'' + \frac{X'}{\varrho} - \frac{N^2 P^2 X}{\varrho^2} - \frac{1}{2} X (X^2 - 1) - \alpha_2 s^2 X &= 0, \\ s'' + \frac{s'}{\varrho} - C^2 s - 2 \frac{\alpha_3}{\alpha_1} s (s^2 - 1) - \frac{\alpha_2}{\alpha_1} X^2 s &= 0, \\ P'' - \frac{P'}{\varrho} - \frac{1}{\beta} X^2 P &= 0, \\ C'' + \frac{C'}{\varrho} - \frac{\alpha_1}{\beta} s^2 C &= 0. \end{aligned} \quad (1.42)$$

[They clearly reduce to the Nielsen–Olesen equations (1.26) if one sets $s = C = 0$.] The asymptotic forms for these fields is given below. There are up to 9 coefficients which are not determined by the equations of motion: for small ϱ , these are x_N , s_0 , c_0 and p_2 (although p_2 is subdominant); for large ϱ , these are x_∞ , s_∞ , p_∞ , c_∞ and

\bar{c}_∞ .

$$\begin{aligned}
 X(\varrho) &= \begin{cases} x_N \varrho^{|N|} \left[1 + \frac{2N^2 p_2 + \alpha_2 s_0^2 - \frac{1}{2}}{4(N+1)} \varrho^2 + O(\varrho^4) \right] & \text{for } \varrho \rightarrow 0, \\ 1 - x_\infty \frac{e^{-\varrho}}{\sqrt{\varrho}} & \text{for } \varrho \rightarrow \infty, \beta < 4, \\ 1 - \frac{N^2 p_\infty^2 \beta}{(\beta - 4)\varrho} e^{-2\varrho/\sqrt{\beta}} & \text{for } \varrho \rightarrow \infty, \beta > 4; \end{cases} \\
 S(\varrho) &= \begin{cases} s_0 \left\{ 1 - \frac{1}{4} \left[2 \frac{\alpha_3}{\alpha_1} (1 - s_0^2) - c_0^2 \right] \varrho^2 + O(\varrho^4) \right\} & \text{for } \varrho \rightarrow 0, \\ s_\infty e^{-[\bar{c}_\infty \ln(\varrho) + c_\infty - \bar{c}_\infty]\varrho} & \text{for } \varrho \rightarrow \infty; \end{cases} \\
 P(\varrho) &= \begin{cases} 1 - |p_2| \varrho^2 + p_4 \delta^{N,1} \varrho^6 + O(\varrho^4) & \text{for } \varrho \rightarrow 0, \\ p_\infty \sqrt{\varrho} e^{-\varrho/\sqrt{\beta}} & \text{for } \varrho \rightarrow \infty; \end{cases} \\
 C(\varrho) &= \begin{cases} c_0 \left[1 + \frac{\alpha_1 s_0^2}{4\beta} \varrho^2 + O(\varrho^4) \right] & \text{for } \varrho \rightarrow 0, \\ c_\infty + \bar{c}_\infty \ln(\varrho) & \text{for } \varrho \rightarrow \infty. \end{cases}
 \end{aligned} \tag{1.43}$$

Note that, numerically, the coefficients in (1.43) need not be the same as those in (1.27) or (1.10), even if they have the same name. Some solutions are shown on figure 1.5.

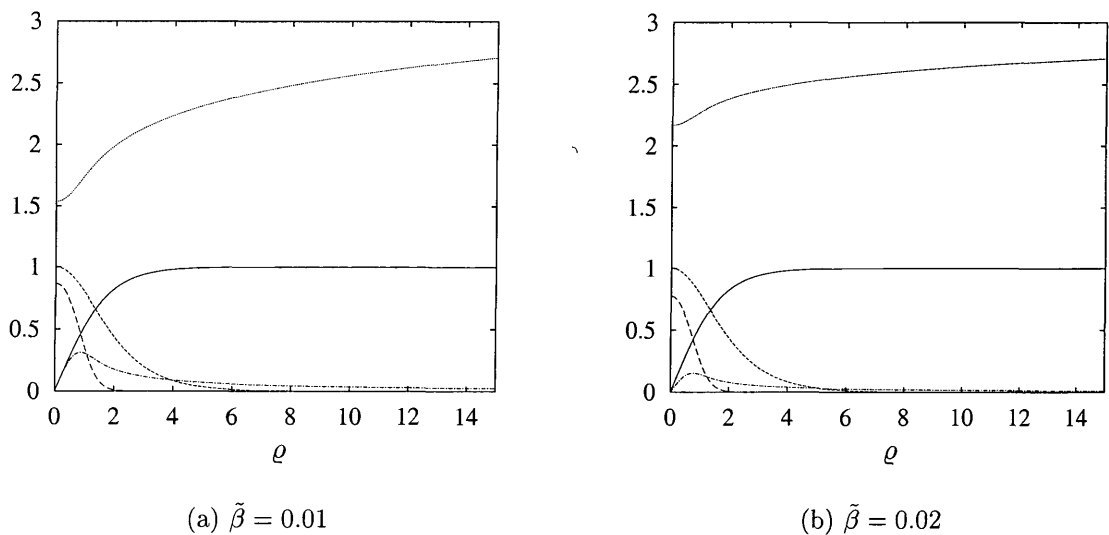


Figure 1.5: The straight superconducting string for $\alpha_1 = 0.01$, $\alpha_2 = 0.5$, $\alpha_3 = 0.1$, $\beta = 1.0$ and (a) $\tilde{\beta} = 0.01$ and (b) $\tilde{\beta} = 0.02$. The plots show X (solid), s (long-dashed), P (short-dashed), C (dotted) and $B_\vartheta \stackrel{\text{def}}{=} G_{rz} = C'$ (dot-dashed).

Part II

The Dynamics of
Topological Defects

The Gauß–Codazzi Formalism for Topological Defects

In this chapter, we briefly introduce the Gauß–Codazzi formalism, which is a powerful tool for considering the embedding of a submanifold \mathcal{S} in a manifold \mathcal{M} . In this thesis, \mathcal{M} will always be the four-dimensional spacetime manifold and \mathcal{S} will be the worldsheet \mathcal{W} of the topological defect in which we are interested. As a consequence, we deal exclusively with the special case of the formalism where the submanifold extends in the timelike direction, *i.e.* the normals of \mathcal{S} in \mathcal{M} are all spacelike. Moreover, we shall restrict ourselves in this introduction to the notions that we will use in later chapters (see [43] for walls and [4] for strings). For a more complete and general description, we refer the reader to [86] and, in a notation closer to ours, to [24–28].

For an infinitesimally thin defect, it is clear that the mathematical abstraction that we call “worldsheet” can be identified with the defect itself, but for the kind of extended defect that concerns us, \mathcal{S} should rather be identified with the defect’s core. For all models introduced in the previous chapter, this is defined by the locus of the points of \mathcal{M} where the Higgs field vanishes, $\Phi = 0$.

Consider a general n -dimensional submanifold \mathcal{S} embedded in the d -dimensional spacetime manifold \mathcal{M} . Then, \mathcal{S} has an orthogonal complement in \mathcal{M} which we denote by ${}^\perp\mathcal{S}$. We shall adopt the convention of noting spacetime indices with lowercase Latin letters (a, b, \dots), indices parallel to \mathcal{S} with uppercase Latin letters (A, B, \dots) and indices perpendicular to \mathcal{S} by Greek letters (μ, ν, \dots).

Let us now coordinatize the spacetime \mathcal{M} with x^a ($a = 0, \dots, d - 1$), \mathcal{S} with

σ^A ($A = 0, \dots, n-1$) and ${}^{\perp}\mathcal{S}$ with ξ^μ ($\mu = 0, \dots, d-n-1$). \mathcal{S} then admits at each point n tangential vectors (or tangents) t_A^a and $n' \stackrel{\text{def}}{=} d-n$ normal vectors (or normals) n_μ^a , which are defined by:

$$t_A^a \stackrel{\text{def}}{=} \left(\frac{\partial}{\partial \sigma^A} \right)^a, \quad n_\mu^a \stackrel{\text{def}}{=} \left(\frac{\partial}{\partial \xi^\mu} \right)^a. \quad (2.1)$$

Moreover, let $X^a(\sigma^A)$ be the coordinates of \mathcal{S} in \mathcal{M} . Then, for each A , the object

$$X^a{}_{,A} \stackrel{\text{notn}}{=} \frac{\partial X^a(\sigma^A)}{\partial \sigma^A}$$

is a vector in \mathcal{M} which is tangent to \mathcal{S} , and can therefore serve to project indices onto it.

As they were defined in (2.1), the n_μ^a exist only on \mathcal{S} itself, i.e. at $\xi^\mu = 0$; we can extend them regularly off the submanifold to form a family of normals on the whole spacetime \mathcal{M} by requiring that, for any μ and ν ,

$$n_\mu^a \nabla_a n_{\nu b} \equiv 0. \quad (2.2)$$

There are still many ways of choosing the families of normals, but we can always choose them in such a way that they are orthonormal in \mathcal{M} , that is:

$$g^{ab} n_{\mu a} n_{\nu b} \equiv -\delta_{\mu\nu}. \quad (2.3)$$

The embedding of \mathcal{S} in \mathcal{M} is naturally described by “fundamental forms” constructed from the normals. The *first fundamental form* of \mathcal{S} in \mathcal{M} is defined as

$$h_{ab} \stackrel{\text{def}}{=} g_{ab} + \sum_{\mu=0}^{d-n-1} n_{\mu a} n_{\mu b} \quad (2.4)$$

and it is the projection tensor of \mathcal{S} , as can be seen by noting that

$$\begin{aligned} h_{ab} h^b{}_c &= h_{ac}, \\ h_{ab} n_\mu^b &= 0. \end{aligned} \quad (2.5)$$

(Note that the first fundamental form lives in \mathcal{M} , not in \mathcal{S} : it is represented by a matrix of size $d \times d$, with at most n^2 non-vanishing elements.)

We can also define the intrinsic metric γ_{AB} , which lives on \mathcal{S} , by projecting the metric g_{ab} with $X^a{}_{,A}$:

$$\gamma_{AB} \stackrel{\text{def}}{=} X^a{}_{,A} X^b{}_{,B} g_{ab} = \frac{\partial X^a}{\partial \sigma^A} \frac{\partial X_a}{\partial \sigma^B}. \quad (2.6)$$

The first fundamental form and the intrinsic metric are equivalent in the sense that

$$\begin{aligned}\gamma_{AB} &= X^a{}_{,A} X^b{}_{,B} h_{ab}, \\ h^{ab} &= X^a{}_{,A} X^b{}_{,B} \gamma^{AB}.\end{aligned}\tag{2.7}$$

γ_{AB} has determinant γ and can be used in \mathcal{S} to determine the Levi-Civita connection $\parallel\nabla$, the Riemann curvature tensor $\parallel R^A{}_{BCD}$, the Ricci tensor $\parallel R_{AB}$ and the scalar curvature $\parallel R$. This corresponds to seeing \mathcal{S} as a manifold in its own right.

The first fundamental form does not contain enough information to represent the full differential structure of \mathcal{S} : we must define at least the *second fundamental form*

$$K_{\mu ab} \stackrel{\text{def}}{=} h^c{}_{(a} h^d{}_{b)} \nabla_c n_{\mu d}.\tag{2.8}$$

For each μ , $K_{\mu ab}$ is also called an extrinsic curvature of \mathcal{S} , because it represents how the submanifold curves in \mathcal{M} away from the hyperplane normal to $n_{\mu}{}^a$. They are clearly symmetric in a and b , and they lie tangential to \mathcal{S} , i.e. $n^a K_{\mu ab} = 0$ for all μ .

If the codimension n' of \mathcal{S} (i.e. the dimension of ${}^\perp\mathcal{S}$) is greater than 1, the choice of normals is not unique. For instance, at each (t, z) , a cosmic string admits two normals $n_1{}^a$ and $n_2{}^a$ (see figure 2.1), but even if we impose orthonormality, we can still rotate rigidly the pair $(n_1{}^a, n_2{}^a)$ around the string to obtain a second pair of normals $(n'_1{}^a, n'_2{}^a)$. This is similar to a gauge choice, with gauge group $\text{SO}(2)$. (Note that the first and second fundamental forms are gauge-independent, in that sense.)

Therefore, if $n' > 1$, we also define the *normal fundamental form* of \mathcal{S} by

$$\beta^\mu{}_{\nu a} \stackrel{\text{def}}{=} n_\mu{}^b \nabla_a n_{\nu b} = -\beta^\nu{}_{\mu a}.\tag{2.9}$$

The $\beta^\mu{}_{\nu a}$ are gauge-dependent; in fact, they are the connection on the normal bundle of \mathcal{S} , and the difference between two normal fundamental forms (corresponding to two choices of normals) is a proper gauge-independent quantity.

It is useful to express the derivatives of the normals in terms of the fundamental tensors:

$$\nabla_a n_{\mu b} = K_{\mu ab} + \sum_{\nu=0}^{d-n-1} \beta^\nu{}_{\mu a} n_{\nu b};\tag{2.10}$$

in particular, for $d = n + 1$ (the case of a domain wall), we have the useful relation:

$$K_{ab} = \nabla_a n_b\tag{2.11}$$

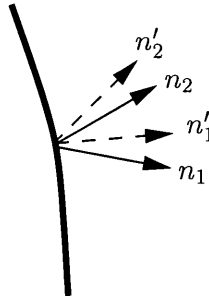


Figure 2.1: Origin of the normal fundamental form. If a submanifold has codimension $n' > 1$, the choice of normals will not be unique. The figure shows two different pairs of (orthonormal) normals on a cosmic string.

(where we dropped the index μ , since there is now only one direction perpendicular to the submanifold, and where it might be necessary to symmetrize the right-hand side over a and b).

The *Gauß identity* provides a link between the d -dimensional geometry of the spacetime and the n -dimensional geometry of the submanifold. In our notation, it is written:

$$\|R^a{}_{bcd} = R^p{}_{qrs} h^a{}_p h^q{}_b h^r{}_c h^s{}_d + \sum_{\mu=0}^{d-n-1} (K^a{}_{\mu c} K_{\mu b d} - K^a{}_{\mu d} K_{\mu b c}). \quad (2.12)$$

Contracting it once, then twice, we obtain:

$$\|R_{ab} = R^p{}_{qrs} h^r{}_p h^q{}_a h^s{}_b + \sum_{\mu=0}^{d-n-1} (K_{\mu} K_{\mu ab} - K_{\mu ac} K_{\mu b}{}^c), \quad (2.13)$$

$$\|R = R + \sum_{\mu=0}^{d-n-1} (K_{\mu}^2 - K_{\mu ab} K_{\mu}{}^{ab} - 2 R_{ab} n_{\mu}{}^a n_{\mu}{}^b). \quad (2.14)$$

In particular, the last equation in flat spacetime ($R_{ab} = 0$) simplifies to

$$\|R = \sum_{\mu=0}^{d-n-1} (K_{\mu}^2 - K_{\mu ab} K_{\mu}{}^{ab}). \quad (2.15)$$

Finally, let us introduce the *Lie derivative* of a tensor field \mathfrak{T} (with components $T_{ab\dots}{}^{cd\dots}$) along the vector field n^a at a point p as

$$\mathcal{L}_n \mathfrak{T}|_p \stackrel{\text{def}}{=} - \lim_{t \rightarrow 0} \frac{\phi_{t*} \mathfrak{T}|_p - \mathfrak{T}|_p}{t}, \quad (2.16)$$

where ϕ_{t*} is the pullback map from the point p^a to a point $p^a + t n^a$. In a curved spacetime, the Lie derivative is the closest object to our usual notion of derivative

that can be defined, since it describes the variation of \mathfrak{T} along the integral curves of n^a .

In terms of the components of \mathfrak{T} , the definition (2.16) implies:

$$\begin{aligned} \mathcal{L}_n T_{ab\dots}{}^{cd\dots} &= n^e \nabla_e T_{ab\dots}{}^{cd\dots} + T_{eb\dots}{}^{cd\dots} \nabla_a n^e + \text{all other lower indices} \\ &\quad - T_{ab\dots}{}^{ed\dots} \nabla_e n^c - \text{all other upper indices} \end{aligned} \quad (2.17a)$$

$$\begin{aligned} &= n^e \partial_e T_{ab\dots}{}^{cd\dots} + T_{eb\dots}{}^{cd\dots} \partial_a n^e + \text{all other lower indices} \\ &\quad - T_{ab\dots}{}^{ed\dots} \partial_e n^c - \text{all other upper indices.} \end{aligned} \quad (2.17b)$$

Effective Motion of a Cosmic String

3.1 Introduction and Chronology

String dynamics is an important topic in the study of cosmic strings. Traditionally, Nielsen–Olesen strings have been either considered in their full field generality (for instance in numerical simulations of their interactions) or in the crude Nambu–Gotō approximation (notably in analytical studies of their dynamics or to determine the properties of cosmic string networks). This approximation consists in replacing the string by an infinitesimally thin vortex-line. Although both approaches have their merits, they also have their limits: the full field action is too complicated to be studied analytically except in the most symmetrical cases, and the Nambu–Gotō action breaks down near cusps and kinks (which just happen to be points of particular interest on the string).

The starting point of the study of string dynamics is of course the action (1.1) with the appropriate Lagrangian density. In this chapter we consider the abelian–Higgs model (1.16),

$$\mathcal{L} = (D_a \Phi) (D^a \Phi)^\dagger - \frac{1}{4} \tilde{F}_{ab} \tilde{F}^{ab} - V(\Phi), \quad (3.1a)$$

$$V(\Phi) = \frac{\lambda}{4} (\Phi^\dagger \Phi - \eta^2)^2. \quad (3.1b)$$

The Nambu–Gotō action

$$S_{\text{NG}} = \int d^2 \sigma \sqrt{-\gamma} \quad (3.2)$$

[where, according to the notation of chapter 2, γ is the determinant of the intrinsic metric (2.6) of the worldsheet coordinatized by σ^A] has been known to approximate

the dynamics of Nielsen–Olesen strings for a quarter of a century [76,42], and has provided a convenient and comparatively easy way to study and simulate the dynamics of these objects. In his original paper [42], Förster not only showed that Nambu–Gotō strings effectively approximated Nielsen–Olesen’s solution, he also described the method to find corrections to this approximation (but he did not do it himself).

In the case of cosmic strings (as opposed to that of dual strings, the context in which Nielsen & Olesen and Förster considered this solution), it may be vital to consider these corrections — even in more general cases than the loop discussed in section 1.1. The reason is that cosmic strings have a finite width, and that in this case the Nambu–Gotō action only approximates accurately the full action when the string’s radii of curvature are large (in a sense that will be made more precise later in this chapter). This condition is badly violated at cusps and kinks on the string; sadly, these points (collectively referred to as “small-scale structure”) have a particular importance for the cosmological implications of strings: it seems that quite generically string loops will radiate most of their energy through their small-scale structure (see for instance [37,44,23]). The rate of energy emission by the loop — which determines its longevity, and therefore its repercussions in cosmology — clearly depends on the quantity of cusps and kinks on it.

Using the Nambu–Gotō action and equations of motion, numerical simulations have shown a certain behaviour for the strings in a network. In particular, they have yielded the rate of energy loss by cosmic loops, via an estimation of the number of cusps and kinks on the worldsheets of the strings. Clearly, it would be of great interest to determine whether strings obeying the full field dynamics produce more or less small-scale structure than their Nambu–Gotō counterparts, and therefore decay faster or slower, respectively. An effort over the last ten years or so (see [71,51], [43,53,52], [29,3]; [6,5]) has yielded an action generalizing the Nambu–Gotō approximation. In this chapter, we rederive this action and, by considering the equations of motion associated with it, we are able to determine whether the worldsheet becomes more or less crinkly. As a matter of terminology, a worldsheet is called *rigid* if it is less crinkly (*i.e.* it has less small-scale structure) when it obeys the full action equations of motion than when it obeys the Nambu–Gotō equations

of motion. Otherwise, it is called *antirigid*.

Following Förster [42], we are going to consider the full action for this model,

$$S = \int d^4x \sqrt{-g} \mathcal{L} \quad (3.3)$$

and, by integrating it over the directions perpendicular to the string's worldsheet, obtain a new action of the form

$$S_{\text{eff}} = \int d^2\sigma \sqrt{-\gamma} \mathcal{L}_{\text{eff}} \quad (3.4)$$

(provided some assumptions hold). In the simplest approximation, this yields the Nambu–Goto action; our goal is to go beyond this “zeroth-order approximation.”

As we have seen in the previous chapter, it is possible to express the abelian–Higgs Lagrangian and equations of motion in terms of real fields X and P_a as

$$\mathcal{L} = (\nabla X)^2 + X^2 P_a^2 - \frac{\beta}{2w_{\text{H}}^2} F_{ab}^2 - \frac{1}{4w_{\text{H}}^2} (X^2 - 1)^2 \quad (3.5)$$

and

$$\square X - X P^2 + \frac{1}{2w_{\text{H}}^2} X (X^2 - 1) = 0, \quad (3.6a)$$

$$\nabla_a F^{ab} + \frac{w_{\text{H}}^2}{\beta} X P^b = 0. \quad (3.6b)$$

(Remember that β is the Bogomol’nyi parameter, and note that we have not yet chosen coordinates such as the string’s width w_{H} is of order unity.)

Apart from the above equations of motion, the formalism described in chapter 2 provides us with “geometrical equations of motion” obtained by taking the Lie derivatives of the metric and the three fundamental forms along the normals. These are

$$\mathcal{L}_\mu g_{ab} = 2 \left(K_{\mu ab} - \sum_{\nu=1,2} \varepsilon_{\mu\nu} \beta_{(a} n_{| \nu | b)} \right), \quad (3.7a)$$

$$\mathcal{L}_\mu h_{ab} = 2K_{\mu ab}, \quad (3.7b)$$

$$\mathcal{L}_\mu K_{\nu ab} = K_{\mu(a}{}^c K_{| \nu | b)c}, \quad (3.7c)$$

$$\mathcal{L}_\mu \beta_a = 0. \quad (3.7d)$$

Note that we assume here that \mathcal{M} , the “background” manifold, is flat: g_{ab} would be the Minkowski metric if we were working in Cartesian coordinates. The need for equation (3.7a) comes from our choice of working with a coordinate system based on the worldsheet \mathcal{W} , which is forced by the form (3.4).

3.2 The Expansion of the Equations of Motion

Following the method presented in chapter 2, we coordinatize the worldsheet \mathcal{W} by two coordinates $\sigma^A (A = 0, 1)$ (which can be imagined to be the “time” t and a ‘ z ’ coordinate along the string). Perpendicularly to \mathcal{W} , we define coordinates ξ^μ by $n_\mu^a = \left(\frac{\partial}{\partial \xi^\mu}\right)^a$ for $\mu = 0, 1$. Then the four vectors $\{\sigma^A, \xi^\mu\}$ form a basis for \mathcal{M} . This choice of “Gaussian” coordinates is motivated by the form of the Nambu–Goto action which we wish to obtain and generalize; however, it has the disadvantage of being only valid within the radii of curvature of \mathcal{W} .

A first remark we could make is that equation (3.7d) integrates immediately to yield

$$\beta_a(\sigma^A, \xi^\mu) = \beta_a(\sigma^A, 0) = \beta_a|_{\mathcal{W}} \stackrel{\text{notn}}{=} \underline{\beta}_a. \quad (3.8)$$

(In this chapter, and in chapter 5, we underline quantities evaluated on \mathcal{W} .)

It is not possible to solve the equations of motion (3.6, 3.7) without any further approximations or Ansätze. We shall therefore restrict ourselves to strings very close to the Nielsen–Olesen vortex, and expand the equations of motion in some (small) parameter ς so that the Nielsen–Olesen solution corresponds to $\varsigma = 0$. The NO solution was found in the case of a static straight string (*i.e.*, a flat worldsheet), but since it also corresponds to a Nambu–Goto string, which is curved but has zero thickness, we expect that the parameter ς is a combination of the string’s width w_H and some typical value \underline{K} for the elements of the string’s extrinsic curvature \underline{K}^a_b at $\xi^\mu = 0$. Namely, we define

$$\varsigma \stackrel{\text{def}}{=} |\underline{K}| w_H. \quad (3.9)$$

Now we must scale all length parameters out of the equations of motion, so that these can be meaningfully expressed as a series in the parameter ς , whose zeroth-order corresponds to the Nambu–Goto equations of motion. To do this, rescale the following coordinates and fields:

$$\xi^\mu \rightarrow x^\mu \stackrel{\text{def}}{=} \xi^\mu / w_H, \quad (3.10a)$$

$$\sigma^A \rightarrow s^A \stackrel{\text{def}}{=} \sigma^A / R, \quad (3.10b)$$

$$K_{\mu ab} \rightarrow \kappa_{\mu ab} \stackrel{\text{def}}{=} R K_{\mu ab}, \quad (3.10c)$$

$$\beta_a \rightarrow R \beta_a, \quad (3.10d)$$

$$P_a \rightarrow w_H P_a, \quad (3.10e)$$

$$\|R_{ab} \rightarrow \|r_{ab} \stackrel{\text{def}}{=} R^2 \|R_{ab}. \quad (3.10f)$$

($R \stackrel{\text{def}}{=} 1/\underline{K}$ is the typical value for the string's radii of curvature.) Then, $\mathcal{L}_\mu \rightarrow w_H \mathcal{L}_\mu$, and the remaining equations (3.7) become,

$$\mathcal{L}_\mu g_{ab} = 2\varsigma \left(\kappa_{\mu ab} - \sum_\nu \varepsilon_{\mu\nu} \beta_{(a} n_{|\nu|b)} \right), \quad (3.11a)$$

$$\mathcal{L}_\mu h_{ab} = 2\varsigma \kappa_{\mu ab}, \quad (3.11b)$$

$$\mathcal{L}_\mu \kappa_{\nu ab} = \varsigma \kappa_{\mu(a}{}^c \kappa_{|\nu|b)c}. \quad (3.11c)$$

We now must apply this rescaling to the equations for X and P_a . The difference in the rescaling for σ^A and ξ^μ will pose a small notational difficulty. Indeed, we have that $\partial^\mu \rightarrow w_H \partial^\mu$ and $D^A \stackrel{\text{def}}{=} \partial^A \rightarrow R D^A$. Therefore,

$$\square X = \frac{1}{R^2} D_A D^A X + \frac{1}{w_H^2} \partial_\mu \partial^\mu X + \frac{\varsigma}{w_H^2} \kappa_\mu \partial^\mu X, \quad (3.12)$$

where $\kappa_\mu \stackrel{\text{def}}{=} \kappa_\mu{}^a{}_a$. Then, equation (3.6a) becomes

$$\partial_\mu \partial^\mu X + \varsigma \kappa_\mu \partial^\mu X + \varsigma^2 D_A D^A X - X P^2 + \frac{1}{2} X (X^2 - 1) = 0. \quad (3.13)$$

Now, turn to F_{ab} . Multiplying equation (3.6b) by w_H yields

$$\begin{aligned} \partial_\mu \partial^\mu P^B + \varsigma (-\partial_\mu D^B P^\mu + \kappa_\mu \partial^\mu P^B) + \varsigma^2 (D_A F^{AB} - \kappa_\mu D^B P^\mu) + \frac{1}{\beta} X^2 P^B &= 0 \\ \partial_\mu F^{\mu\nu} + \varsigma (-D_A \partial^\nu P^A + \kappa_\mu F^{\mu\nu}) + \varsigma^2 D_A D^A P^\nu + \frac{1}{\beta} X^2 P^\nu &= 0 \end{aligned} \quad (3.14)$$

(for $b = B$ and $b = \nu$ respectively).

To summarize, the equations to solve are

$$\mathcal{L}_\mu g_{ab} = 2\varsigma \left(\kappa_{\mu ab} - \sum_\nu \varepsilon_{\mu\nu} \beta_{(a} n_{|\nu|b)} \right), \quad (3.15a)$$

$$\mathcal{L}_\mu h_{ab} = 2\varsigma \kappa_{\mu ab}, \quad (3.15b)$$

$$\mathcal{L}_\mu \kappa_{\nu ab} = \varsigma \kappa_{\mu(a}{}^c \kappa_{|\nu|b)c}, \quad (3.15c)$$

$$0 = \partial_\mu \partial^\mu X + \varsigma \kappa_\mu \partial^\mu X + \varsigma^2 D_A D^A X - X P^2 + \frac{1}{2} X (X^2 - 1), \quad (3.15d)$$

$$\begin{aligned} 0 = \partial_\mu \partial^\mu P^B + \varsigma (-\partial_\mu D^B P^\mu + \kappa_\mu \partial^\mu P^B) + \varsigma^2 (D_A F^{AB} - \kappa_\mu D^B P^\mu) \\ + \frac{1}{\beta} X^2 P^B, \end{aligned} \quad (3.15e)$$

$$0 = \partial_\mu F^{\mu\nu} + \varsigma (-D_A \partial^\nu P^A + \kappa_\mu F^{\mu\nu}) + \varsigma^2 D_A D^A P^\nu + \frac{1}{\beta} X^2 P^\nu. \quad (3.15f)$$

Next, we must expand the fields in powers of the dimensionless parameter ς ,

$$\begin{aligned}
g_{ab} &= g_{ab}^{(0)} + \varsigma g_{ab}^{(1)} + \frac{1}{2}\varsigma^2 g_{ab}^{(2)} + \mathcal{O}(\varsigma^3), \\
h_{ab} &= h_{ab}^{(0)} + \varsigma h_{ab}^{(1)} + \frac{1}{2}\varsigma^2 h_{ab}^{(2)} + \mathcal{O}(\varsigma^3), \\
\kappa_{\mu ab} &= \kappa_{\mu ab}^{(0)} + \varsigma \kappa_{\mu ab}^{(1)} + \frac{1}{2}\varsigma^2 \kappa_{\mu ab}^{(2)} + \mathcal{O}(\varsigma^3), \\
P_a &= P_a^{(0)} + \varsigma P_a^{(1)} + \frac{1}{2}\varsigma^2 P_a^{(2)} + \mathcal{O}(\varsigma^3), \\
X &= X^{(0)} + \varsigma X^{(1)} + \frac{1}{2}\varsigma^2 X^{(2)} + \mathcal{O}(\varsigma^3).
\end{aligned} \tag{3.16}$$

Before we consider the equations order by order, we should note a few facts. First, that we have expanded P_a , and therefore we must replace $P^a = g^{ab}P_b$ everywhere, where g^{ab} is found at each order by expanding the relation $g^{ac}g_{bc} = \delta^a_b$. Second, since σ^A and ξ^μ are of same order, we have that $\partial_\mu \sim \varsigma D_A$.

Moreover, it is possible to know the background metric to all orders exactly. The expansion of any quantity Q off the worldsheet takes the form,

$$Q = Q|_{\mathcal{W}} + x^\mu (\mathcal{L}_\mu Q)|_{\mathcal{W}} + \frac{1}{2}x^\mu x^\nu (\mathcal{L}_\mu \mathcal{L}_\nu Q)|_{\mathcal{W}} + \dots,$$

and in the case where Q is g_{ab} , the series has a finite number of terms, because

$$\begin{aligned}
\mathcal{L}_\mu \mathcal{L}_\nu \kappa_{\rho ab} &= 0, \\
\mathcal{L}_\mu \mathcal{L}_\nu \mathcal{L}_\rho \sqrt{-g} &= 0.
\end{aligned} \tag{3.17}$$

In fact, one finds that,

$$g_{ab} = \begin{pmatrix} \gamma_{AB} + 2\varsigma x^\mu \underline{\kappa}_{\mu AB} + \varsigma^2 x^\mu x^\nu \underline{\kappa}_{\mu AC} \underline{\kappa}_{\nu B}{}^C & \varsigma x^\rho \varepsilon_{\rho\nu} \underline{\beta}_{-A} \\ \varsigma x^\rho \varepsilon_{\mu\rho} \underline{\beta}_{-B} & -\delta_{\mu\nu} \end{pmatrix}, \tag{3.18}$$

$$\frac{1}{2}\sqrt{-g} = \sqrt{-\gamma} \left[1 + \varsigma x^\mu \underline{\kappa}_\mu + \frac{1}{2}\varsigma^2 x^\mu x^\nu (\underline{\kappa}_\mu \underline{\kappa}_\nu - \underline{\kappa}_{\mu AB} \underline{\kappa}_\nu{}^{AB}) \right]. \tag{3.19}$$

In particular, note that $g_{\mu\nu} = g_{\mu\nu}^{(0)}$; this will simplify the equations of motion later on.

3.2.1 The Zeroth Order and the Nambu Action

Inserting the expansion for the fields into the equations of motion and setting $\varsigma = 0$ leads to

$$\mathcal{L}_\mu g_{ab}^{(0)} = \mathcal{L}_\mu h_{ab}^{(0)} = \mathcal{L}_\mu \kappa_{\mu ab}^{(0)} = 0, \tag{3.20a}$$

$$\partial_\mu (g^{(0)\mu a} \partial_a X^{(0)}) - X^{(0)} g^{(0)ab} P_a^{(0)} P_b^{(0)} + \frac{1}{2} X^{(0)} (X^{(0)2} - 1) = 0, \quad (3.20b)$$

$$\partial_\mu (g^{(0)\mu a} g^{(0)bB} P_b^{(0)}) + \frac{1}{\beta} X^{(0)2} g^{(0)bB} P_b^{(0)} = 0, \quad (3.20c)$$

$$\partial_\mu (g^{(0)\mu a} g^{(0)\nu b} F_{\mu\nu}^{(0)}) + \frac{1}{\beta} X^{(0)2} g^{(0)\nu b} P_b^{(0)} = 0. \quad (3.20d)$$

The three geometrical equations integrate immediately:

$$\begin{aligned} g_{ab}^{(0)} &= \begin{pmatrix} \gamma_{AB} & 0 \\ 0 & -\delta_{\mu\nu} \end{pmatrix}, \\ h_{ab}^{(0)} &= \underline{h}_{ab}, \\ \kappa_{\mu ab}^{(0)} &= \underline{\kappa}_{\mu ab}. \end{aligned} \quad (3.21)$$

[Note that $g_{\mu\nu}$ is written in Cartesian coordinates (which for $\varsigma = 0$ are equivalent to our Gaussian coordinates); it would be more useful in cylindrical coordinates, in which case we replace $-\delta_{\mu\nu}$ by $-\text{Diag}(1, \varrho^2)$.]

We now must insert $g^{(0)ab}$ into the equations for $X^{(0)}$ and $P_a^{(0)}$. Remembering that X depends only on ϱ , and making the usual Nielsen–Olesen Ansatz¹ $X^{(0)} = X(\varrho)$, $P_a^{(0)} = P(\varrho) \nabla_a \vartheta$, we find that X and P must satisfy,

$$\begin{aligned} X'' + \frac{X'}{\varrho} - \frac{P^2}{\varrho^2} X - \frac{1}{2} X (X^2 - 1) &= 0, \\ P'' - \frac{P'}{\varrho} - \frac{X^2 P}{\beta} &= 0, \end{aligned} \quad (3.22)$$

where a prime denotes differentiation with respect to ϱ . Equations (3.22) are of course the Nielsen–Olesen equations, and we can solve them numerically. The solutions for X and P are plotted in figure 3.1. Insertion of the Nielsen–Olesen functions to approximate the full X, P_a into the action (3.3, 3.5) leads to the Nambu–Goto action.

3.2.2 The First Order

Inserting the expansion of the fields into (3.15) and retaining only the terms proportional to ς , we find

$$\mathcal{L}_\mu g_{ab}^{(1)} - 2 (\underline{\kappa}_{\mu ab} - \varepsilon_{\mu\nu} \underline{\beta}_{(a} n_{\nu b)}) = 0, \quad (3.23a)$$

$$\mathcal{L}_\mu h_{ab}^{(1)} - 2 \underline{\kappa}_{\mu ab} = 0, \quad (3.23b)$$

¹We consider $N = 1$ for simplicity.

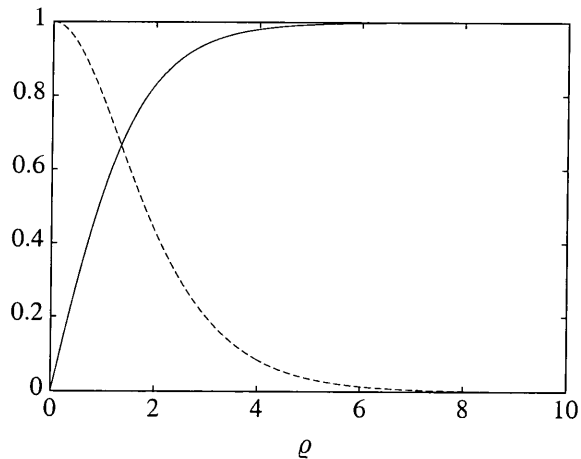


Figure 3.1: The Higgs field X (solid) and the polar gauge field P_ϑ of the Nielsen–Olesen solution.

$$\mathcal{L}_\mu \kappa_{\nu ab}^{(1)} - \underline{\kappa}_{\mu(a}{}^c \underline{\kappa}_{|\nu|b)c} = 0, \quad (3.23c)$$

$$\begin{aligned} -\partial_\mu \partial_\mu X^{(1)} - \underline{\kappa}_\mu \partial_\mu X^{(0)} + P_\mu^{(0)} P_\mu^{(0)} X^{(1)} + 2P_\mu^{(0)} P_\mu^{(1)} X^{(0)} \\ + \frac{1}{2} X^{(1)} (X^{(0)2} - 1) = 0, \end{aligned} \quad (3.23d)$$

$$\begin{aligned} \partial_\mu \left(\underline{\beta}_A x^\nu \varepsilon_{\nu\rho} F_{\mu\rho}^{(0)} \right) - \partial_\mu \partial_\mu P_A^{(1)} + \frac{1}{\beta} X^{(0)2} P_A^{(1)} \\ + \frac{1}{\beta} X^{(0)2} \underline{\beta}_A x^\mu \varepsilon_{\mu\nu} P_\nu^{(0)} = 0, \end{aligned} \quad (3.23e)$$

$$-\partial_\mu F_{\mu\nu}^{(1)} - \underline{\kappa}_\mu F_{\mu\nu}^{(0)} + \frac{1}{\beta} X^{(0)2} P_\nu^{(1)} + 2\frac{1}{\beta} X^{(0)} X^{(1)} P_\nu^{(0)} = 0. \quad (3.23f)$$

As for the zeroth order, the geometrical equations (3.23a–3.23c) integrate easily to give

$$\begin{aligned} g_{ab}^{(1)} &= \underline{g}_{ab}^{(1)} + 2(x^\mu \underline{\kappa}_{\mu ab} - x^\mu \underline{\beta}_{(a} n_{\nu b)}), \\ h_{ab}^{(1)} &= \underline{h}_{ab}^{(1)} + 2x^\mu \underline{\kappa}_{\mu ab}, \\ \kappa_{\mu ab}^{(1)} &= \underline{\kappa}_{ab}^{(1)} + x^\nu \underline{\kappa}_{\mu(a}{}^c \underline{\kappa}_{\mu b)c}. \end{aligned}$$

Equation (3.23e) is solved [3] by the Ansatz

$$P_A^{(1)} = -\omega_A x^\nu \varepsilon_{\nu\sigma} P_\sigma^{(0)}, \quad (3.24)$$

where $\omega_a \stackrel{\text{def}}{=} \frac{1}{2} \varepsilon^\nu{}_\mu \beta^\mu{}_\nu a$ is called the twist vector. Therefore, we are left with three equations (3.23d, 3.23f) for $X^{(1)}$, $P_\varrho^{(1)}$ and $P_\vartheta^{(1)}$. To simplify them, notably by eliminating the the extrinsic curvature terms, we decompose them in cylindrical harmon-

ics,

$$\begin{aligned}
 X^{(1)} &= \kappa_\mu \frac{x^\mu}{\varrho} \Xi(\varrho), \\
 P_\vartheta^{(1)} &= \kappa_\mu \frac{x^\mu}{\varrho} \Lambda(\varrho), \\
 P_\varrho^{(1)} &= \kappa_\mu \frac{x^\mu}{\varrho} \Psi(\varrho).
 \end{aligned} \tag{3.25}$$

With this Ansatz the remaining equations become

$$-\Xi'' - \frac{\Xi'}{\varrho} + \frac{\Xi}{\varrho} \left[1 + P_{\text{NO}}^2 + \frac{\varrho^2}{2} (3X_{\text{NO}}^2 - 1) \right] + 2 \frac{X_{\text{NO}} P_{\text{NO}}}{\varrho^2} \Lambda = X'_{\text{NO}}, \tag{3.26a}$$

$$-\Lambda'' + \frac{\Lambda'}{\varrho} + \Psi' - \frac{\Psi}{\varrho} + \frac{X_{\text{NO}}^2 \Lambda}{\beta} + 2 \frac{X_{\text{NO}} P_{\text{NO}} \Sigma}{\beta} = P'_{\text{NO}}, \tag{3.26b}$$

$$-\Lambda' + \Psi + \frac{\varrho^2 X_{\text{NO}}^2 \Psi}{\beta} = \varrho P'_{\text{NO}}. \tag{3.26c}$$

Equations (3.26) can be seen not to admit solutions for Ξ , Λ and Ψ which are smooth and bounded throughout the ϱ -axis (see also discussion in [29]). Therefore, we must consider only the trivial solution,

$$\Xi = \Lambda = \Psi = 0. \tag{3.27}$$

3.2.3 The Second Order

Considering the terms at order ζ^2 in (3.15), we obtain the following equations:

$$\mathcal{L}_\mu g_{ab} - 4\kappa_{\mu ab}^{(1)} = 0, \tag{3.28a}$$

$$\mathcal{L}_\mu h_{ab}^{(2)} - 4\kappa_{\mu ab}^{(1)} = 0, \tag{3.28b}$$

$$\mathcal{L}_\mu \kappa_{\nu ab} - 2 \left(\kappa_{\mu(a}{}^c \kappa_{|\nu|b)c}^{(1)} + \kappa_{\mu(a}{}^{(1)c} \kappa_{|\nu|b)c} \right) = 0, \tag{3.28c}$$

$$\begin{aligned}
 & -\partial_\mu \partial_\mu X^{(2)} + x^\nu \kappa_{\mu AB} \kappa_\nu{}^{AB} \partial^\mu X^{(0)} + P_\mu^{(0)} P_\mu^{(0)} X^{(2)} \\
 & + 2P_\mu^{(0)} P_m u^{(2)} X^{(0)} + \frac{1}{2} X^{(2)} (3X^{(0)2} - 1) = 0,
 \end{aligned} \tag{3.28d}$$

$$-\partial \left(\underline{\omega}_A x^\nu \varepsilon_{\nu\rho} F_{\mu\rho}^{(0)} \right) - \partial_\mu \partial_\mu P_A^{(2)} = 0 \tag{3.28e}$$

$$-\partial_\mu F_{\mu\nu}^{(2)} + x^\rho \kappa_{\mu AB} \kappa_\rho{}^{AB} F_{\mu\nu}^{(0)} + \frac{1}{\beta} X^{(0)} P_\nu^{(2)} + \frac{2}{\beta} X^{(0)} X^{(2)} P_\nu^{(0)} = 0. \tag{3.28f}$$

Again, the geometric equations integrate easily, and (as for the first order) we expand the fields in cylindrical harmonics to get rid of the curvature terms:

$$\begin{aligned}
 X^{(2)} &= \frac{1}{2} \underline{\kappa}_{\mu AB}^2 \xi(\varrho) + x^{\mu\nu} \underline{\kappa}_{\mu AB} \underline{\kappa}_{\nu}{}^{AB} \bar{\xi}(\varrho), \\
 P_{\vartheta}^{(2)} &= \frac{1}{2} \underline{\kappa}_{\mu AB}^2 \lambda(\varrho) + x^{\mu\nu} \underline{\kappa}_{\mu AB} \underline{\kappa}_{\nu}{}^{AB} \bar{\lambda}(\varrho), \\
 P_{\varrho}^{(2)} &= \varepsilon_{\rho\mu} x^{\mu\nu} \underline{\kappa}_{\rho AB} \underline{\kappa}_{\nu}{}^{AB} \bar{\psi}(\varrho)
 \end{aligned} \tag{3.29}$$

(where $x^{\mu\nu} \stackrel{\text{def}}{=} \frac{x^\mu x^\nu}{\varrho^2} - \frac{1}{2} \delta^{\mu\nu}$).

This leaves us five equations for the five fields $\xi, \bar{\xi}, \lambda, \bar{\lambda}$ and $\bar{\psi}$, which split into two sets of coupled equations, for unbarred and barred variables:

$$-\xi'' - \frac{\xi'}{\varrho} + \frac{\xi}{\varrho^2} \left[P_{\text{NO}}^2 + \frac{\varrho^2}{2} (3X_{\text{NO}}^2 - 1) \right] + 2 \frac{X_{\text{NO}} P_{\text{NO}}}{\varrho^2} \lambda + \varrho X'_{\text{NO}} = 0, \tag{3.30a}$$

$$-\lambda'' + \frac{\lambda'}{\varrho} + \frac{X_{\text{NO}}^2 \lambda}{\beta} + 2 \frac{X_{\text{NO}} P_{\text{NO}} \xi}{\beta} + \varrho P'_{\text{NO}} = 0 \tag{3.30b}$$

and

$$-\bar{\xi}'' - \frac{\bar{\xi}'}{\varrho} + \frac{\bar{\xi}}{\varrho^2} \left[4 + P_{\text{NO}}^2 + \frac{\varrho^2}{2} (3X_{\text{NO}}^2 - 1) \right] + 2 \frac{X_{\text{NO}} P_{\text{NO}}}{\varrho^2} \bar{\lambda} + \varrho X'_{\text{NO}} = 0 \tag{3.31a}$$

$$-\bar{\lambda}'' + \frac{\bar{\lambda}'}{\varrho} + 2\bar{\psi}' - 2\frac{\bar{\psi}}{\varrho} + \frac{X_{\text{NO}}^2 \bar{\lambda}}{\beta} + 2 \frac{X_{\text{NO}} P_{\text{NO}} \bar{\xi}}{\beta} + \varrho P'_{\text{NO}} = 0 \tag{3.31b}$$

$$4\bar{\psi} - 2\bar{\lambda}' + \frac{\varrho^2 X_{\text{NO}}^2 \bar{\psi}}{\beta} + \varrho^2 P'_{\text{NO}} = 0 \tag{3.31c}$$

These equations admit regular solutions and can therefore be easily solved numerically; the result of these integrations is presented on figure 3.2. It satisfies the following asymptotic behaviours at the origin:

$$\begin{aligned}
 \xi, \bar{\xi}, \bar{\psi} &\sim \varrho, \\
 \lambda &\sim \varrho^2, \\
 \bar{\lambda} &\sim \text{const.}
 \end{aligned} \tag{3.32}$$

3.3 The Effective Action and Equations of Motion

3.3.1 The Effective Action

If we insert the solutions $g_{ab}^{(n)}, \sqrt{g}^{(n)}, h_{ab}^{(n)}, \kappa_{\mu ab}^{(n)}, X^{(n)}$ and $P_{\mu}^{(n)}$ found in the previous sections into the action (3.3, 3.5), we can carry out the resulting integral on directions perpendicular to \mathcal{W} , and obtain an effective action for the abelian–Higgs model based

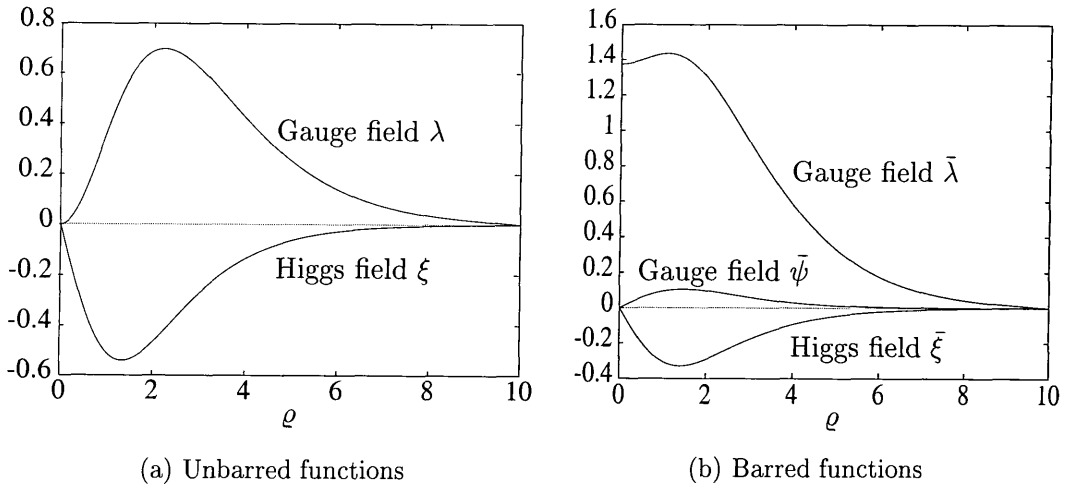


Figure 3.2: The unbarred and barred functions for the second order solution, for the critical case $\beta = 1$.

on the Nielsen–Olesen solution. This is Anderson’s action [3]

$$S = -\mu \int d^2\sigma \sqrt{-\lambda} \left\{ 1 - \zeta^2 \frac{\alpha_1}{\mu} \kappa_{\mu AB}^2 + \zeta^4 \frac{1}{\mu} \left[\left(\alpha_2 + \frac{1}{2} \alpha_3 \right) (\kappa_{\mu AB}^2)^2 + \alpha_3 \kappa_{\mu AB} \kappa_{\nu}^{AB} \kappa_{\mu CD} \kappa_{\nu}^{CD} \right] \right\}. \quad (3.33)$$

The four parameters μ, α_i are numerical coefficients obtained by integrating over ${}^\perp\mathcal{W}$; since we only know the solutions numerically, these coefficients must be found in the same way. They are plotted against β^{-1} in figures 3.3 and 3.4, and are shown in table B.1. They are given by

$$\mu = 2\pi\eta^2 \int_0^\infty \varrho d\varrho \left[X'_{\text{NO}}{}^2 + \frac{X_{\text{NO}}^2 P_{\text{NO}}^2}{\varrho^2} + \frac{\beta P_{\text{NO}}^2}{\varrho^2} + \frac{1}{4} (X_{\text{NO}}^2 - 1)^2 \right], \quad (3.34a)$$

$$\alpha_1 = \frac{\pi\eta^2}{2} \int_0^\infty \varrho^3 d\varrho \left[X'_{\text{NO}}{}^2 + \frac{X_{\text{NO}}^2 P_{\text{NO}}^2}{\varrho^2} + \frac{\beta P_{\text{NO}}^2}{\varrho^2} + \frac{1}{4} (X_{\text{NO}}^2 - 1)^2 \right], \quad (3.34b)$$

$$\alpha_2 = \frac{\pi}{4} \int_0^\infty d\varrho \left[\varrho^2 X'_{\text{NO}} (2\xi - \bar{\xi}) + \beta P'_{\text{NO}} (2\lambda - \bar{\lambda} - \varrho\bar{\psi}) + 4\beta\varrho P_{\text{NO}}^2 \right], \quad (3.34c)$$

$$\alpha_3 = \frac{\pi}{4} \int_0^\infty d\varrho \left[2\varrho^2 X'_{\text{NO}} \bar{\xi} + \beta P'_{\text{NO}} (\bar{\lambda} + \varrho\bar{\psi}) - 4\beta\varrho P_{\text{NO}}^2 \right]. \quad (3.34d)$$

3.3.2 The Effective Equations of Motion

In order to derive the effective equations of motion of the string, we must express the effective action (3.33) in terms of the worldsheet coordinates X^a , with respect

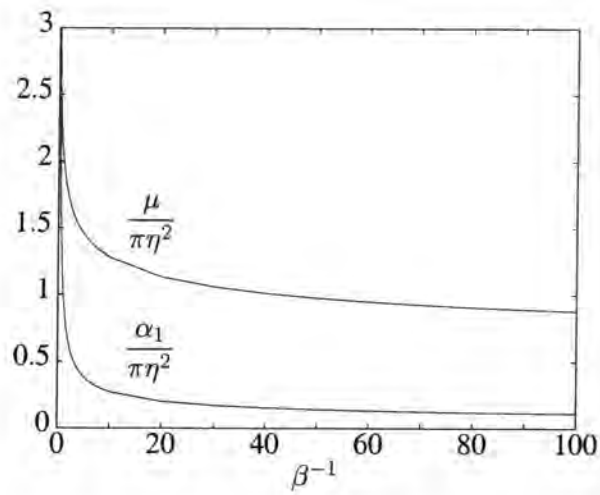


Figure 3.3: The parameters $\mu/(\pi\eta^2)$ and $\alpha_1/(\pi\eta^2)$ as functions of the inverse Bogomol'nyi parameter $1/\beta$.

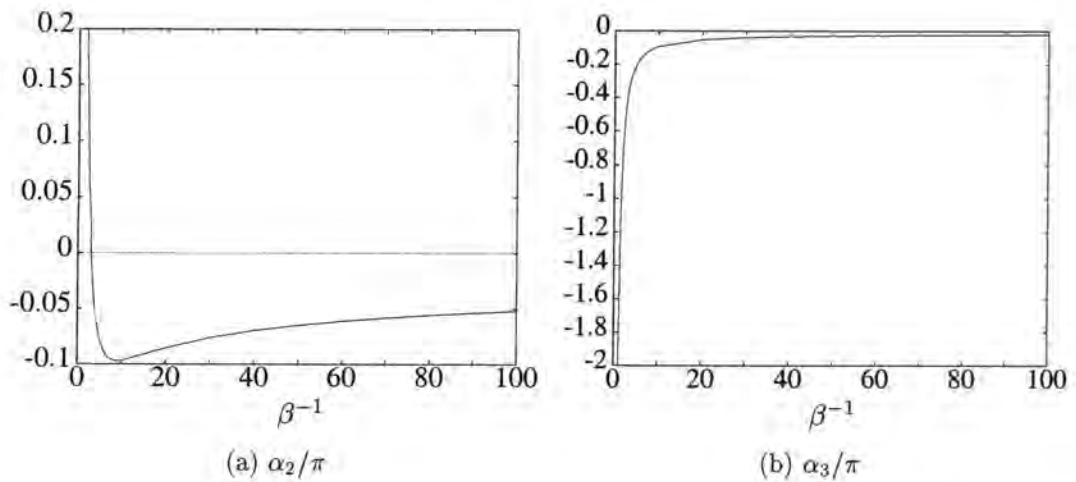


Figure 3.4: The parameters α_2/π and α_3/π as functions of $1/\beta$.

to which we are varying it. To do this, note that

$$\underline{\kappa}_{\mu AB} = n_{\mu a, A} X^a{}_{,B} = -n_{\mu a} X^a{}_{,AB} = -n_{\mu a} X^a{}_{;AB}. \quad (3.35)$$

Hence, defining

$$N_{CD}^{AB} \stackrel{\text{def}}{=} X^{a;A}{}_{;C} X_{a;D}{}^{;B}, \quad (3.36)$$

we see that

$$\begin{aligned} \underline{\kappa}_{\mu AB}^2 &= -X^{a;AB} X_{a;AB} = -N_{BA}^{AB}, \\ \underline{\kappa}_{\mu AB} \underline{\kappa}_{\nu}{}^{AB} \underline{\kappa}_{\mu CD} \underline{\kappa}_{\nu}{}^{CD} &= X^{a;AB} X_{a;CD} X^{b;CD} X_{b;AB} = N_{BD}^{AC} N_{CA}^{DB}. \end{aligned}$$

Now, the connection on the worldsheet is given by

$$\| \Gamma_B{}^A{}_C = \frac{1}{2} \gamma^{AE} (\gamma_{BE,C} + \gamma_{CE,B} - \gamma_{BC,E}) = \gamma^{AE} X^a{}_{,E} X_{a,BC}, \quad (3.37)$$

and the Riemann tensor [either directly from the above connection or via the Gauß equation (2.12)] is

$$\| r_{ABCD} = X^a{}_{;AC} X_{a;BD} - X^a{}_{;AD} X_{a;BC}. \quad (3.38)$$

We may therefore, using the identity $R_{ABCD} = \frac{1}{2} R (\gamma_{AC} \gamma_{BD} - \gamma_{AD} \gamma_{BC})$ and the symmetries of N_{CD}^{AB} , infer the following useful relations:

$$\| r^A{}_B = \frac{1}{2} \| r \delta^A{}_B = -N_{BC}^{CA} \quad (3.39a)$$

$$\| r = -N_{BA}^{AB} \quad (3.39b)$$

$$\begin{aligned} N_{BD}^{AC} N_{CA}^{DB} &= X^{a;AB} X_a{}^{;CD} (\| r_{ACBD} + X^b{}_{AD} X_{b;BC}) \\ &= \frac{1}{2} \| r^2 + N_{BC}^{AD} N_{AD}^{CB}. \end{aligned} \quad (3.39c)$$

Therefore, we can also express the effective action (3.33) as

$$S = -\mu \int d^2 \sigma \sqrt{-\lambda} \left\{ 1 - \varsigma^2 \frac{\alpha_1}{\mu} \| r + \varsigma^4 \frac{1}{\mu} \left[\left(\alpha_2 + \frac{1}{2} \alpha_3 \right) \| r^2 + \alpha_3 N_{BC}^{AD} N_{AD}^{CB} \right] \right\}. \quad (3.40)$$

[Note that in (3.33) the term $\underline{\kappa}_{\mu AB}^2$ multiplying ς^2 is in fact $\underline{\kappa}_{\mu AB}^{(0)2}$, which is equal to $\| r^{(0)}$ by (2.15), since $\underline{\kappa}_{\mu}^{(0)} = 0$.] The variations of the constituent terms of (3.40) are

$$\delta \sqrt{-\gamma} = \frac{1}{2} \sqrt{-\gamma} \gamma^{AB} \delta \gamma_{AB} = \frac{1}{2} \sqrt{-\gamma} \gamma^{AB} X^a{}_{;A} \delta X_{a;B}, \quad (3.41a)$$

$$\begin{aligned} \delta (\| r) &= -2 X^{a;AB} \delta X_{a;AB} + 4 N_{AB}^{DA} X^{a,B} \delta X_{a,D} \\ &= -2 X^{a;AB} \delta X_{a;AB} - 2 \| r X^{a,C} \delta X_{a,C}, \end{aligned} \quad (3.41b)$$

$$\delta (N_{BC}^{AD} N_{AD}^{CB}) = 4 \delta X_{a;AB} X^{a;CD} N_{CD}^{AB} - 4 X^a{}_F \delta X_{a,A} \gamma^{AF} N_{BC}^{ED} N_{ED}^{CB}. \quad (3.41c)$$

Noting that $\Theta \stackrel{\text{def}}{=} \int \sqrt{-\gamma} \parallel_r d^2\sigma$ is proportional to the Euler characteristic of the worldsheet (which is a topological invariant), or from the above equations, we see that the α_1 term will not contribute to the equations of motion. The \parallel_r^2 term gives

$$\begin{aligned} 3 (\gamma^{AB} X^a{}_{,A} \parallel_r^2)_{;B} - 4 (\parallel_r X^{a;AB})_{;AB} &= (X^{a,B} \parallel_r^2 - 4 \parallel_r{}_{,A} X^{a;AB})_{;B} \\ &= -4 \parallel_r{}_{;AB} X^{a;AB}. \end{aligned} \quad (3.42)$$

In this calculation we used the Riemann identity $[D_A, D_B]X^a{}_{,C} = \parallel_r{}_{CDAB} X^{a,D}$, which implies $X^{a;AB}{}_{;B} = \parallel_r{}^{AB} X^a{}_{,B} = \frac{1}{2} \parallel_r X^{a,A}$.

The $N_{BC}^{AD} N_{AD}^{CB}$ term gives

$$3 (X^{a,A} N_{BC}^{ED} N_{AD}^{EB})_{;A} + 3 (N_{CD}^{AB} X^{a;CD})_{;AB}. \quad (3.43)$$

Inserting into this the following relation

$$\begin{aligned} N_{CD;A}^{AB} X^{a;CD} &= X^{b;B}{}_{;DA} X_{b;C}{}^{;A} X^{\mu;CD} = \frac{1}{2} (X^b{}_{;DA} X_{b;C}{}^{;A})_{;B} X^{a;CD} \\ &= -\frac{1}{4} (\parallel_r \gamma_{CD})_{;B} X^{a;CD} = 0, \end{aligned} \quad (3.44)$$

we finally find that the equations of motion for the worldsheet to fourth order in ς are

$$\begin{aligned} \frac{\mu}{\varsigma^4} \square X^a &= -2 (\alpha_2 + 2\alpha_3) \parallel_r{}_{;AB} X^{a;AB} + 3\alpha_3 X^{a,A} (N_{BC}^{ED} N_{ED}^{CB})_{;A} \\ &\quad + 4\alpha_3 N_{CD}^{AB} X^{a;CD}{}_{;AB}. \end{aligned} \quad (3.45)$$

(Note that for $\varsigma = 0$ this reduces to the Nambu equation, $\square X^a = 0$, and that there are no contributions at order ς^2 .)

We can now express this equation of motion in terms of the fundamental forms.

Using (3.35) and

$$X^a{}_{;AB} = X^a{}_{,AB} - \Gamma_A{}^C{}_B X^a{}_{,C}, \quad (3.46a)$$

$$X_{a,D} X^a{}_{;AB} = 0, \quad (3.46b)$$

it follows that

$$\begin{aligned} X^a{}_{;AB} &= \eta^{ab} X_{b;AB} = (\gamma^{CD} X^a{}_{,C} X^b{}_{,D} - \delta^{\mu\nu} n_\mu{}^a n_\nu{}^b) X_{b;AB} \\ &= -\delta^{\mu\nu} n_\mu{}^a n_\nu{}^b X_{b,AB} = \delta^{\mu\nu} n_\mu{}^a \underline{\mathbb{E}}_{\mu AB}. \end{aligned} \quad (3.47)$$

Contracting the equations of motion with $n_\mu{}^a$ and with $X^a{}_{,P}$ gives us equations of motion parallel and perpendicular to \mathcal{W} :

$$-\frac{\mu}{\zeta^4} \underline{\kappa}_{\mu A}{}^A = (4\alpha_2 + 2\alpha_3) \parallel r_{;AB} \underline{\kappa}_\mu{}^{AB} + 4\alpha_3 \delta^{\nu\rho} \underline{\kappa}_\nu{}^{AC} \underline{\kappa}_\rho{}^{BD} n_\mu{}^a X_{a;CDAB}, \quad (3.48a)$$

$$0 = 3\alpha_3 (N_{EF}^{CD} N_{CD}^{FE})_{,P} + 4\alpha_3 N_{EF}^{CD} \gamma^{AE} \gamma^{BF} X^a{}_{,P} X_{a;CDAB}. \quad (3.48b)$$

(This last equality is an identity for the unperturbed worldsheet.) Therefore, the equations of motion also read

$$\begin{aligned} \frac{\mu}{\zeta^4} \underline{\kappa}_\mu = & - (4\alpha_2 + 2\alpha_3) \parallel r_{;AB} \underline{\kappa}_\mu{}^{AB} + 4\alpha_3 \underline{\kappa}_\nu{}^{AC} \underline{\kappa}_\nu{}^{BD} \left(- \underline{\kappa}_{\mu CA;AB} - \varepsilon_{\mu\rho} \underline{\omega}_B \underline{\kappa}_{\rho CD;A} \right. \\ & \left. - \varepsilon_{\mu\rho} \underline{\omega}_A \underline{\kappa}_{\rho CD;B} - \underline{\kappa}_{\rho CD} \underline{\kappa}_\rho{}^E{}_A \underline{\kappa}_{\mu EB} - \varepsilon_{\mu\rho} \underline{\omega}_{A;B} \underline{\kappa}_{\rho CD} + \underline{\kappa}_{\mu CD} \underline{\omega}_a \underline{\omega}_B \right). \end{aligned} \quad (3.49)$$

In this notation the Nambu equation assumes the familiar form

$$\underline{\kappa}_\mu = 0. \quad (3.50)$$

3.4 Three Illustrative Trajectories

In this section we shall derive the corrections to the motion of three test trajectories: a collapsing circular loop, a travelling wave and a helical breather. Then, we will determine from this corrected motion whether these three string solutions are rigid or antirigid. A more general discussion of the rigidity of strings beyond the Nambu limit is postponed until section 3.5.

Before we consider the corrections to these trajectories, let us briefly introduce their Nambu characteristics and discuss what we would expect to find.

The loop trajectory [64] is given by

$$X^a(\tau, \sigma) = (\tau, \cos(\tau) \cos(\sigma), \cos(\tau) \sin(\sigma), 0), \quad (3.51)$$

(where τ and σ are the worldsheet coordinates σ^0 and σ^1) and collapses to a point after a time $\Delta\tau = \pi/2 = L/4$, where $L = \oint d\sigma = 2\pi$ is the length of the closed loop. This is a good trajectory for investigating the differences between the Nambu–Gotō and Anderson’s actions, (3.2) and (3.33), because at $\tau = \Delta\tau$ the extrinsic curvatures invariants of the worldsheet become singular, that is $\zeta \rightarrow \infty$ and the Nambu–Gotō action breaks down. Of course, the corrected action also breaks down, but since it is to fourth order it should remain valid longer than the Nambu–Gotō

action. Therefore, we should observe roughly three zones for the collapse of the loop: 1° Both the Nambu–Gotō and Anderson’s actions are valid, 2° The Nambu–Gotō action breaks down, but Anderson’s remains valid and 3° Anderson’s action breaks down. Intuitively, rigidity would be indicated by a retardation of the divergence of the curvature invariants, *i.e.*, of the collapse.

The travelling wave is a variant of the flat worldsheet where we allow the superimposition of a displacement depending only on one of the light-cone variables of the worldsheet, $\sigma_{\pm} = \sigma \pm \tau$. That is, the travelling wave is described by

$$X^a(\tau, \sigma) = (\tau, f(\tau - \sigma), g(\tau - \sigma), \sigma). \quad (3.52)$$

This has been shown to be a solution to the full field theory [45], and since this is clearly also a solution of the Nambu equations $\square X^a = 0$, we anticipate that no corrections will be found.

Finally, the helical breather (see *e.g.* [83]) is given by

$$X^a(\tau, \sigma) = \left(\tau, \sqrt{1 - q^2} \cos(\tau) \cos(\sigma), \sqrt{1 - q^2} \cos(\tau) \sin(\sigma), q\sigma \right), \quad (3.53)$$

where q is a free parameter such that $q \rightarrow 0$ gives the collapsing loop and $q \rightarrow 1$ gives the flat worldsheet. For $0 < q < 1$ the trajectory is never singular and the extrinsic curvature peaks at approximately $\sqrt{1 - q^2}/q^2$. Rigidity would be indicated by a preference for lower extrinsic curvature, and therefore a negative correction to the amplitude of breathing oscillation.

3.4.1 The Collapsing Loop

In Cartesian coordinates, the position of a collapsing loop centered at the origin is

$$X^a(\tau, \sigma) = (\tau, Z(\tau) \cos(\sigma), Z(\tau) \sin(\sigma), 0), \quad (3.54)$$

where $Z(\tau)$ is the time-varying radius of the loop. The normals of the worldsheet are given by $n_{\mu a} X^a_{,A} = 0$, and are

$$\begin{aligned} n_0^a &= (\dot{Z}, \cos(\sigma), \sin(\sigma), 0) / \sqrt{1 - \dot{Z}^2}, \\ n_1^a &= (0, 0, 0, 1). \end{aligned} \quad (3.55)$$

Then,

$$\begin{aligned}
 \underline{\omega}_A &= \underline{\kappa}_{1AB} = 0, \\
 \underline{\kappa}_{0AB} &= \frac{1}{\sqrt{1 - \dot{Z}^2}} \begin{pmatrix} \ddot{Z} & 0 \\ 0 & -Z \end{pmatrix}, \\
 \gamma_{AB} &= \begin{pmatrix} 1 - \dot{Z}^2 & 0 \\ 0 & -Z^2 \end{pmatrix}, \\
 \Gamma_A{}^\tau{}_B &= \begin{pmatrix} -\frac{\dot{Z}\ddot{Z}}{1 - \dot{Z}^2} & 0 \\ 0 & \frac{Z\dot{Z}}{1 - \dot{Z}^2} \end{pmatrix}, \\
 \Gamma_A{}^\sigma{}_B &= -\frac{\dot{Z}}{Z} \begin{pmatrix} 0 & 1 \\ 1 & 0 \end{pmatrix}
 \end{aligned} \tag{3.56}$$

and the equation of motion to order ζ^0 is

$$\underline{\kappa}_0 = \frac{Z\ddot{Z} + 1 - \dot{Z}^2}{Z(1 - \dot{Z}^2)^{3/2}} = 0, \tag{3.57}$$

which admits as general solution:

$$Z_0(\tau) = k \cos\left(\frac{\tau - \tau_0}{k}\right). \tag{3.58}$$

Choosing $\tau_0 = 0, k = 1$, we obtain the canonical loop trajectory (3.51).

Now we want to solve Eq. (3.49) for a corrected radius $Z(\tau) = Z_0(\tau) + \delta Z(\tau)$.

Inserting (3.56), the right-hand side of (3.49) becomes:

$$4(\alpha_2 + \alpha_3) \parallel r_{,AB} \underline{\kappa}_2{}^{AB} = 32(\alpha_2 + \alpha_3) \sec^8(\tau) \tan(\tau) [7 \sec^2(\tau) - 6]. \tag{3.59}$$

The left-hand side of (3.49) can be obtained by varying the expression (3.57), whereby we obtain

$$\delta \ddot{Z} + 2 \tan(\tau) \delta \dot{Z} - \delta Z = 32 \frac{\zeta^4}{\mu} (\alpha_2 + \alpha_3) \sec^8(\tau) \tan(\tau) [7 \sec^2(\tau) - 6]. \tag{3.60}$$

The solution can be obtained by varying the constants of (3.58), and is

$$\delta Z = 32 \frac{\zeta^4}{\mu} (\alpha_2 + \alpha_3) \left[\frac{7}{40} \sec^5(\tau) + \frac{1}{60} \sec^3(\tau) + \frac{1}{15} \sec(\tau) - \frac{31}{120} \cos(\tau) - \frac{\tau}{8} \sin(\tau) \right]. \tag{3.61}$$

Clearly, (3.61) tells us that the rigidity of the string will be determined by the combination $\alpha_2 + \alpha_3$. This is plotted on figure 3.5a and is negative for the range of β that we consider. This means (figure 3.5b) that the loop collapses faster and, according to the discussion at the beginning of this section, is antirigid.

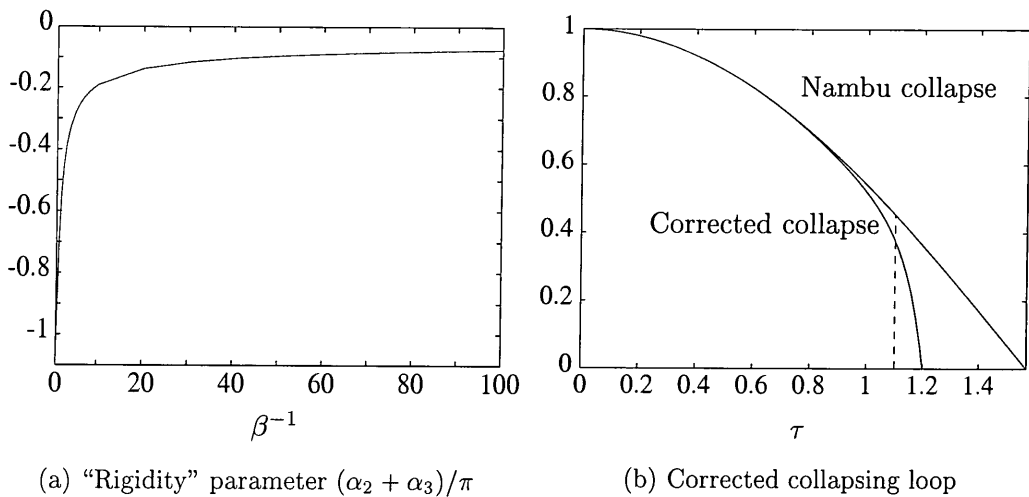


Figure 3.5: The corrected collapsing loop. (a) The “rigidity” parameter $(\alpha_2 + \alpha_3)/\pi$ as a function of the inverse Bogomol’nyi parameter $1/\beta$. (b) Comparison of the Nambu collapse of a loop with the corrected collapse, for $\beta = 1$ and a (large) value of $\zeta = 1/10$.

Note that the approximation breaks down when $|K_{0AB}| \simeq O(1/w_H)$, *i.e.* when $\cos \tau = O(w_H)$; for $\zeta = 1/10$ as in figure 3.5b this happens at $\tau \simeq 1.1$, which is indeed the point where the two solutions start to differ significantly. This is indicated on the figure by a vertical dashed line.

3.4.2 The Travelling Wave

The travelling wave is a worldsheet which has position

$$X^a = (\tau, f(\tau - \sigma), g(\tau - \sigma), \sigma) \quad (3.62)$$

and normals

$$\begin{aligned} n_0^a &= (0, g', -f', 0) / \sqrt{f'^2 + g'^2}, \\ n_1^a &= (f'^2 + g'^2, f', g', f'^2 + g'^2) / \sqrt{f'^2 + g'^2}. \end{aligned} \quad (3.63)$$

We denote by a prime “ $'$ ” the differentiation with respect to the function’s argument, *i.e.* $\tau - \sigma$. Writing

$$\begin{aligned} \lambda(\tau - \sigma) &\stackrel{\text{def}}{=} f'^2 + g'^2, \\ \zeta(\tau - \sigma) &\stackrel{\text{def}}{=} (f''g' - f'g'') / \lambda, \\ k_0(\tau - \sigma) &\stackrel{\text{def}}{=} (f''g' - f'g'') / \sqrt{\lambda}, \\ k_1(\tau - \sigma) &\stackrel{\text{def}}{=} (f'f'' + g'g'') / \sqrt{\lambda}, \end{aligned} \quad (3.64)$$

we have:

$$\begin{aligned}
\underline{\omega}_A &= \zeta \begin{pmatrix} 1 \\ -1 \end{pmatrix}, \\
\underline{\kappa}_{\mu AB} &= k_\mu \begin{pmatrix} 1 & -1 \\ -1 & 1 \end{pmatrix}, \\
\gamma_{AB} &= \begin{pmatrix} 1 - \lambda & \lambda \\ \lambda & -1 - \lambda \end{pmatrix}, \\
\Gamma_B^A C &= \frac{\lambda'}{2} \begin{pmatrix} 1 \\ -1 \end{pmatrix} \otimes \begin{pmatrix} -1 & 1 \\ 1 & -1 \end{pmatrix},
\end{aligned} \tag{3.65}$$

and it is straightforward to see that all terms in the right-hand side of (3.49) vanish separately: as expected, we find no corrections.

3.4.3 The Helical Breather

The helical breather trajectory is given by

$$X^a = (\tau, Z(\tau) \cos(\sigma), Z(\tau) \sin(\sigma), q\sigma), \tag{3.66a}$$

$$n_0^a = (0, q \sin(\sigma), -q \cos(\sigma), Z) / \sqrt{q^2 + Z^2}, \tag{3.66b}$$

$$n_1^a = (\dot{Z}, \cos(\sigma), \sin(\sigma), 0) / \sqrt{1 - \dot{Z}^2} \tag{3.66c}$$

and describes the worldsheet of a helical sting (*i.e.*, a corkscrew) with breathing parameter q . It is a generalization of the flat cosmic string loop, for the latter is obtainable by taking the limit $q \rightarrow 0$; the limit $q \rightarrow 1$ is the flat worldsheet. With our choice of normals, we obtain

$$\begin{aligned}
\underline{\omega}_A &= -\frac{q}{\sqrt{1 - \dot{Z}^2} \sqrt{q^2 + Z^2}} \begin{pmatrix} 0 \\ 1 \end{pmatrix}, \\
\underline{\kappa}_{0AB} &= -\frac{q\dot{Z}}{\sqrt{q^2 + Z^2}} \begin{pmatrix} 0 & 1 \\ 1 & 0 \end{pmatrix}, \\
\underline{\kappa}_{1AB} &= \frac{1}{\sqrt{1 - \dot{Z}^2}} \begin{pmatrix} \ddot{Z} & 0 \\ 0 & -Z \end{pmatrix}, \\
\gamma_{AB} &= \begin{pmatrix} 1 - \dot{Z}^2 & 0 \\ 0 & -(q^2 + Z^2) \end{pmatrix};
\end{aligned} \tag{3.67}$$

hence, the equation of motion to zeroth order is

$$\frac{\ddot{Z}}{(1 - \dot{Z}^2)^{3/2}} + \frac{Z}{(q^2 + Z^2)(1 - \dot{Z}^2)^{1/2}} = 0, \tag{3.68}$$

which admits for general solution

$$Z_0(\tau) = \sqrt{k^2 - q^2} \cos\left(\frac{\tau - \tau_0}{k}\right). \quad (3.69)$$

Choosing again $k = 1, \tau_0 = 0$, and calling

$$\Omega(\tau) \stackrel{\text{def}}{=} \cos^2(\tau) + q^2 \sin^2(\tau), \quad (3.70)$$

we find

$$\begin{aligned} \underline{\omega}_A &= -\frac{q}{\Omega} \begin{pmatrix} 0 \\ 1 \end{pmatrix}, \\ \underline{\kappa}_{0AB} &= -q \sqrt{\frac{1 - q^2}{\Omega}} \sin(\tau) \begin{pmatrix} 0 & 1 \\ 1 & 0 \end{pmatrix}, \\ \underline{\kappa}_{1AB} &= -\sqrt{\frac{1 - q^2}{\Omega}} \cos(\tau) \begin{pmatrix} 1 & 0 \\ 0 & 1 \end{pmatrix}, \\ \gamma_{AB} &= \Omega \begin{pmatrix} 1 & 0 \\ 0 & -1 \end{pmatrix}. \end{aligned} \quad (3.71)$$

The zeroth order solution (3.69 with $q = 1, \tau_0 = 0$) is called a “breather,” because it smoothly oscillates from one helicity to the other (a “right-handed” corkscrew to a “left-handed” one) and back.

Then, the right-hand side of equation (3.49) becomes

$$-32\zeta^4 \sqrt{1 - q^2} \cos(\tau) \Omega^{-9/2} (\beta_1 - \beta_2 \Omega^{-1} + \beta_3 \Omega^{-2} - \beta_4 \Omega^{-3}), \quad (3.72)$$

where we have defined the following numerical coefficients

$$\begin{aligned} \beta_1 &\stackrel{\text{def}}{=} 6 [(\alpha_2 + \alpha_3) + \alpha_2 q^2], \\ \beta_2 &\stackrel{\text{def}}{=} 7(\alpha_2 + \alpha_3) + (38\alpha_2 + 22\alpha_3)q^2 + (7\alpha_2 - 3\alpha_3)q^4, \\ \beta_3 &\stackrel{\text{def}}{=} 5q^2 [(7\alpha_2 + 5\alpha_3) + (7\alpha_2 + 2\alpha_3)q^2], \\ \beta_4 &\stackrel{\text{def}}{=} 15q^4(2\alpha_2 + \alpha_3). \end{aligned} \quad (3.73)$$

As with the loop, the left-hand side of (3.49) is obtained by varying the trace of $\underline{\kappa}_1$:

$$\begin{aligned} \delta(\underline{\kappa}_1) &= \Omega^{-3/2} \delta \ddot{Z} + 2\Omega^{-5/2} (1 - q^2) \sin(\tau) \cos(\tau) \delta \dot{Z} \\ &\quad + \Omega^{-5/2} [q^2 - (1 - q^2) \cos^2(\tau)] \delta Z, \end{aligned} \quad (3.74)$$

so that the corrected equation of motion is

$$\begin{aligned} \delta \ddot{Z} + 2 \frac{1 - q^2}{\Omega} \sin(\tau) \cos(\tau) \delta \dot{Z} + \frac{q^2 - (1 - q^2) \cos^2(\tau)}{\Omega} \delta Z \\ = -32 \frac{\zeta^4}{\mu} \sqrt{1 - q^2} \cos(\tau) \Omega^{-3} (\beta_1 - \beta_2 \Omega^{-1} + \beta_3 \Omega^{-2} - \beta_4 \Omega^{-3}). \end{aligned} \quad (3.75)$$

We give an exact solution to this equation in appendix A; for now it is more instructive to consider the quasiflat case, $q \rightarrow 1$. Let us pose $\Delta^2 \stackrel{\text{def}}{=} 1 - q^2 \ll 1$; then, (3.75) becomes

$$\delta\ddot{Z} + \delta Z = -32 \frac{\zeta^4 \Delta^3}{\mu} [(\alpha_2 + \alpha_3) \cos(\tau) - (2\alpha_2 + \alpha_3) \cos(\tau) \sin^2(\tau)] \quad (3.76)$$

and the corrected trajectory can be written [at $O(\zeta^8)$]

$$\begin{aligned} Z_0 + \delta Z = & \Delta \left[1 - \frac{\zeta^4 \Delta^2}{\mu} (2\alpha_2 + \alpha_3) \right] \cos \left\{ \left[1 + \frac{4\zeta^4 \Delta^2}{\mu} (2\alpha_2 + 3\alpha_3) \right] \tau \right\} \\ & + \frac{\zeta^4 \Delta^3}{\mu} (2\alpha_2 + \alpha_3) \cos(3\tau). \end{aligned} \quad (3.77)$$

Comparing this with the unperturbed solution, we see that the effect of the correction is threefold:

- It alters the frequency, sending $\tau \rightarrow [1 + 4\zeta^4 \Delta^2 (2\alpha_2 + 3\alpha_3)/\mu] \tau$. Since both α_3 and $\alpha_2 + \alpha_3$ are negative, this reduces the frequency, an effect we would say tends to make the worldsheet rigid.
- It modifies the amplitude of the oscillation by a factor $1 - \zeta^4 \Delta^2 (2\alpha_2 + \alpha_3)/\mu$, which could be either greater or smaller than 1, depending on β ; figure 3.6a shows that $2\alpha_2 + \alpha_3$ is positive for subcritical β and negative for supercritical β . Therefore, the amplitude is increased for $\beta < 1$ and decreased for $\beta > 1$.
- It adds a higher frequency oscillation if $\beta \neq 1$.

For simplicity, let us consider the case $\beta = 1$; then,

$$Z_0 + \delta Z = \Delta \cos \left[\left(1 + \frac{8\zeta^4 \Delta^2}{\mu} \alpha_3 \right) \tau \right], \quad (3.78)$$

i.e. the only effect of the correction is to reduce the frequency of oscillation of the breather, which would seem to be unambiguously rigid. (See figure 3.6.)

However, for general β , we observe a curious property: suppose that we initialize the correction at the instant of maximal velocity rather than maximal amplitude, $\delta Z(-\pi/2) = \delta\dot{Z}(-\pi/2) = 0$, we find

$$\begin{aligned} Z_0 + \delta Z = & \Delta \left[1 - \frac{\zeta^4 \Delta^2}{\mu} (2\alpha_2 + 9\alpha_3) \right] \sin \left\{ \left[1 + \frac{4\zeta^4 \Delta^2}{\mu} (2\alpha_2 + 3\alpha_3) \right] \tau' \right\} \\ & - \frac{\zeta^4 \Delta^3}{\mu} (2\alpha_2 + \alpha_3) \sin(3\tau') + O(\zeta^8) \end{aligned} \quad (3.79)$$

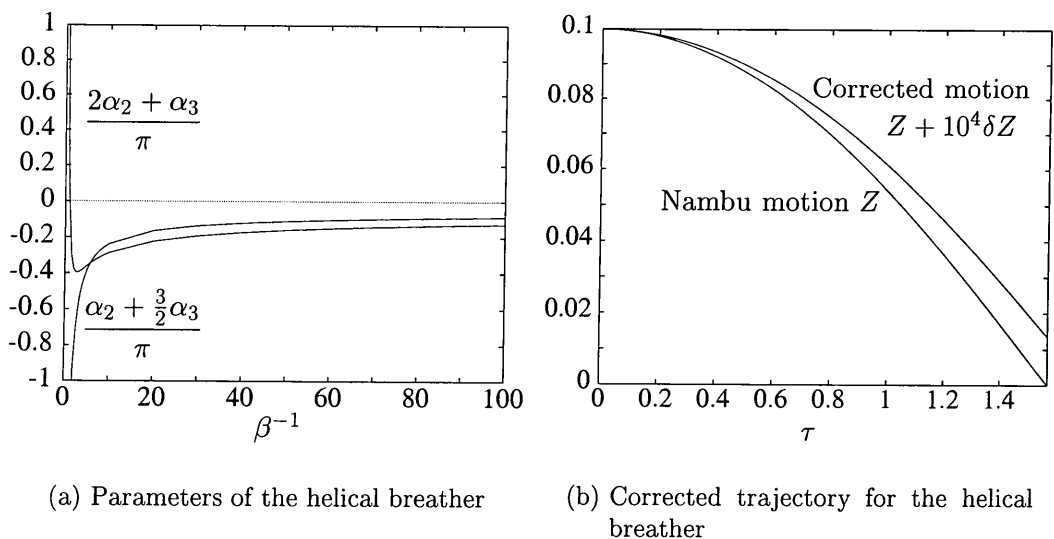


Figure 3.6: The corrected helical breather. (a) The parameters $(\alpha_2 + \frac{3}{2}\alpha_3)/\pi$ and $(2\alpha_2 + \alpha_3)/\pi$ appearing in the equations of motion and solutions of the helical breather, as functions of β . (b) The corrected breather trajectory for $\beta = 1, \Delta = \varsigma = 1/10$. (In fact, the effect is so small that we have plotted $Z + 10^4 \delta Z$.)

(where $\tau' = \tau + \pi/2$). This time the amplitude is increased for all β . If we consider again $\beta = 1$, this reduces to

$$Z_0 + \delta Z = \Delta \left(1 - \frac{8\varsigma^4 \Delta^2}{\mu} \alpha_3 \right) \sin \left[\left(1 + \frac{8\varsigma^4 \Delta^2}{\mu} \alpha_3 \right) \tau' \right]. \quad (3.80)$$

Although it is not clear from this formula, an analysis of the Ricci curvature \parallel_{τ} near $\tau' = 0$ shows that it is increased, which we would call antirigidity. (A calculation of the extrinsic curvature for the general solution rather than this particular case is included at the end of appendix A.)

3.5 The Worldsheet Rigidity from the Action

To summarize the findings of the previous section, we could say that, although for the collapsing loop we found that the worldsheet was unambiguously antirigid, it was much more difficult to tell in the case of the helical breather. In fact, we found that it was not possible to determine directly from the corrected motion whether it behaved rigidly or antirigidly, and had to compute the corrections to the worldsheet's curvature; in doing so, we found that — for $\beta = 1$ — the string could behave either way, depending on the initial conditions.

In this section, we wish to consider the question of the worldsheet rigidity in more detail, using an argument originally due to Polyakov [81]. We abandon our attempts to determine the rigidity of the worldsheet directly via the corrected dynamics of the string to concentrate on the very definition of rigidity (respectively antirigidity), namely a decrease (increase) of the small-scale structure on the worldsheet.

Let us perform a rescaling of the worldsheet coordinates, that is $X^a \rightarrow \lambda X^a$. These transformations alter of course the scale of crinkles on \mathcal{W} and magnify or reduce the small-scale structure, depending on whether $\lambda \lesseqgtr 1$. Rigidity would be indicated by an extremum of the energy (or the action) with respect to the parameter λ , as illustrated in figure 3.7.

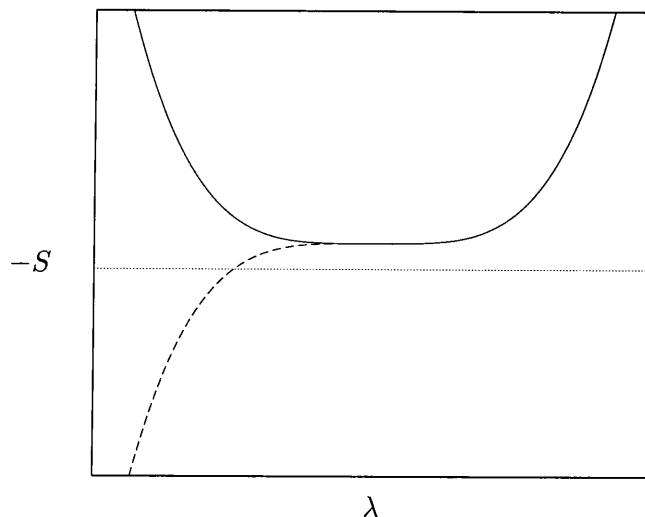


Figure 3.7: Illustration of Polyakov's argument for a rigid worldsheet (solid line) and an antirigid worldsheet.

Let us consider then the fourth-order action, which we can write as

$$\begin{aligned}
 -S = \mu \int d^2\sigma \sqrt{-\gamma} - \zeta^2 \alpha_1 \int d^2\sigma \sqrt{-\gamma} M_{\mu\mu} + \zeta^4 \alpha_2 \int d^2\sigma \sqrt{-\gamma} M_{\mu\mu}^2 \\
 + \zeta^4 \alpha_3 \int d^2\sigma \sqrt{-\gamma} M_{\mu\nu} M_{\mu\nu},
 \end{aligned} \tag{3.81}$$

where $M_{\mu\nu} \stackrel{\text{def}}{=} \underline{\kappa}_{\mu AB} \underline{\kappa}_{\nu}{}^{AB}$. As $M_{\mu\nu} M_{\mu\nu} = M_{\mu\mu}^2 - 2 \det(M)$, this can be rewritten as

$$-S = \mu A - \zeta^2 \alpha_1 \Theta + \zeta^4 [(\alpha_2 + \alpha_3) I_1 - 2\alpha_3 I_2], \tag{3.82}$$

with A the area of the worldsheet for the range of $\{\tau, \sigma\}$ being integrated over, Θ proportional to the Euler character of \mathcal{W} and

$$I_1 = \int d^2\sigma \sqrt{-\gamma} M_{\mu\mu}^2, \tag{3.83a}$$

$$I_2 = \int d^2\sigma \sqrt{-\gamma} \det(M). \quad (3.83b)$$

So now perform the rescaling $X^a \rightarrow \lambda X^a$ as mandated by the argument. Then,

$$\begin{aligned} \gamma_{AB} &\rightarrow \lambda^2 \gamma_{AB}, \\ \underline{\kappa}_{\mu AB} &\rightarrow \lambda \underline{\kappa}_{\mu AB}, \\ I_i &\rightarrow \lambda^{-2} I_i \end{aligned} \quad (3.84)$$

and hence

$$-S \rightarrow \lambda^2 \mu A + \varsigma^2 \alpha_1 \Theta + \lambda^{-2} \varsigma^4 [(\alpha_2 + \alpha_3) I_1 - 2\alpha_3 I_2]. \quad (3.85)$$

We know that $\alpha_3, \alpha_2 + \alpha_3 < 0$, and clearly $I_1 > 0$, so in order to determine the shape of $S(\lambda)$ we only need to determine the sign of $\det(M)$. For this purpose, we can work in the conformal gauge, $\gamma_{AB} = \eta_{AB}$, where we find

$$\begin{aligned} \det(M) &= (\underline{\kappa}_{000} \underline{\kappa}_{111} - \underline{\kappa}_{100} \underline{\kappa}_{011})^2 - 2(\underline{\kappa}_{011} \underline{\kappa}_{110} - \underline{\kappa}_{111} \underline{\kappa}_{010})^2 \\ &\quad - 2(\underline{\kappa}_{000} \underline{\kappa}_{110} - \underline{\kappa}_{100} \underline{\kappa}_{010})^2. \end{aligned} \quad (3.86)$$

If we impose the Nambu equations of motion, $\underline{\kappa}_{\mu} = 0$, this determinant is strictly negative. Hence, since μA is positive, we see that $S(\lambda)$ is unbounded below. We must therefore conclude that *the string is generically antirigid*. This does not mean that all trajectories are antirigid, but rather that they cannot all be rigid. Let us now illustrate this with the three cases that we have considered in the previous section.

- **Collapsing loop**

In this case, $\det(M) = 0$ because the loop is flat and therefore has only one non-vanishing second fundamental form. As noted in section 3.4.1, the parameter $\alpha_2 + \alpha_3$ then determines alone the rigidity behaviour of the worldsheet. Since this parameter is negative, $S(\lambda)$ is unbounded and this solution is antirigid.

- **Travelling wave**

Here $M_{\mu\nu} = 0$ altogether.

- **Helical breather**

In this final case, both $M_{\mu\nu}$ and $\det(M)$ are non-zero. Although the string is generically antirigid (due to an unstable mode) some trajectory corrections may have vanishing projection onto that unstable mode, and be rigid.

From the discussion in section 3.4.3, it is clear that whether the the correction projects or not onto the unstable mode depends on the parameter q and on the initial condition. Let us trade q for Δ and pose $\Sigma = \sin(\tau_0)$. Figure 3.8 shows the zones in the parameter space (Δ^2, Σ^2) where the worldsheet is rigid and antirigid. (The computations to compose the figure require the solution for arbitrary q of appendix A, and we therefore postpone them until then.)

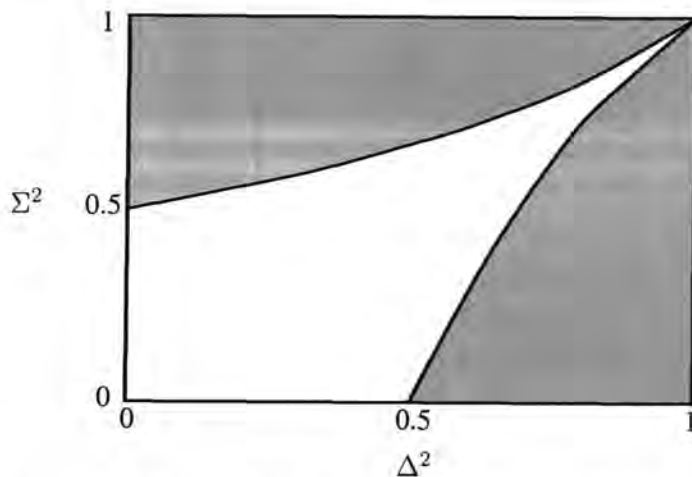


Figure 3.8: Diagram showing the regions of rigidity and antirigidity (shaded) for the helical breather and $\beta = 1$. $\Delta^2 = 1 - q^2$ and $\Sigma = \sin(\tau_0)$ are the two parameters upon which the rigidity depends.

3.6 Outlook

In this chapter we have determined that cosmic strings are generically antirigid when considered beyond the Nambu limit. Cosmologically, this implies that string networks will have a shorter life — and less impact — than previously believed. This result is somewhat annoying in a more “mathematical” way. The main reason for finding the effective motion and determining the rigidity of the worldsheet was that the Nambu approximation would not be valid at the small-scale structure. By finding that the quantity of small-scale structure was actually increased by going further than the zero-thickness limit, we have in a sense contradicted our assumption that finding corrections to the Nambu–Goto action would improve our knowledge of the string’s dynamics. We would somehow had preferred to find that the corrected dynamics of the string was rigid; this would have given us an *a posteriori* confirmation that indeed we know more about the string’s motion now. But there is still

hope that this will indeed be the case when we consider the gravity of the defect, an important ingredient that is still missing in this analysis.

The method used in this chapter to obtain the effective motion consisted in expanding the fields off the worldsheet, and integrating the action S over these perpendicular directions to obtain a quantity based on \mathcal{W} . This method relies crucially on our use of the custom-made system of Gaussian coordinates. However, it was mentioned earlier in this chapter that this basis's existence and uniqueness is only guaranteed up to a distance R of the string's core. Therefore, we should not be allowed to integrate the action outside the interval $\varrho = (0, R)$. What makes the method work is that all our fields (including the gauge field P_a) are massive, and therefore fall off exponentially rapidly to their vacuum values (1.27). By the time the coordinate system breaks down, all integrands are effectively zero and we do not make any mistakes by integrating the action up to infinity.

Consequently, one can genuinely wonder whether this method can (or should) be applied in the presence of massless fields (such as the graviton in pure General Relativity and the dilaton in Brans–Dicke or stringy extensions of it), since these would not benefit from this rapid falloff at infinity. A similar problem occurs with global strings (whose field decays as $1/\varrho^2$ at large distances). Of course, the integrands of the action could still all fall off exponentially despite the presence of massless fields, and the effective action method might still work; only an explicit calculation could tell.

For simplicity, we shall consider the dynamics of gravitating walls rather than strings. We shall then see (in chapter 5) that there is another way of finding the effective equations of motion for a defect, which does not require the integration of the effective action. Before we can do this, however, we need to know more about the gravitation of plane-symmetric domain walls, which will play a rôle similar to that of the Nielsen–Olesen string in this chapter.

Gravitating Plane-Symmetric Domain Walls

4.1 Introduction

For some time, topological defects — in particular cosmic strings — have been believed to hold the key to some important observations that the standard Big Bang model cannot explain alone. Most spectacularly, the standard model fails to predict the existence of cosmological structures in the Universe (galaxies and clusters of galaxies) because of the Cosmological Principle (CP), which postulates that at large scales the Universe is homogeneous and isotropic; these symmetries are used to derive of the Robertson–Walker metric, upon which the Big Bang scenario is based. Although the CP is in agreement with the Universe that we observe today at scales much larger than the size of galaxy clusters, these symmetries actually make the early Universe so completely homogeneous that gravity cannot be invoked to explain the formation of cosmic structure.

To remedy this situation, several explanations have been proposed, which should be regarded as fixes to be patched to the standard cosmological model. The first possibility is that gravity was not well described by General Relativity in the early Universe. There are good reasons to believe that this is indeed the case, such as the non-minimal coupling of matter to gravity in the low energy limit of string theories (which gave birth to the so-called string cosmology, and most notably the “pre-Big Bang” scenarios). The second explanation originates in the Friedmann equations (the Einstein equations for the Robertson–Walker metric), which in certain special

circumstances admit exponentially fast growing Universe solutions. Such a period in the early Universe may indeed have happened, and is called an inflationary epoch. Inflation was originally proposed to solve the flatness problem, but it was soon found to provide seeds to the growth of cosmic structures. Indeed, during inflation, the Universe is believed to have increased by about 60 e-folds ($\simeq 10^{26}$); this would have blown up tiny quantum fluctuations into cosmic-sized inhomogeneities which could have served as seeds for gravitational collapse. The third possibility is the existence of topological defects. In particular, moving cosmic strings would have created inhomogeneities in their wake which could have caused the formation of galaxies or galaxy clusters (see [59,89] and references therein).

Although global abelian strings seem so be ruled out as potential causes of gravitational seeding [2,79] because of the power spectrum that they generate, recent claims of a non-Gaussian signature in the Cosmological Microwave Background Radiation (CMBR) [41,78,77] would indicate, if they are verified [22,10], that inflation cannot account by itself for observations, and that topological defects may have existed and influenced the seeding of cosmic structure after all. (Almost all inflationary models predict a purely Gaussian spectrum, but see for instance [84].) Even if these claims turn out to be unfounded, topological defects are formed quite generically in phase transitions in the early Universe [63], and ideally we should be able to explain this lack of impact. By contrast, it has been so far impossible to integrate realistically the inflationary paradigm into particle physics (with the possible exception of “topological inflation” scenario, as we shall see later), because of the very specific potential required.

Among the different kinds of topological defects, domain walls are possibly the most interesting, gravitationally speaking. First, their metric is not static like that of most of the other defects but time-dependent, as was shown by Vilenkin [87] and Ipser & Sikivie [60] using Israel’s thin wall formalism [61]; the wall exhibits a de Sitter-like expansion along its parallel directions. (This is the case even though the Higgs scalar field is static! In fact, domain wall spacetimes cannot be static if one imposes a reflection symmetry around the wall’s core; see [47] for an example.) Second, the wall exhibits a cosmological horizon at a finite proper distance from its core, although this horizon is a consequence of the coordinates used, which were

chosen so that the flat spacetime wall lies along two spatial directions and at the origin of the third one. The proposal by Hill, Schramm and Fry (HSF) [58] that soft topological defects — meaning topological defects formed at a late time — could lead to cosmic structure caused some interest and prompted diverse attempts to find thick domain wall solutions [92,91,50,75] (with or without gravity). Indeed, walls in the HSF scenario are thick and light (“soft”), because at the time of their formation the scalar field’s VEV η is much smaller than the Planck energy. Unfortunately, HSF walls were discovered to be incompatible with the CMBR [62,66], and extended defects were again out of fashion.

One of the problems of the inflationary paradigm is that it cannot be easily incorporated in the particle physical models of the early Universe, because it requires a very particular potential to agree with observations. However, it was recently noted [88,69,70] that the core of topological defects formed very close to the Planck time would provide ideal conditions for inflation: these regions are in effect dominated by the vacuum energy of the Higgs field (which is trapped at the top of its potential by the topology of the defect). Although such defects would usually be called “thin” because the Higgs VEV is comparable to the Planck scale, it was noted that this thickness would be of the same order than the de Sitter horizon as seen from within the defect’s core. Thus, the idea of inflating topological defects was born; these defects are of course in a strongly gravitating situation, and an in-depth analysis of this situation has never yet been performed. In this chapter, we examine plane-symmetric thick domain walls, following all the possible solutions, from the very weakly to the strongly gravitating ones.

4.2 Plane-Symmetric Spacetimes

We consider the action (1.1) with $\mathcal{L} = \mathcal{L}_G + \mathcal{L}_M$ where

$$\mathcal{L}_G = -\frac{R}{16\pi G}, \quad (4.1a)$$

$$\mathcal{L}_M = (\nabla_a \Phi)(\nabla^a \Phi) - U(\Phi). \quad (4.1b)$$

Here, Φ is a real scalar field (the “Higgs” field) and $U(\Phi)$ is a symmetry-breaking potential which has a discrete set of degenerate minima. R is the spacetime’s Ricci

scalar. We assume that the spacing between the minima of $U(\Phi)$ is proportional to a parameter η (the Higgs VEV which sets the symmetry breaking scale) and that $U(\Phi)$ is characterised by a scale $V_F = U(\Phi_F)$, where Φ_F is a local maximum situated between two minima of the potential.

Let us start by scaling the dimensionful parameters via

$$\begin{aligned}\Phi &= \eta X, \\ \epsilon &\stackrel{\text{def}}{=} 8\pi G\eta^2;\end{aligned}\tag{4.2}$$

the parameter ϵ then characterises the strength of the gravitational interaction of the Higgs field. Let us also rescale the potential by letting $V(X) = U(\eta\Phi)/V_F$; with this choice, $V(X_F) = 1$, where $X_F = \Phi_F/\eta$ is a false vacuum. So far, there is only one scale in this problem, the Higgs boson's mass, whose inverse is the domain wall's thickness w_H :

$$w_H \stackrel{\text{def}}{=} \frac{1}{\sqrt{\lambda\eta}} = \sqrt{\frac{\epsilon}{8\pi G V_F}}.\tag{4.3}$$

Without loss of generality, we can set $w_H = 1$, which simply means that we measure distances in units of w_H .

Although all the results of this chapter will remain valid for any general potential satisfying these (and possibly other) conditions, we shall consider two particular potentials, both for illustrative purposes and to allow us to perform numerical simulations to refine our analytical results. These potentials are the Goldstone (or “ $\lambda\Phi^4$ ”) and the sine-Gordon (sG) potentials, given respectively by

$$V(X) = (X^2 - 1)^2\tag{4.4}$$

and

$$V(X) = \frac{1}{2}[1 + \cos(X)].\tag{4.5}$$

In terms of the new field X , the action and equations of motion are

$$-S = \frac{1}{2\epsilon} \int dx^4 \sqrt{-g} \left\{ R - 2\epsilon [(\nabla_a X)(\nabla^a X) - V(X)] \right\}.\tag{4.6}$$

and

$$\square X = -\frac{1}{2} \frac{\partial V}{\partial X}\tag{4.7a}$$

$$R_{ab} = \epsilon [2 \nabla_a X \nabla_b X - g_{ab} V(X)],\tag{4.7b}$$

where g_{ab} is the metric tensor from which R_{ab} is built. Note that if $X \equiv X_F$, then the Einstein equation (4.7b) reduces to

$$G_{ab} = -\epsilon g_{ab} = \frac{R}{4} g_{ab}, \quad (4.8)$$

whose solution is a four-dimensional de Sitter spacetime [56, page 124]. In this case, ϵ clearly plays the rôle of an effective cosmological constant. We call this a “false vacuum-de Sitter” (vdS) solution.

Let us now turn to the metric: we shall demand that it has planar symmetry, *i.e.* Killing vector fields ∂_x, ∂_y and $x\partial_y - y\partial_x$, and reflection symmetry around the wall’s core, which we can place at $z = 0$, where z now measures the proper distance from the wall. The metric can then be written as

$$ds^2 = A^2(z) dt^2 - B^2(t, z) (dx^2 + dy^2) - dz^2. \quad (4.9)$$

Although this is the most general metric with the symmetries that we impose, the fact that the Higgs field is static, $\dot{X} = 0$, means that

$$R_{tz} = \frac{1}{AB} (A'\dot{B} - A\dot{B}') = 0, \quad (4.10)$$

which (setting an integration constant to zero) implies $B(t, z) = b(t)A(z)$. Then

$$R^t_t - R^x_x \sim \frac{\dot{b}^2}{b^2} - \frac{\ddot{b}}{b} = 0, \quad (4.11)$$

which imposes $b(t) = e^{kt}$ for some constant k . The coupled scalar-Einstein equations then finally reduce to

$$X'' + 3\frac{A'}{A}X' = \frac{1}{2}\frac{\partial V}{\partial X}, \quad (4.12a)$$

$$\frac{A''}{A} = -\frac{\epsilon}{3} [2X'^2 + V(X)], \quad (4.12b)$$

$$\left(\frac{A'}{A}\right)^2 = \frac{k^2}{A^2} + \frac{\epsilon}{3} [X'^2 - V(X)]. \quad (4.12c)$$

Equation (4.12c) fixes the constant k .

Before solving the above equations (4.12), let us pause to consider what we mean by a “wall solution.” We know now that $X = X_F$ and a de Sitter spacetime will always be a solution of these equations, which we do not want to call a wall, since

the Higgs field remains in its false vacuum value throughout space. Putting $X = X_F$ into (4.12b, 4.12c), we get

$$\begin{aligned} A(z) &= \cos(kz), \\ k^2 &= \frac{\epsilon}{3} \end{aligned} \tag{4.13}$$

and therefore

$$ds^2 = \cos^2(kz) dt^2 - e^{2kt} \cos^2(kz) (dx^2 + dy^2) - dz^2. \tag{4.14}$$

Although this is a rather unfamiliar form for the de Sitter metric, it can be cast into the usual $ds^2 = d\tau^2 - e^{2k\tau} d\mathbf{x}^2$ by transforming the t and z coordinates to τ and ζ , such that $e^{k\tau} = e^{kt} \cos(kz)$ and $\zeta = \tan(kz)e^{-kt}/k$.

In section 4.5, we will investigate which solutions are admitted by the system of equations (4.12). In particular, we want to know which solutions are stable or unstable in what range of the parameter ϵ . Clearly, the vdS solution is a solution for all values of ϵ , but it is not necessarily always stable; indeed, this solution is *always* unstable to the scalar field rolling down the potential to the same minimum $+1$ or -1 throughout spacetime. We are not interested in this trivial instability; the one that interests us here is the instability to decay into a domain wall configuration.

We define a domain wall solution to be a function $X(z)$ of the proper distance from the wall such that $X(0) = X_F$. Moreover, we shall require that the function $(X(z) - X_F)$ be odd, which corresponds to imposing that X tends to different vacua as $z \rightarrow \pm\infty$, i.e. that the solution is topological. Concerning the boundary conditions, we shall see that when gravity is switched on, the Higgs field may not have the time to reach its true vacuum value at the horizon (which will be for us the limit of validity of the coordinates in the z -direction). Therefore we cannot impose $X_h \stackrel{\text{def}}{=} X(z_h) = \pm 1$. However, we see from equation (4.12a) that as we reach the horizon and $A \rightarrow 0$, A'/A blows up and if we want the solution to be regular we must require $X'_h \stackrel{\text{def}}{=} X'(z_h) = 0$. Moreover, we shall only consider solutions which have reflection symmetry around $z = 0$, which means $A'(0) = 0$. Finally, we can choose t so that $A(0) = 1$.

4.3 Analytical Predictions

In this section, we would like to see if it is possible to determine any properties of the solutions of equations (4.12) analytically. First, we know that wall solutions do exist in flat spacetime, and therefore we expect that for small ϵ these solutions will still exist by continuity, albeit perturbed by the inclusion of gravity. In particular, they will exhibit a cosmological horizon at some very large proper distance z_h . As ϵ increases, we expect the horizon to move closer to the defect's core, until roughly $\epsilon = O(1)$, at which point the horizon moves inside the domain wall. One of two things could then happen.

1. The scalar field ignores the proximity of the horizon and falls away minutely from the false vacuum. That is, X_h can be arbitrary close to the false vacuum X_F without being actually identical to it. Of course, since this solution's energy would be dominated by its vacuum contribution, we would expect the Einstein equation to be close to (4.8) and the resulting spacetime to be almost de Sitter; however, a wall solution would exist for all values of ϵ .
2. The scalar field admits two qualitatively different types of solution. In the first kind, the field at the horizon remains relatively close to the true vacuum value, $X_h = O(1)$; and in the second kind $X(z) \equiv X_F$, and the spacetime is *exactly* de Sitter. These two kinds of solution should be separated by a phase transition at some particular value ϵ_{\max} . Contrary to the previous case, wall solutions would not exist at all beyond the phase transition.

Figure 4.1 shows schematically the evolution of X_h with ϵ in two scenarios above. (We have used in this discussion and in the figure the fact that $X'(z) \geq 0$ and therefore $X_h = X_F$ implies $X(z) \equiv X_F$. See figure 4.4.) From the work of Basu & Vilenkin [12], and our own work from chapter 6 (which predates this research), we would expect the second scenario to hold. Our goal in this section is to determine analytically whether a wall solution can be found for all values of ϵ , and if the vdS solution is stable for all values of ϵ . This will establish (beyond any numerical uncertainty) which of the two possibilities above is realized.

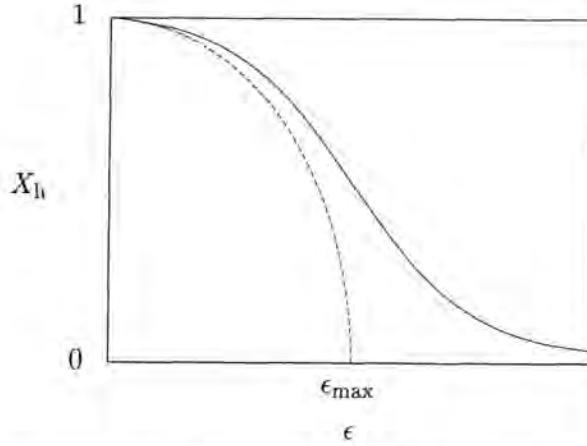


Figure 4.1: The evolution of $X_h(\epsilon)$ in the two different scenarios. In the first scenario (solid line), X_h can take arbitrarily small values. In the second, we observe a phase transition at some ϵ_{\max} , after what $X_h = 0$.

4.3.1 Existence of a Wall Solution

For a nontrivial wall solution, we require that $X(0)' > 0$ and $X'(z_h) = 0$. Taking the derivative of the scalar equation (4.12a) yields

$$X''' = -3\frac{A'}{A}X'' + X' \left[-3\frac{A''}{A} + 3\left(\frac{A'}{A}\right)' + \frac{1}{2}\frac{\partial^2 V}{\partial X^2} \right] = -3\frac{A'}{A}X'' + F(z)X', \quad (4.15)$$

where [using (4.12b)]

$$F(z) = 3\epsilon X'^2 + 3\frac{k^2}{A^2} + \frac{1}{2}\frac{\partial^2 V}{\partial X^2}. \quad (4.16)$$

Now, at $z = 0$, (4.12c) gives $0 < 3k^2 = \epsilon[1 - X'(0)^2]$, and thus

$$X'''(0) = X'(0) \left[3\epsilon - 6k^2 + \frac{1}{2}\frac{\partial^2 V}{\partial X^2} \right] > X'(0) \left[\epsilon + \frac{1}{2}\frac{\partial^2 V}{\partial X^2} \right], \quad (4.17)$$

Therefore, if $\epsilon > |V''(X_F)|/2$, $X''' > 0$ and X' is increasing and can never vanish at the horizon. We conclude that *there can be no wall solution for*

$$\epsilon > \frac{1}{2} |V''(X_F)|. \quad (4.18)$$

This condition becomes $\epsilon > 2$ for the Goldstone model and $\epsilon > 1/4$ for the sine-Gordon model.

4.3.2 Stability of the Vacuum-de Sitter Solution

We know that the vdS solution exists for all values of ϵ , and that for $\epsilon > |V''(X_F)|/2$ it is the only solution. However, we still need to determine the stability of this solution to decaying into a domain wall solution for smaller values of ϵ .

To do this, consider a vdS solution, $A(z) = \cos(kz)$, $X = X_F$ and $k^2 = \epsilon/3$. This solution will be stable if there is no perturbation $\xi(t, z)$ of X_F which is odd in z and growing in time. Setting $X = X_F + \xi$, we note that the corrections to the geometry are $O(\xi^2)$ (and thus negligible). The question of the stability of the vdS solution then translates into whether the following linearized equation for ξ

$$\xi'' - 3k \tan(kz) \xi' - \sec^2(kz) (\ddot{\xi} + 2k\dot{\xi}) - \frac{1}{2} \frac{\partial V}{\partial X} = 0 \quad (4.19)$$

admits any solutions of the type described above.

We find that (4.19) does indeed admit unstable solutions for

$$k^2 = \frac{\epsilon}{3} < \frac{1}{8} |V''(X_F)|,$$

the leading instability being given by

$$\xi = e^{k\nu t} \sin(kz) \cos^\nu(kz), \quad (4.20)$$

where

$$\nu = -\frac{5}{2} + \frac{1}{2k} \sqrt{9k^2 - 2V''(X_F)}. \quad (4.21)$$

Thus for

$$\epsilon < \epsilon_{\max} \stackrel{\text{def}}{=} \frac{3}{8} |V''(X_F)|, \quad (4.22)$$

the vdS solution is unstable to decay into a wall solution. Numerically, we then have

$$\epsilon_{\max} = \begin{cases} \frac{3}{2} & \text{for Goldstone,} \\ \frac{3}{16} = 0.1875 & \text{for sine-Gordon.} \end{cases} \quad (4.23)$$

In the interval $(\epsilon_{\max}, \frac{4}{3}\epsilon_{\max})$, we must resort to numerical methods to decide which solution is the true one.

4.3.3 A More General Perturbation

One might be worried that the previous analysis might not be correct because it was not carried out in a global coordinate system for de Sitter spacetime. Indeed, it is conceivable that there exists some perturbation which is bounded in time in the patch covered by our coordinates $\{t, x, y, z\}$ but unbounded elsewhere on the de

Sitter hyperboloid. Let us consider here the global system of coordinates $\{\tilde{t}, \chi, \theta, \phi\}$, in which the metric takes the Robertson–Walker form [56]

$$ds^2 = d\tilde{t}^2 - \frac{1}{k^2} \cosh(k\tilde{t})^2 \left\{ d\chi^2 + \sin^2(\chi) [d\theta^2 + \sin^2(\theta) d\phi^2] \right\}. \quad (4.24)$$

Then one can check that the equation to be satisfied by a perturbation $\xi(t, \chi)$ is (in the Goldstone case)

$$\ddot{X} + 3k \tanh(kz) \dot{X} - k^2 \operatorname{sech}^2(k\tilde{t}) [X'' + 2 \cot(\chi) X'] = 2X. \quad (4.25)$$

The condition that X be odd in z translates to X being odd in χ around $\chi = \pi/2$. Separating variables, $X(\tilde{t}, \chi) = \xi(\tilde{t}) \mu(\chi)$, we get

$$\mu'' + 2 \cot(\chi) \mu' - \frac{C}{k^2} \mu = 0, \quad (4.26a)$$

$$\ddot{\xi} + 3k \tanh(k\tilde{t}) \dot{\xi} - [2 + C \operatorname{sech}^2(k\tilde{t})] \xi = 0, \quad (4.26b)$$

where C is a constant. The first equation is solved by $\mu = \cos(\chi)$ or $\mu = \cot(\chi)$; the latter being singular, we choose $\mu = \cos(\chi)$, which implies $C = -3k^2$. It is then possible to find the general solution of the equation for ξ , which is given in terms of the hypergeometric function ${}_2F_1(a, b; c; z)$ by

$$\begin{aligned} \xi(t) = & \alpha \operatorname{sech}^2(k\tilde{t})^{\frac{3}{4}-\gamma} {}_2F_1\left(-\frac{3}{4}-\gamma, \frac{5}{4}-\gamma; 1-2\gamma; \operatorname{sech}^2(k\tilde{t})\right) + \\ & \beta \operatorname{sech}^2(k\tilde{t})^{\frac{3}{4}+\gamma} {}_2F_1\left(-\frac{3}{4}+\gamma, \frac{5}{4}+\gamma; 1+2\gamma; \operatorname{sech}^2(k\tilde{t})\right) \end{aligned} \quad (4.27)$$

where α and β are constants and

$$\gamma = \frac{\sqrt{9k^2 + 8}}{4k}. \quad (4.28)$$

For the purposes of checking when this solution is stable, we can set $\beta = 0$ because the second hypergeometric function falls off to zero for large \tilde{t} . The first hypergeometric function, on the other hand, explodes at $\tilde{t} \rightarrow \infty$ for any value of k , and thus of ϵ , although its values remain smaller longer for large k .

Transforming back this perturbation into our original set of coordinates $\{t, x, y, z\}$, we find

$$\xi(t, x, y, z) = \sin(kz) \zeta^{-\nu/2} {}_2F_1\left(-\frac{\nu+4}{2}, -\frac{\nu}{2}; -\frac{2\nu+3}{2}; \zeta\right), \quad (4.29)$$

where

$$\zeta^{-1} \stackrel{\text{def}}{=} 1 + \cos^2(kz) \left[\sinh(kt) - \frac{k^2}{2} \rho^2 e^{kt} \right]^2 \quad (4.30)$$

and ν is the parameter defined in (4.21). Therefore, this depends on $\rho^2 \stackrel{\text{def}}{=} x^2 + y^2$, and the de Sitter solution decays into a solution of a kind we do not consider in this chapter.

4.4 Weak Gravity

In flat spacetime, $A = 1$ and we can integrate equation (4.12a) to get an implicit solution $z(X)$ which we could in principle invert to get $X(z)$:

$$X'^2 = V(X) \quad \Rightarrow \quad z = \int_{X_F}^X \frac{dY}{\sqrt{V(Y)}}. \quad (4.31)$$

For small ϵ , therefore, we expect to find wall solutions close to equation (4.31).

Let us therefore expand all quantities in powers of ϵ and solve order by order:

$$\begin{aligned} X(z) &= X^{(0)}(z) + \epsilon X^{(1)}(z) + \epsilon^2 X^{(2)}(z) + O(\epsilon^3), \\ A(z) &= A^{(0)}(z) + \epsilon A^{(1)}(z) + \epsilon^2 A^{(2)}(z) + O(\epsilon^3). \end{aligned} \quad (4.32)$$

To zeroth order, we find of course that $X^{(0)}$ is given by the flat spacetime solution (4.31) and that $A^{(0)} = 1$. To order ϵ , we then obtain the following equations:

$$X^{(1)''} = -3A^{(1)'}X^{(0)'} + \frac{1}{2}X^{(1)} \frac{\partial^2 V}{\partial X^2} \Big|_{X^{(0)}(z)}, \quad (4.33a)$$

$$A^{(1)''} = -\frac{1}{3} [2X^{(0)'}{}^2 + V(X^{(0)})] = -X^{(0)'}{}^2. \quad (4.33b)$$

The boundary conditions for $X^{(1)}$ and $A^{(1)}$ are

$$A^{(1)}(0) = A^{(1)'}(0) = 0; \quad X^{(1)}(0) = 0, X^{(1)} \rightarrow 0 \quad \text{for large } z. \quad (4.34)$$

Then we can integrate (4.33) to get

$$A^{(1)} = - \iint V(X^{(0)}) dz = - \int \frac{dX}{\sqrt{V}} \int dX \sqrt{V}, \quad (4.35a)$$

$$X^{(1)} = -\frac{3}{2} X^{(0)'} \int \frac{dz}{X^{(0)'}{}^2} \left(A^{(1)'} - \frac{k^2}{\epsilon^2} \right) \quad (4.35b)$$

and also,

$$k^2 = \epsilon^2 \left[A^{(1)'}{}^2 + \frac{2}{3} (X^{(1)} X^{(0)''} - X^{(0)'} - X^{(1)'}) \right] = -\frac{2}{3} \epsilon^2 X^{(0)'}(0) X^{(1)'}(0). \quad (4.36)$$

4.4.1 The Goldstone Model

Consider the specific case of the Goldstone model, $V(X) = (X^2 - 1)^2$, with the usual flat spacetime kink solution $X(z) = \tanh(z)$ (figure 4.2). Then, equations (4.33,

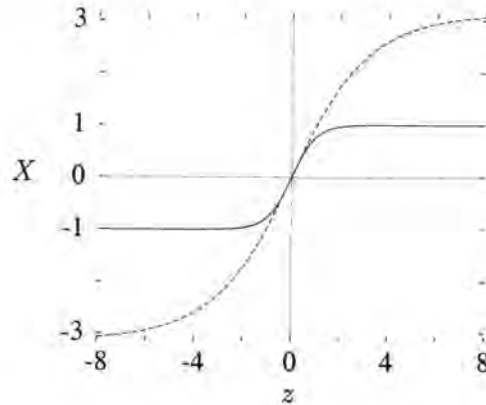


Figure 4.2: The flat spacetime solutions $X = \tanh(z)$ for the Goldstone model (solid line) and $X = 4 \arctan(e^{z/2}) - \pi$ for the sine-Gordon model of section 4.4.2.

4.36) give:

$$X^{(1)} = -\frac{1}{6} \operatorname{sech}^2(z) [3z + \tanh(z)], \quad (4.37a)$$

$$A^{(1)} = -\frac{2}{3} \ln \cosh(z) - \frac{1}{6} \tanh^2(z). \quad (4.37b)$$

To summarize, to first order we find

$$X = \tanh(z) - \frac{\epsilon}{6} \operatorname{sech}^2(z) [3z + \tanh(z)] + O(\epsilon^2), \quad (4.38a)$$

$$A = 1 - \frac{\epsilon}{3} \left[2 \ln \cosh(z) - \frac{1}{2} \tanh^2(z) \right] + O(\epsilon^2), \quad (4.38b)$$

$$k = \frac{2}{3} \epsilon + O(\epsilon^2). \quad (4.38c)$$

This solution is compared with the one found numerically on figure 4.3.

4.4.2 The Sine-Gordon Model

Now, let us consider the potential $V(X) = \frac{1}{2} (1 + \cos X) = \cos^2(X/2)$. This time, equation (4.31) gives

$$X^{(0)} = 4 \arctan(e^{z/2}) - \pi. \quad (4.39)$$

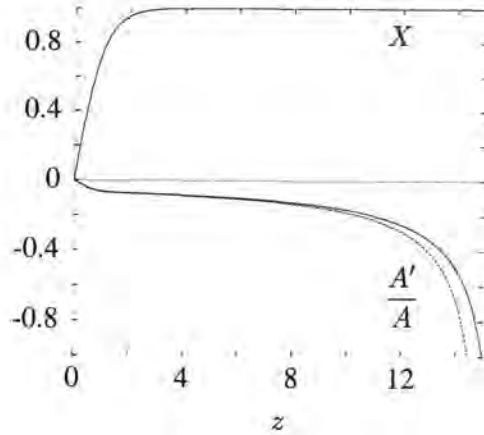


Figure 4.3: Comparison between the numerical solution (solid line) and the first order approximation equation (4.38). At this scale the two solutions for the scalar field are superposed. This is done for $\epsilon = 1/10$.

The backreaction to order $O(\epsilon^2)$ this time is given by

$$X = 4 \arctan \left(e^{z/2} \right) - \pi - 6\epsilon z \operatorname{sech} \left(\frac{z}{2} \right), \quad (4.40a)$$

$$A = 1 - 4\epsilon \ln \cosh \left(\frac{z}{2} \right), \quad (4.40b)$$

$$k = 2\epsilon. \quad (4.40c)$$

4.5 Strong Gravity

If $\epsilon \ll 1$, our expansion breaks down, and we must solve the equations (4.12) numerically. In fact, we can split this problem in two parts by rewriting (4.12b) as

$$\left(\frac{A'}{A} \right)' + \left(\frac{A'}{A} \right)^2 + \frac{\epsilon}{3} [2X'^2 + V(X)] = 0, \quad (4.41)$$

and solving the following equations

$$X' = Y, \quad (4.42a)$$

$$Y' = -3YZ + \frac{1}{2} \frac{\partial V}{\partial X}, \quad (4.42b)$$

$$Z' = -\frac{\epsilon}{3} [2Y^2 + V(X)] - Z^2 \quad (4.42c)$$

for X, Y and $Z \stackrel{\text{def}}{=} A'/A$. Then, of course, one obtains $A(z)$ by exponentiation of the integral of $Z(z)$, and k via equation (4.12c). The boundary conditions required for a wall solution are $X(0) = Z(0) = Y(z_h) = 0$.

In this section, we consider only the Goldstone case; the results for sine-Gordon are rather similar, and we postpone their presentation to the next section. To solve

these equations, we have used the routine SOLVDE from [82]. Typically, we obtain wall solutions such as the one shown on figure 4.4. As we can see, X does not go to its asymptotic value $X = \pm 1$ at the horizons (and consequently the energy density does not vanish there).

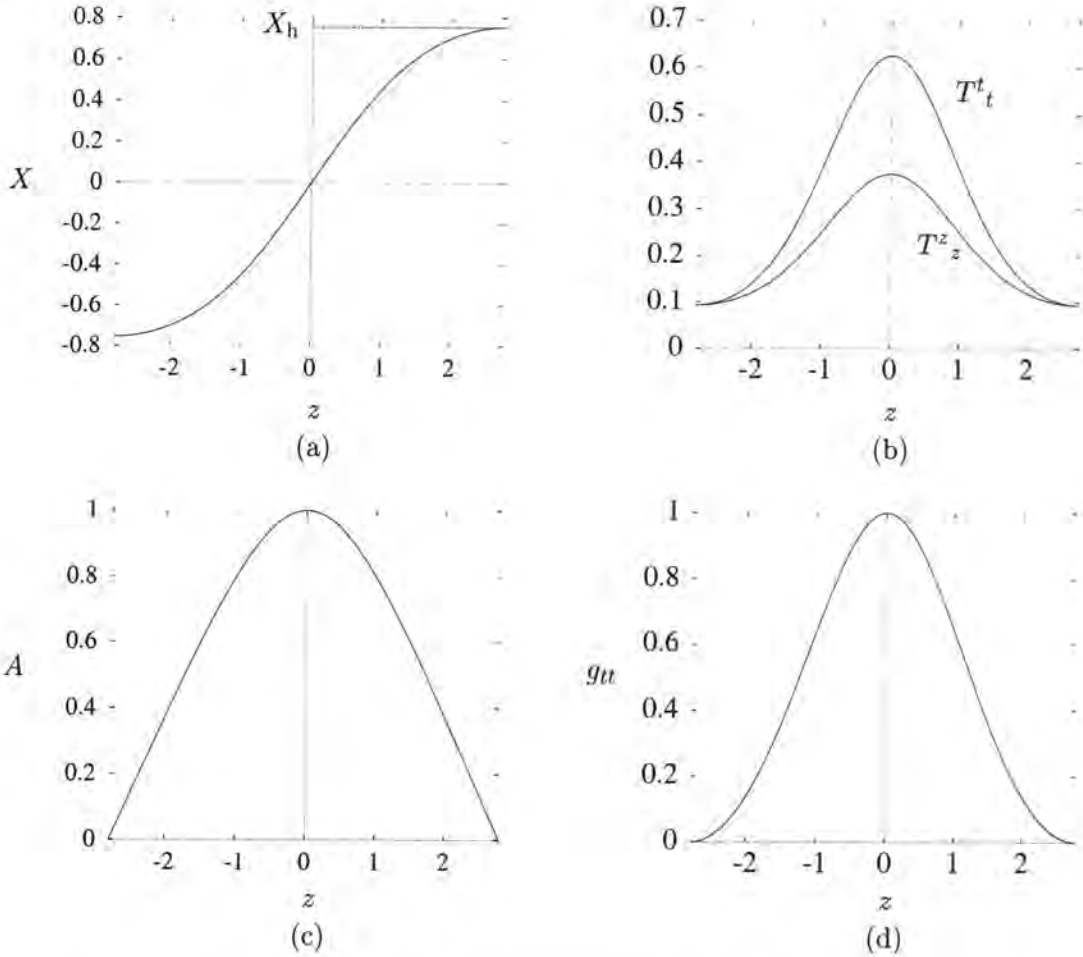


Figure 4.4: Numerical solution of the equations (4.42) for the Goldstone model. This solution was obtained for $\epsilon = 0.9$ (in which case the horizon was situated at a proper distance $z_h = 2.789$). The figure shows (a) the Higgs field, (b) the energy momentum tensor $T^x_x = T^y_y = T^t_t$ and T^z_z , (c) the function $A(z)$ and (d) the metric component $g_{tt}(z) = A^2(z)$.

We want to follow the solutions numerically from the weak to the strong gravity sectors. In section 4.3 we argued that for $\epsilon < \epsilon_{\max} = 1.5$ the de Sitter solution should be unstable to decay into a wall solution, whereas for $\epsilon > 2$ wall solutions could not exist any more. This implies that there exists a phase transition between the two regimes, and this is what we want to check numerically. To do this, we see from the general shape of the wall solutions for the scalar field X , and from the

fact that $X_F = 0$, that it suffices to follow the evolution with ϵ of the value X_h . The “wall phase” corresponds to $X_h > 0$ and the vdS phase to $X_h = 0$. The result is presented in figure 4.5a. Part b of this figure shows the evolution of the proper distance to the horizon; for very small ϵ , we see that this tends to the dashed line $z_h = 3/2\epsilon$, but quadratic corrections quickly spoil the agreement.

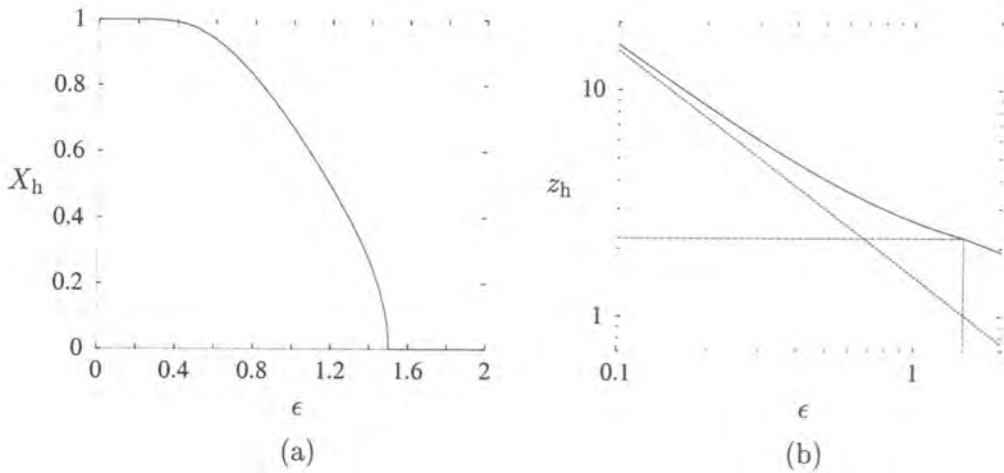


Figure 4.5: (a) The evolution of X_h as a function of ϵ . (b) Log-log plot of the proper distance to the horizon as a function of ϵ (solid line) compared with the first order prediction of $z_h = 3/2\epsilon$ (dashed line). The dash-dotted line indicates the phase transition at $\epsilon = 3/2$, $X_h \approx 2.221$: compare part (a) with figure 4.1.

Figure 4.5a is typical of a second-order phase transition (the first derivative of X_h is discontinuous) with order parameter ϵ . At the phase transition, we have the vdS solution, for which the distance to the horizon is given by $A^2(z) = 0$, *i.e.* $\cos(kz_h) = 0$. With $k = \epsilon^2/3$ and $\epsilon_{\max} = 3/2$, which gives $z_h = \pi/\sqrt{2} \approx 2.221$. This is in good agreement with the observation (dot-dashed line in figure 4.5b), and confirms and refines the analytic results of section 4.3: in the zone $\epsilon \in (\epsilon_{\max}, \frac{4}{3}\epsilon_{\max})$ we find vdS solutions.

4.6 Domain Walls in a de Sitter or Anti-de Sitter Background

In this section we want to show that it is rather straightforward to consider domain wall solutions in a de Sitter or anti-de Sitter background. First of all, adding a cosmological constant consists in replacing the Einstein tensor $G_{ab} = R_{ab} - \frac{1}{2}g_{ab}R$ by $G_{ab} + \Lambda g_{ab}$ in (4.7b), and the equations of motion (4.12) must be modified as

follows:

$$X'' + 3\frac{A'}{A}X' = \frac{1}{2}\frac{\partial V}{\partial X}, \quad (4.43a)$$

$$\frac{A''}{A} = -\frac{\epsilon}{3}[2X'^2 + V(X)] - \frac{1}{3}\Lambda, \quad (4.43b)$$

$$\left(\frac{A'}{A}\right)^2 = \frac{k^2}{A^2} + \frac{\epsilon}{3}[X'^2 - V(X)] - \frac{1}{3}\Lambda. \quad (4.43c)$$

There are two qualitatively different cases: if $\Lambda > 0$ the background is de Sitter, and if $\Lambda < 0$ the wall is embedded in anti-de Sitter spacetime. The latter case is of particular interest because the effect of the cosmological constant counteracts that of the effective cosmological constant created by the wall's backreaction [see equation (4.8) and the discussion attached to it]. Note as well that, strictly speaking, for an anti-de Sitter background, $k^2 < 0$ if we want the reflection symmetry around $z = 0$. For the metric to be real, this would then imply $b(t) = \cos(kt)$, which requires the $\{x, y\}$ sections to be hyperbolic [35]. However, this does not affect the equations of motion, and we will not discuss it further; for a more detailed discussion of domain walls in an anti-de Sitter background, see [36].

Now, let us notice that when $X \equiv 0$ (i.e., the vdS solution) equations (4.43) reduce to equations (4.12) if we replace ϵ by $\Lambda_{\text{eff}} \stackrel{\text{def}}{=} \epsilon + \Lambda$. The analytical argument of section 4.3.2 was carried out using the vdS solution, and should still be valid upon replacement of ϵ by the effective cosmological constant Λ_{eff} . This means that we should still observe a phase transition, since now there are no more wall solutions for $\Lambda > \frac{3}{8}|V''(V_F)|$. Numerically, one can check that varying ϵ and Λ with Λ_{eff} fixed always gives the the same vdS solution. For the wall solutions, the terms with ϵ multiplying X' clearly spoil this invariance.

Figure 4.6 shows the evolution of the value of X_h as a function of ϵ and Λ for both models we considered. Λ takes the values $-0.3, -0.2, \dots, 0.3$ in these figures. (In the sG case, figure 4.6b, we do not see any curves for $\Lambda = 0.2$ or 0.3 because the condition tells us that for $\Lambda > 3/16 = 0.1875$ the only solutions are vdS.) Notice that in the Goldstone case (figure 4.6a) the curves seem to have retained some of the translational symmetry of the vdS solutions.

Figure 4.7 shows the evolution of the proper distance to the horizon as a function of ϵ and Λ for the same values of the parameter Λ . Note that at the phase transition

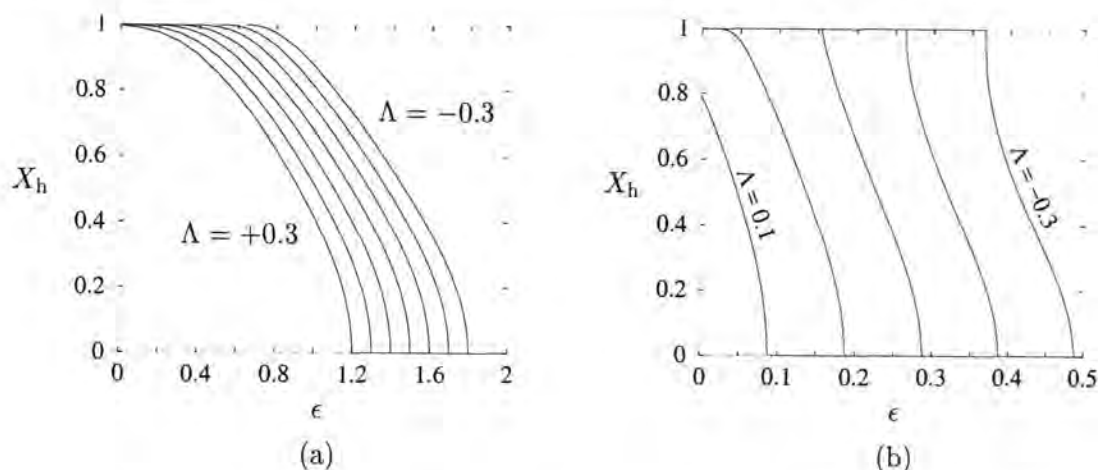


Figure 4.6: Evolution of X_h as a function of ϵ and Λ (from right to left, $\Lambda = -0.3, -0.2, \dots, 0.2, 0.3$). (a) shows the Goldstone case, and (b) shows the sine-Gordon case. In (b) we have actually divided X_h by π to help the comparison with case (a).

this distance is always the same ($\pi/\sqrt{2}$ for Goldstone and 2π for sine-Gordon), as expected from the discussion above.

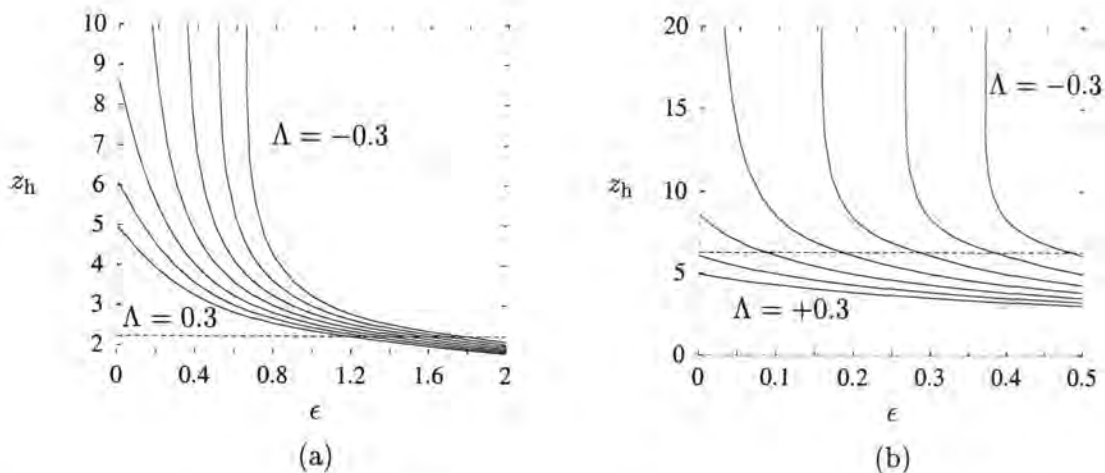


Figure 4.7: Distance from the wall to the horizon, as a function of ϵ , for the same values of Λ as in figure 4.6. (a) was obtained for the Goldstone model and (b) for sine-Gordon. Again, the broken lines show the values of z_h at the phase transition.

Now let us turn to the solution in the anti-de Sitter case, $\Lambda < 0$. We now find *three* qualitatively distinct solutions. For very small ϵ , the wall's self-gravitation cannot compete with the anti-de Sitter expansion and A'/A is strictly positive; in fact, it is easy to check that the solution plotted on figure 4.8a is $A(z) = \cosh(\sqrt{|\Lambda|/3}z)$. As one increases ϵ , the metric potential A is observed to decrease close to the wall's core, whereas the Higgs profile is slightly smoothed (figure 4.8b). This is the begin-

ning of a complete change in the metric function $A(z)$: as the wall's gravitational interaction is switched on, A assumes the shape of a "double well," with a local maximum at the imposed boundary value $A(0) = 1$ and two local minima symmetrically situated at $A(\pm z_m)$ for some z_m . As ϵ increases, this double well becomes deeper, whereas z_m moves away from the wall. Notice that so far the function $A(z)$ is strictly positive, and therefore none of these solutions exhibit an horizon. Eventually, however, for some critical value ϵ_c of ϵ , the two minima of $A(z)$ vanish as $z_m \rightarrow \infty$ (figure 4.8c). For $\epsilon > \epsilon_c$, the metric potential becomes negative at a finite distance z_h , thus giving rise to the wall's horizon.

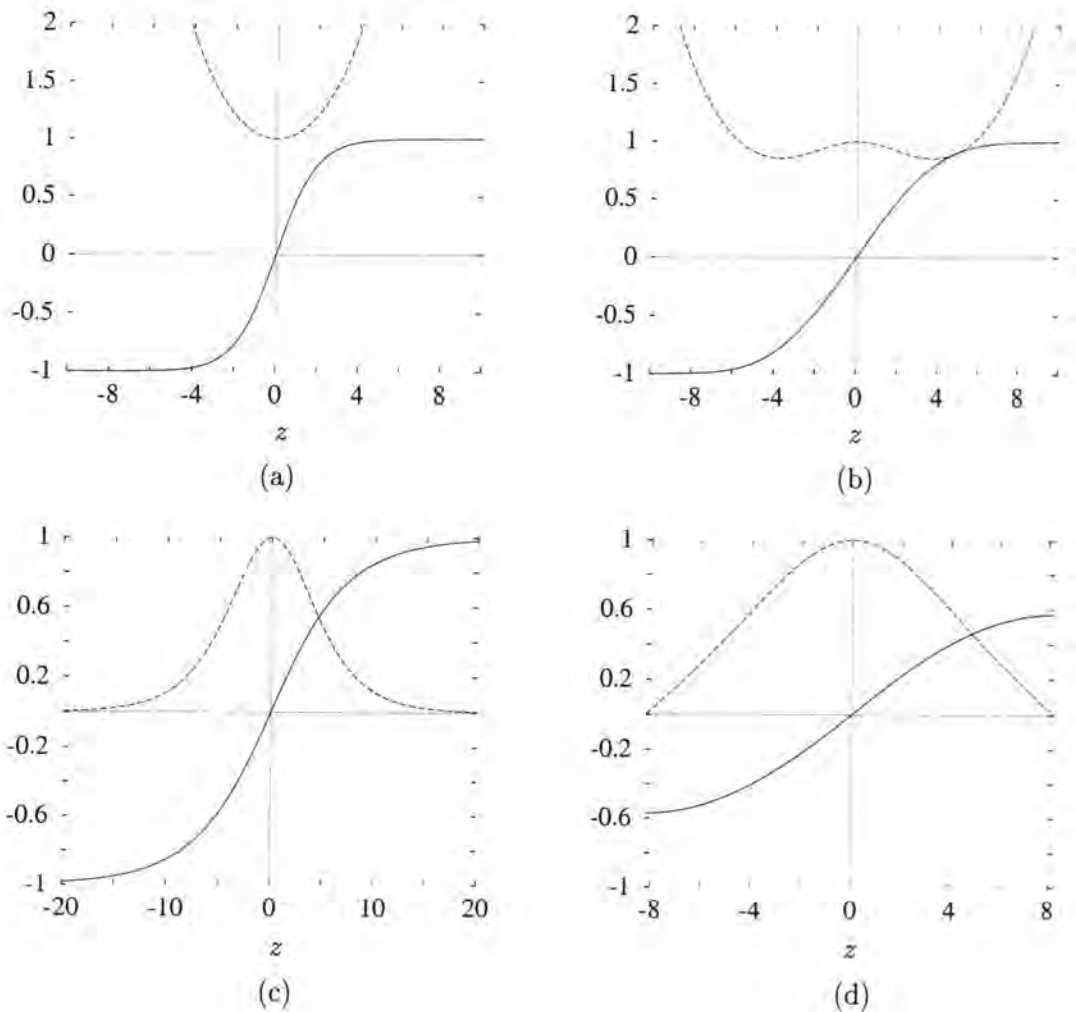


Figure 4.8: Solutions $X(z)$ (solid lines) and $A(z)$ to the sine-Gordon equations for $\Lambda = -0.3$ and $\epsilon = 0$ (a); 0.2 (b); $0.367\dots$ (c) and 0.4 (d).

Figure 4.9 shows the parameter space (Λ, ϵ) , and the different kinds of solution that we find. It is interesting to note that the two lines separating the three phases

seem to run parallel with each other in both cases, indicating that a phenomenon similar to the triple point observed in the phase diagram of water never occurs. This is to be expected, since as long as the wall does not have an event horizon it is constrained to take its asymptotic value at infinity. (Of course, this topological constraint does not imply that the lines are parallel, merely that they cannot meet in the physical range $\epsilon > 0$; figure 4.9 then suggests that the range of the parameter ϵ over which the value of the Higgs field at the horizon is allowed to drop from 1 to 0 is approximately constant.)

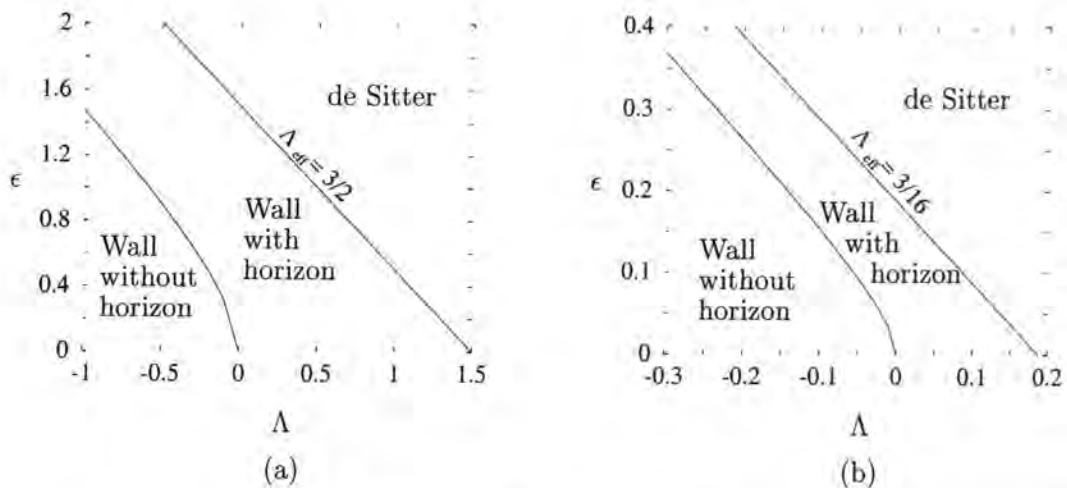


Figure 4.9: Parameter space (Λ, ϵ) and the types of solutions found numerically for (a) Goldstone and (b) sine-Gordon.

Finally, we can show a bifurcation diagram for this phase transition by plotting a normalized action \bar{S} against ϵ for the different solutions (figure 4.10). Using the form of our metric, we find that

$$R = 6 \left(\frac{A''}{A} + \frac{A'^2}{A^2} - \frac{k^2}{A^2} \right), \quad (4.44)$$

and from (4.12b, 4.12c) we get

$$S = \int d^4x \sqrt{-g} (\mathcal{L}_G + \mathcal{L}_M) = \eta^2 \int d^4x e^{2kt} A^3 V(X) = N \int_0^{z_h} dz A^3 V(X) \quad (4.45)$$

where N contains the integrations over t, x and y . The normalized action is then $\bar{S} = S/N$. For the vdS solution, $\bar{S} = 2/3k = 2/\sqrt{3\epsilon}$.

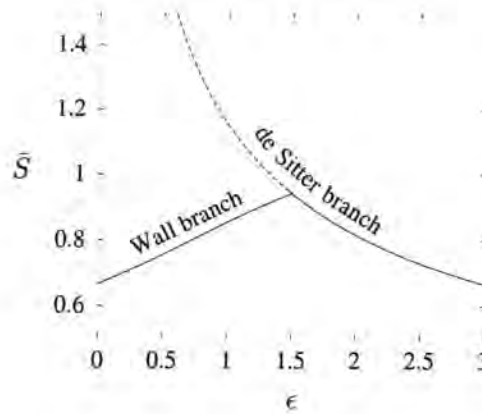


Figure 4.10: Bifurcation diagram for the gravitating Goldstone wall. We plot here the normalized action \bar{S} as a function of ϵ . Solid lines indicate the stable solutions found numerically, and the dashed line represents the unstable de Sitter solution.

4.7 Discussion and Conclusion

The lack of existence of wall solutions for $\epsilon > \epsilon_{\max}$ and the phase transition by which this occurs are two interesting results obtained in this chapter. We can gain a different insight on this phenomenon by considering the topology of the wall and vdS spacetimes; let us start with the de Sitter solutions, whose well-known topology [56] is pictured on figure 4.11.

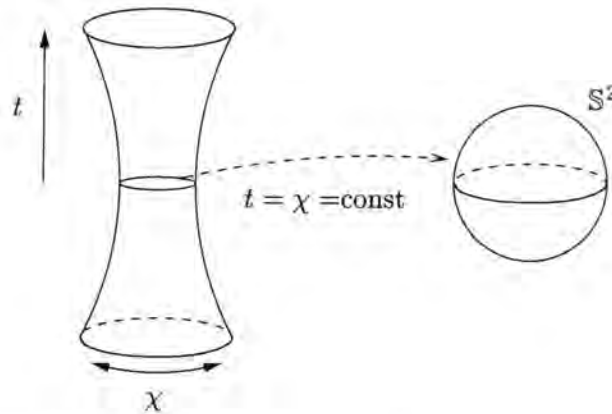


Figure 4.11: The de Sitter hyperboloid and its spherical section, obtained by fixing the time coordinate as well as one spatial coordinate, χ in this case.

The four-dimensional de Sitter spacetime can be viewed as a hyperboloid embedded in five-dimensional Minkowski spacetime $ds^2 = dv^2 - dw^2 - dx^2 - dy^2 - dz^2$, with equation

$$v^2 - w^2 - x^2 - y^2 - z^2 = -k^{-2}. \quad (4.46)$$

Introducing global coordinates on the hyperboloid, the four-dimensional metric can be written as (4.24)

$$ds^2 = d\tilde{t}^2 - \frac{1}{k^2} \cosh(k\tilde{t})^2 [d\chi^2 + \sin(\chi)^2 (d\theta^2 + \sin(\theta)^2 d\phi^2)]. \quad (4.47)$$

We see that the sections of constant \tilde{t} are described by three-dimensional spheres of radius $[\cosh(k\tilde{t})/k]^2$. This radius is increasing exponentially fast (recall the exponential form for this metric from page 54) which is why the de Sitter spacetime is said to describe an inflating universe.

Let us now consider the wall solutions, whose metric is given by (4.9),

$$ds^2 = A^2(z) dt^2 - B^2(t, z) (dx^2 + dy^2) - dz^2, \quad (4.48)$$

with $B(t, z) = A(z) e^{kt}$. Defining a new set of coordinates by

$$\begin{aligned} x^* &\stackrel{\text{def}}{=} A(z) e^{kt} x, \\ y^* &\stackrel{\text{def}}{=} A(z) e^{kt} y, \\ t^* - z^* &\stackrel{\text{def}}{=} -\frac{1}{k} A(z) e^{kt}, \\ t^* + z^* &\stackrel{\text{def}}{=} \frac{1}{k} A(z) e^{-kt} - k(x^2 + y^2) A(z) e^{kt}, \end{aligned} \quad (4.49)$$

the metric can be written

$$ds^2 = dt^{*2} - dx^{*2} - dy^{*2} - dz^{*2} - \left(1 - \frac{A'^2}{k^2}\right) dz^2. \quad (4.50)$$

This is very close to the five-dimensional Minkowski metric, and we can cast (4.50) into that form by defining a fifth variable

$$w^* \stackrel{\text{def}}{=} \int_0^z \sqrt{1 - \frac{A'^2(z)}{k^2}} dz; \quad (4.51)$$

we then see the wall spacetime as a four-dimensional hypersurface embedded in the flat five-dimensional spacetime, just like the de Sitter hyperboloid.

To find what this hypersurface is, note that in the “starred” coordinates, z is given implicitly by

$$k^2 (t^{*2} - x^{*2} - y^{*2} - z^{*2}) = -A^2(z), \quad (4.52)$$

which, in terms of the variable w^* , must be rewritten

$$t^{*2} - x^{*2} - y^{*2} - z^{*2} = -\frac{A^2[z(w^*)]}{k^2}. \quad (4.53)$$

For de Sitter, $A(z) = \cos(kz)$, $w^* \equiv \sin(kz)/k$, and (4.53) reduces to the hyperboloid (4.46). For the wall solutions, we can only work analytically in the small- ϵ limit; for sine-Gordon solutions, we find

$$w^* = \int_0^z \operatorname{sech}(z/2) dz = 4 \arctan(e^{z/2}) - \pi = X^{(0)}(z). \quad (4.54)$$

The hypersurface is then given by a hyperboloid which has been squashed in the w^* direction,

$$t^{*2} - x^{*2} - y^{*2} - z^{*2} = -\frac{1}{4\epsilon^2} [1 + 4\epsilon \ln \cosh(w^*/2)]. \quad (4.55)$$

The spatial section of this hypersurface is plotted, for $\epsilon = 1/30$, on figure 4.12. The wall is situated at the rim of the discus, in the region of high curvature, whereas far from it the hypersurface is flat, and the horizons on either side of the defect are situated at the poles of the ellipsoid. The two characteristic lengths of the problem, w_H and z_h , are roughly the two radii of the ellipsoid, the Higgs width corresponding to its fixed “height” (as shown in the figure) and the proper distance to the horizon to its “width.”

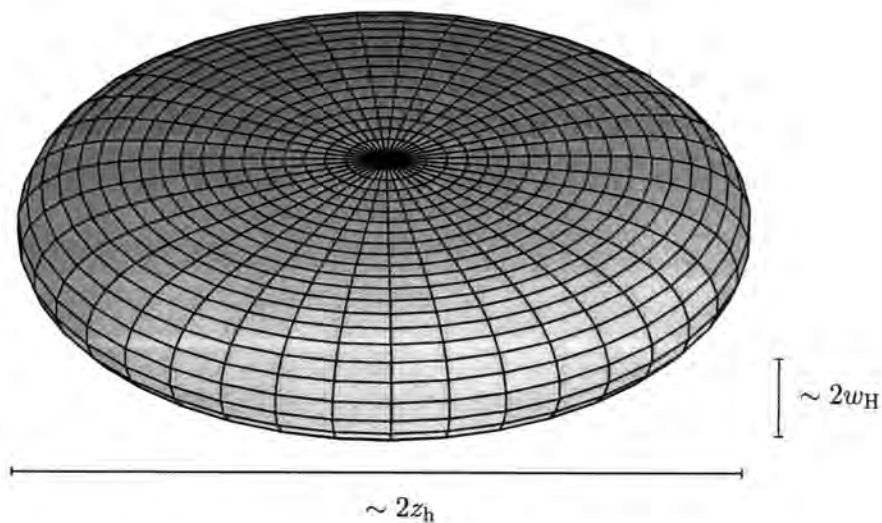


Figure 4.12: The $t^* = z^* = 0$ (ellipsoidal) section of the weakly gravitating sine-Gordon domain wall, here for $\epsilon = 1/30$.

We now see what happens to the solutions as we vary ϵ : for very small ϵ , the spatial section of the hypersurface is an ellipsoid which is very squashed, since z_h is very large. As ϵ increases, this squashing becomes less and less pronounced, until (at $\epsilon = \epsilon_{\max}$) the ellipsoid becomes the de Sitter sphere.

The reason for the disappearance of wall solutions at large gravitational coupling seems to be linked to the compactness of the wall's spatial section, which (as for de Sitter) is topologically identical to \mathbb{S}^3 . This phenomenon had already been observed by Avis & Isham [8] (and was rederived recently by Espichán Carrillo *et al.* [40]), who studied solutions of $\lambda\Phi^4$ theory in a spatially closed interval of \mathbb{R} . They found that when the interval becomes too small, all topological solutions cease to exist. What is new here is that it is the wall's self-gravity which compactifies spacetime at its own characteristic scale. (Most recently, a similar phenomenon was also observed in the case of monopoles [72].)

The Dynamics of Curved Gravitating Domain Walls

5.1 Introduction

When we have seen in chapter 3 that the motion of cosmic strings was inherently antirigid, we also remarked that our analysis was lacking a potentially important ingredient: gravity. In the previous chapter we have investigated the profound impact of the Higgs's self-gravity, not only on the spacetime surrounding it but also on the existence of topological solutions. In this chapter, we wish to bring these elements together and determine the dynamics of gravitating curved walls.

A special motivation for this research lies in the claims (see for instance [16,33,32]) that gravitating defects, strings or walls, might be totally geodesic. We have seen in the case of the string that the Nambu–Goto dynamics could be expressed in terms of the extrinsic curvatures as $\underline{\kappa}_\mu = 0$ for all μ ; this is quite general and also applies to the case of walls, as we shall see later. A “totally geodesic” defect satisfies the more restrictive dynamical condition $\underline{\kappa}_{\mu ab} = 0$ — in other words, the cores of these defects do not actually curve inside the background spacetime. There is some concern that this result is due to some overrestrictive assumptions, in particular regarding the form of the defect's metric. Sadly, this work is still in progress, and we will not be able, in this thesis, to settle definitely the question of whether the string is totally geodesic or not.

In the conclusion to chapter 3, we have noted that the effective action method might not work in the presence of gravity because the latter is mediated by a massless

particle. There is, however, another method to obtain the effective dynamics of a defect which does not require the integration of the action. In this method, which we follow here, the equations of motion at each order n are obtained from integrability constraints at order $n + 1$. Clearly, its disadvantage is that we must solve the field equations to one order higher than that of the effective equations of motion that we want to obtain.

We consider a domain wall identical to the “ $\lambda\Phi^4$ ” wall of the previous chapter, that is, we investigate the dynamics derived from the action

$$\begin{aligned} S &= S_G + S_M = \int dx^4 \sqrt{-g} (\mathcal{L}_G + \mathcal{L}_M), \\ \mathcal{L}_G &= -\frac{R}{16\pi G}, \\ \mathcal{L}_M &= (\nabla_a \Phi) (\nabla^a \Phi) - \lambda (\Phi^2 - \eta^2)^2, \end{aligned} \tag{5.1}$$

where all the “matter” parameters (Φ , λ and η) have the same interpretation as before. The gravitation Lagrangian \mathcal{L}_G is again the usual Hilbert action, with R being the spacetime Ricci scalar.

We introduce the new field X and the gravitational coupling ϵ by (4.2), which is

$$\begin{aligned} \Phi &= \eta X, \\ \epsilon &\stackrel{\text{def}}{=} 8\pi G\eta^2. \end{aligned} \tag{5.2}$$

This time, however, we do not yet rescale the coordinates, but explicitly keep w_H in the equations; the action and equations of motion become:

$$\bar{S} \stackrel{\text{def}}{=} -\frac{2\epsilon}{\eta^2} S = \int d^4x \sqrt{-g} \left\{ R - \frac{2\epsilon}{w_H} \left[w_H^2 (\nabla_a X) (\nabla^a X) - (X^2 - 1)^2 \right] \right\} \tag{5.3}$$

and

$$\square X = -\frac{2}{w_H^2} X (X^2 - 1), \tag{5.4a}$$

$$R_{ab} = \epsilon \left[2 (\nabla_a X) (\nabla^a X) - \frac{1}{w_H^2} g_{ab} (X^2 - 1)^2 \right]. \tag{5.4b}$$

5.2 The Equations of Motion

We are now going to use the Gauß–Codazzi formalism to reformulate the equations (5.4) in terms of the “geometrical” quantities introduced in chapter 2. The

wall is seen as a worldvolume \mathcal{W} embedded in the spacetime manifold \mathcal{M} . We can therefore define a single family of unit normals $n^a \stackrel{\text{def}}{=} (\partial/\partial z)^a$ (where we have defined the coordinates in such a way that the wall's core lies at $z = 0$) and compute the first and second fundamental forms for the defect; since the wall has codimension 1, there is no need to define the normal fundamental form, as it vanishes.

The equations of motion for the fundamental forms are can be found by taking Lie derivatives as in chapter 3; we get

$$\begin{aligned}\mathcal{L}_n h_{ab} &= 2K_{ab}, \\ \mathcal{L}_n K &= -K_{ab}^2 - \epsilon \left[2X_{,z}^2 + \frac{1}{w_H^2} (X^2 - 1)^2 \right], \\ \mathcal{L}_n K_{ab} &= -\frac{\epsilon}{w_H^2} h_{ab} (X^2 - 1)^2 + 2\epsilon (\hat{D}_a X) (\hat{D}^a X) + 2K_{ac} K_b^c - \parallel R_{ab} - K K_{ab}.\end{aligned}\tag{5.5}$$

Here, \hat{D}_a are the covariant derivatives parallel to the worldvolume.

The equations for X and R_{ab} can also be written in this “3+1” fashion. In fact, the diagonal equations for R_{ab} are identical to the equations for K_{ab} and K above; thus the only missing equations are the scalar and the non-diagonal Einstein equations, which read

$$X_{,zz} + K X_{,z} = 2X (X^2 - 1) + w_H^2 \hat{D}^2 X,\tag{5.6}$$

$$\hat{D}_b K^b_a - \hat{D}_a K = 2\epsilon X_{,z} \hat{D}_a X.\tag{5.7}$$

To summarize, the equations of motion that we must solve are

$$\mathcal{L}_n h_{ab} = 2K_{ab},\tag{5.8a}$$

$$\begin{aligned}\mathcal{L}_n K_{ab} &= -\frac{\epsilon}{w_H^2} h_{ab} (X^2 - 1)^2 + 2\epsilon (\hat{D}_a X) (\hat{D}^a X) + 2K_{ac} K_b^c \\ &\quad - \parallel R_{ab} - K K_{ab},\end{aligned}\tag{5.8b}$$

$$\mathcal{L}_n K = -K_{ab}^2 - \epsilon \left[2X_{,z}^2 + \frac{1}{w_H^2} (X^2 - 1)^2 \right],\tag{5.8c}$$

$$X_{,zz} = -K X_{,z} + 2X (X^2 - 1) + w_H^2 \hat{D}^2 X,\tag{5.8d}$$

$$\hat{D}_b K^b_a = \hat{D}_a K + 2\epsilon X_{,z} \hat{D}_a X.\tag{5.8e}$$

We can now rescale the coordinate z : $z \rightarrow u \stackrel{\text{def}}{=} z/w_H$ and set $w_H = 1$. Since from (2.17b) $\mathcal{L}_n \equiv \partial/\partial z$, this yields

$$h'_{ab} = 2K_{ab},\tag{5.9a}$$

$$K'_{ab} = -\epsilon h_{ab} (X^2 - 1)^2 + 2\epsilon (\hat{D}_a X) (\hat{D}^a X) + 2K_{ac} K_b{}^c - \parallel R_{ab} - K K_{ab}, \quad (5.9b)$$

$$K' = -K_{ab}^2 - \epsilon \left[2X'^2 + (X^2 - 1)^2 \right], \quad (5.9c)$$

$$X'' = -K X' + 2X (X^2 - 1) + \hat{D}^2 X, \quad (5.9d)$$

$$\hat{D}_b K^b{}_a = \hat{D}_a K + 2\epsilon X' \hat{D}_a X, \quad (5.9e)$$

where a prime denotes differentiation with respect to the perpendicular variable u . From now on, we will omit equation (5.9e), because it does not contribute to the determination of the effective dynamics.

Finally, we want to rescale K_{ab} and $\sigma^A = \{t, x, y\}$ as well. Following the method of chapter 3, we would rescale K_{ab} by a quantity $1/\varsigma$ characterising the wall's extrinsic radius of curvature, $\varsigma \stackrel{\text{def}}{=} |\underline{K}|$. However, we must realize that there are now two contributions to K_{ab} , coming from the wall's self-gravity and from its bending, which are respectively of order $O(\epsilon)$ and $O(\varsigma)$. Hence we must consider the cases $\epsilon > \varsigma$ and $\epsilon < \varsigma$ separately. Moreover, the wall also has a cosmological horizon situated at a finite proper distance $u \sim 1/\epsilon$ away from it, and now both the distances $R \stackrel{\text{def}}{=} 1/\varsigma$ and $1/\epsilon$ represent limits to the validity of our system of coordinates. We deal with this problem by rescaling the coordinates differently in the two cases.

5.3 The Gravity-Dominated Case ($\epsilon > \varsigma$)

In this case, we set

$$K_{ab} = \epsilon \kappa_{ab}, \quad (5.10)$$

$$\sigma^A = x^A / \epsilon.$$

Noting that, by the Gauß equation, this implies that $\parallel R_{ab}$ must be rescaled as

$$\parallel R_{ab} = \epsilon^2 \parallel r_{ab}, \quad (5.11)$$

and writing D_a for the rescaled derivative \hat{D}_a , equations (5.9) then become

$$h'_{ab} = 2\epsilon \kappa_{ab}, \quad (5.12a)$$

$$\kappa'_{ab} = -h_{ab} (X^2 - 1)^2 + \epsilon \left[2\kappa_{ab} \kappa_{bd} h^{cd} - \parallel r_{ab} - \kappa \kappa_{ab} \right] + 2\epsilon^2 D_a X D_b X, \quad (5.12b)$$

$$\kappa' = -3 (X^2 - 1)^2 - \epsilon (\parallel r + \kappa^2) + \epsilon^2 h^{ab} D_a X D_b X, \quad (5.12c)$$

$$X'' = 2X (X^2 - 1) - \epsilon \kappa X' + \epsilon^2 a^{ab} D_a D_b X. \quad (5.12d)$$

(The equation for κ_{ab} was modified using that for X .)

We see that the equations do not depend on the parameter ς , which makes this case easier to solve. We can apply our method and expand all the quantities in ϵ ,

$$\begin{aligned} h_{ab} &= h_{ab}^{(0)} + \epsilon h_{ab}^{(1)} + \epsilon^2 h_{ab}^{(2)} + O(\epsilon^3), \\ \kappa_{ab} &= \kappa_{ab}^{(0)} + \epsilon \kappa_{ab}^{(1)} + \epsilon^2 \kappa_{ab}^{(2)} + O(\epsilon^3), \\ \parallel r_{ab} &= \parallel r_{ab}^{(0)} + \epsilon \parallel r_{ab}^{(1)} + \epsilon^2 \parallel r_{ab}^{(2)} + O(\epsilon^3), \\ X &= X^{(0)} + \epsilon X^{(1)} + \epsilon^2 X^{(2)} + O(\epsilon^3), \end{aligned} \tag{5.13}$$

and solve the equations order by order. The procedure is the same for all the cases that we consider in this chapter, and it is only completely shown for this case.

5.3.1 The Zeroth Order

At zeroth order, the equations (5.12) reduce to

$$h_{ab}^{(0)'} = 0, \tag{5.14a}$$

$$\kappa_{ab}^{(0)'} = -h_{ab}^{(0)} (X^2 - 1)^2, \tag{5.14b}$$

$$\kappa^{(0)'} = -3(X^2 - 1), \tag{5.14c}$$

$$X^{(0)''} = 2(X^{(0)2} - 1)X^{(0)} \tag{5.14d}$$

and are of course solved by

$$X^{(0)}(u) = \tanh(u), \tag{5.15a}$$

$$h_{ab}^{(0)} = \underline{h}_{ab}, \tag{5.15b}$$

$$\kappa_{ab}^{(0)} = \underline{\kappa}_{ab} - \underline{h}_{ab} f_0(u), \tag{5.15c}$$

$$\kappa^{(0)} = \underline{\kappa} - 3f_0(u), \tag{5.15d}$$

where, as usual, underlined quantities are evaluated at the worldvolume, and we define

$$\begin{aligned} f_n(u) &\stackrel{\text{def}}{=} \int du u^n \text{sech}(u)^4, \\ F_n(u) &\stackrel{\text{def}}{=} \int du f_n(u). \end{aligned} \tag{5.16}$$

(All of the functions that we shall define for notational simplicity will be such as they vanish at $u = 0$.) This zeroth order can be compared with the results that we

obtained in the previous chapter. Although we did not compute the fundamental forms there, these can be checked to be

$$h_{ab}^{\text{PS}} = A^2(u) \text{diag} (1, -e^{4\epsilon t/2}, -e^{4\epsilon t/2}), \quad (5.17a)$$

$$K^a_b{}^{\text{PS}} = \frac{A'(u)}{A(u)} h^a_b{}^{\text{PS}}. \quad (5.17b)$$

Note how h_{ab}^{PS} is of order 1, but K_{ab}^{PS} is of order ϵ : this is why we did not rescale h_{ab} . The appearance of a zeroth-order contribution for the extrinsic curvature in (5.15c) is due to the rescaling $K_{ab} \rightarrow \kappa_{ab}$ in this chapter.

5.3.2 The First Order

If we consider the terms proportional to ϵ , the equations of motion become

$$h_{ab}^{(1)'} = 2\kappa_{ab}^{(0)}, \quad (5.18a)$$

$$\begin{aligned} \kappa_{ab}^{(1)'} = - \left(\|\gamma_{ab}^{(0)} + \kappa^{(0)} \kappa_{ab}^{(0)} \right) + 2\kappa_{ac}^{(0)} \kappa_{bd}^{(0)} h^{(0)cd} - h_{ab}^{(1)} (X^{(0)2} - 1)^2 \\ - 4h_{ab}^{(0)} X^{(0)} (X^{(0)2} - 1) X^{(1)}, \end{aligned} \quad (5.18b)$$

$$\kappa^{(1)'} = - \left(\|\gamma^{(0)} + \kappa^{(0)2} \right) - 12X^{(0)} (X^{(0)2} - 1) X^{(1)}, \quad (5.18c)$$

$$X^{(1)''} - 2(3X^{(0)2} - 1) X^{(1)} = -\kappa^{(0)} X^{(0)'}. \quad (5.18d)$$

Taking into account the zeroth order solution, the equation for $X^{(1)}$ is

$$X^{(1)''} - 2(3X^{(0)2} - 1) X^{(1)} = -(\underline{\kappa}^{(0)} - 3f_0) X^{(0)'}. \quad (5.19)$$

Noting that $X^{(0)'}$ is the zero-mode of the operator $\partial_u^2 - 2(3X^{(0)2} - 1)$, we must conclude that

$$\underline{\kappa}^{(0)} = 0. \quad (5.20)$$

This is the first integrability condition, obtained at order ϵ^1 but giving an equation of motion at order ϵ^0 . (This confirms that to zeroth order the wall obeys the Nambu dynamics.) We can obtain this condition in a more general way by noting that f_0 is an odd function of u , then multiplying equation (5.19) by $X^{(0)'}$ to obtain

$$\begin{aligned} [X^{(1)''} - 2(3X^{(0)2} - 1) X^{(1)}] X^{(0)'} &\equiv (X^{(1)'} X^{(0)'} - X^{(1)} X^{(0)''})' \\ &= -(\underline{\kappa}^{(0)} - 3f_0) X^{(0)'^2}. \end{aligned} \quad (5.21)$$

Integrating over \mathbb{R} then yields the constraint $\underline{\kappa}^{(0)} = 0$. The solution for $X^{(1)}$ is

$$X^{(1)} = -\frac{1}{6} [3u + \tanh(u)] \operatorname{sech}(u)^2. \quad (5.22)$$

We then get

$$h_{ab}^{(1)} = \underline{h}_{ab}^{(1)} + 2\underline{\kappa}_{ab} u - 2\underline{h}_{ab}^{(0)} F_0(u), \quad (5.23a)$$

$$\begin{aligned} \kappa_{ab}^{(1)} = & \underline{\kappa}_{ab}^{(1)} + \left(2\underline{\kappa}_{ac}^{(0)} \underline{\kappa}_b^{(0)c} - \|\underline{r}_{ab}^{(0)}\| \right) u - \underline{h}_{ab}^{(1)} f_0(u) \\ & - \underline{\kappa}^{(0)} [F_0(u) + 2f_1(u)] + \underline{h}_{ab}^{(0)} G_1(u), \end{aligned} \quad (5.23b)$$

$$\kappa^{(1)} = \underline{\kappa}^{(1)} - \|\underline{r}^{(0)}\| u + 3G_0(u), \quad (5.23c)$$

where

$$G_0(u) \stackrel{\text{def}}{=} \int du [4 \tanh(u) \operatorname{sech}(u)^2 X^{(1)}(u) - 3f_0^2(u)], \quad (5.24)$$

$$G_1(u) \stackrel{\text{def}}{=} 2f_0(u)F_0(u) + G_0(u).$$

5.3.3 The Second and Third Orders

Keeping the terms in $O(\epsilon^2)$ in (5.12) we get

$$h_{ab}^{(2)'} = 2 \kappa_{ab}^{(1)}, \quad (5.25a)$$

$$\begin{aligned} \kappa_{ab}^{(2)'} = & - \left(\|\underline{r}_{ab}^{(1)}\| + \kappa^{(0)} \kappa_{ab}^{(1)} + \kappa^{(1)} \kappa_{ab}^{(0)} \right) \\ & - 2 \left(\kappa_{ac}^{(0)} \kappa_{bd}^{(0)} h^{(1)cd} + \kappa_{ac}^{(0)} \kappa_{bd}^{(1)} h^{(0)cd} + \kappa_{ac}^{(1)} \kappa_{bd}^{(0)} h^{(0)cd} \right) \\ & - h_{ab}^{(2)} (X^{(0)2} - 1)^2 - 4h_{ab}^{(1)} X^{(0)} (X^{(0)2} - 1) X^{(1)} \\ & - 4h_{ab}^{(0)} (X^{(0)2} - 1) X^{(2)} - 2h_{ab}^{(0)} (3X^{(0)2} - 1) X^{(1)2}, \end{aligned} \quad (5.25b)$$

$$\begin{aligned} \kappa^{(2)'} = & - \left(\|\underline{r}^{(1)}\| + 2\kappa^{(0)} \kappa^{(1)} \right) - 12X^{(0)} (X^{(0)2} - 1) X^{(2)} \\ & - 6 (3X^{(0)2} - 1) X^{(1)2}, \end{aligned} \quad (5.25c)$$

$$X^{(2)''} - 2 (3X^{(0)2} - 1) X^{(2)} = - (\kappa^{(1)} X^{(0)'})' + \kappa^{(0)} X^{(1)'} + 6X^{(0)} X^{(1)2}. \quad (5.25d)$$

We consider again the equation for $X^{(2)}$ first; replacing all the lower order contributions, we obtain

$$X^{(2)''} - 2 (3X^{(0)2} - 1) X^{(2)} = -\underline{\kappa}^{(1)} X^{(0)'} + \text{terms odd in } u. \quad (5.26)$$

Multiplying by $X^{(0)'}$ and integrating over \mathbb{R} , we find that

$$\underline{\kappa}^{(1)} = 0 \quad (5.27)$$

and thus the wall still obeys the Nambu–Gotō dynamics at first order in ϵ .

Anticipating that we will find the first corrections to the Nambu motion at second order, *i.e.* from the X -equation at third order, we do not need to compute all the terms of $h_{ab}^{(2)}$, $\kappa_{ab}^{(2)}$ and $\kappa^{(2)}$; in fact, all we need is the even contribution to $\kappa^{(2)}$, because all other terms in the equation for $X^{(3)}$ will be odd. A rather long calculation yields

$$\begin{aligned}\kappa^{(2)} &= \kappa_{ab}^{(2)} h^{(0)ab} - \kappa_{ab}^{(1)} h^{(1)ab} - \kappa_{ab}^{(0)} h^{(2)ab} \\ &= \underline{\kappa}^{(2)} + u^2 \underline{\kappa}_{ab}^{(0)} \parallel_{r^{(0)ab}} + \text{terms odd in } u.\end{aligned}\quad (5.28)$$

We finally come to the equation at third order. The equation for $X^{(3)}$ is

$$\begin{aligned}X^{(3)''} - 2(3X^{(0)2} - 1)X^{(3)} &= -\left(\underline{\kappa}^{(2)} + u^2 \underline{\kappa}_{ab}^{(0)} \parallel_{r^{(2)ab}}\right) X^{(0)'} \\ &+ \text{terms odd in } u.\end{aligned}\quad (5.29)$$

Therefore, multiplying by $X^{(0)'}$ and integrating over the real line gives

$$\left[\underline{\kappa}^{(2)} f_0(u) + \underline{\kappa}_{ab}^{(0)} \parallel_{r^{(0)ab}} f_2(u) \right]_{-\infty}^{\infty} = 0, \quad (5.30)$$

which yields the lowest-order corrections to the Nambu effective action,

$$\begin{aligned}\underline{\kappa} &= -\epsilon^2 \frac{f_2(u)|_{-\infty}^{\infty}}{f_0(u)|_{-\infty}^{\infty}} \underline{\kappa}_{ab}^{(0)} \parallel_{r^{(0)ab}} + O(\epsilon^3) \\ &= -\frac{\epsilon^2}{2} \left(\frac{\pi^2}{6} - 1 \right) \underline{\kappa}_{ab}^{(0)} \parallel_{r^{(0)ab}} + O(\epsilon^3).\end{aligned}\quad (5.31)$$

5.4 The Curvature-Dominated Case ($\varsigma > \epsilon$)

If $\varsigma > \epsilon$, K_{ab} will be of order ς , and we let

$$\begin{aligned}K_{ab} &= \varsigma \kappa_{ab}, \\ \sigma^A &= x^A / \varsigma,\end{aligned}\quad (5.32)$$

which implies $\parallel R_{ab} = \varsigma^2 \parallel r_{ab}$. The equations then depend on two parameters, ς and

$$\varkappa \stackrel{\text{def}}{=} \frac{\epsilon}{\varsigma} < 1. \quad (5.33)$$

and are

$$h'_{ab} = 2\varsigma \kappa_{ab}, \quad (5.34a)$$

$$\kappa'_{ab} = \varsigma (2\kappa_{ac}\kappa_b^c - \kappa\kappa_{ab} - \parallel r_{ab}) - \varkappa h_{ab} (X^2 - 1)^2 + 2\varsigma^2 \varkappa D_a X D_b X, \quad (5.34b)$$

$$\kappa' = -\varsigma (\kappa^2 + \parallel r) - 3\varkappa (X^2 - 1)^2 + 2\varsigma^2 \varkappa h^{ab} D_a X D_b X, \quad (5.34c)$$

$$X'' = 2X (X^2 - 1) - \varsigma\kappa X' + \varsigma^2 D^2 X. \quad (5.34d)$$

The gravitational coupling of the Higgs field is characterized by \varkappa now, and note that although ς and \varkappa are small, we do not know their relative sizes. We must now expand all the fields in terms of these two parameters and solve order by order.

Let us start with the flat spacetime case, $\varkappa = 0$, when the equations reduce to

$$h'_{ab} = 2\varsigma\kappa_{ab}, \quad (5.35a)$$

$$\kappa'_{ab} = \varsigma (2\kappa_{ac}\kappa_b^c - \kappa\kappa_{ab} - \parallel r_{ab}), \quad (5.35b)$$

$$\kappa' = -\varsigma (\kappa^2 + \parallel r), \quad (5.35c)$$

$$X'' = 2X (X^2 - 1) - \varsigma\kappa X' + \varsigma^2 \hat{D}^2 X. \quad (5.35d)$$

In this case, we can compute $\parallel r_{ab}$ from equation (2.15) — in particular, $\parallel r_{ab}^{(0)} = \kappa_{ac}^{(0)} \kappa_b^{(0)c}$. Solving order by order in ς , we obtain to $O(\varsigma^2)$

$$h_{ab} = \underline{h}_{ab} + 2\varsigma \underline{\kappa}_{ab}^{(0)} u + \varsigma^2 \left(2\underline{\kappa}_{ab}^{(1)} u + \underline{\kappa}_{ab}^{(0)} \underline{\kappa}_b^{(0)c} u^2 \right), \quad (5.36a)$$

$$\begin{aligned} \kappa_{ab} = \underline{\kappa}_{ab} + \varsigma \underline{\kappa}_{ac}^{(0)} \underline{\kappa}_b^{(0)c} u + \varsigma^2 \left[\left(2\underline{\kappa}_{ac}^{(0)} \underline{\kappa}_{bd}^{(0)} \underline{h}^{(1)cd} + 2\underline{\kappa}_{(a}^{(0)c} \underline{\kappa}_{b)c}^{(1)} \right) u \right. \\ \left. + \left(2\underline{\kappa}_{ac}^{(0)} \underline{\kappa}_{bd}^{(0)} \underline{\kappa}^{(0)cd} + \frac{1}{2} \underline{\kappa}_{ab}^{(0)2} \right) u^2 \right], \end{aligned} \quad (5.36b)$$

$$\kappa = \underline{\kappa} - \varsigma \underline{\kappa}_{ab}^{(0)2} u + \varsigma^2 \left[\left(\underline{\kappa}_{ac}^{(0)} \underline{\kappa}_b^{(0)c} \underline{h}^{(1)ab} - 2\underline{\kappa}_{ab}^{(0)} \underline{\kappa}^{(1)ab} \right) u - \underline{\kappa}_{ab}^{(0)3} u^2 \right], \quad (5.36c)$$

$$X = X^{(0)} + \varsigma^2 X^{(2)} \quad (5.36d)$$

where

$$X^{(2)} = \operatorname{sech}^2(u) \int_0^u du \cosh^4(u) \int_{-\infty}^u du u \underline{\kappa}_{ab}^2 \operatorname{sech}^4(u) \quad (5.37)$$

is an odd function of u . This is enough to obtain the first corrections to the Nambu dynamics; at order ς^3 , the equation (5.35d) multiplied by $X^{(0)'}$ reads

$$(X^{(3)'} X^{(0)'} - X^{(3)} X^{(0)''})' = - \left(\underline{\kappa}^{(2)} + \underline{\kappa}_{ab}^{(0)3} u^2 \right) X^{(0)'}{}^2 + \text{terms odd in } u \quad (5.38)$$

and therefore integrating over \mathbb{R} yields the corrected equation of motion for the wall,

$$\underline{\kappa} = -\frac{\varsigma^2}{2} \left(\frac{\pi^2}{6} - 1 \right) \underline{\kappa}_{ab}^{(0)3} + O(\varsigma^3). \quad (5.39)$$

This is the same as equation (5.31), once we replace the value for $\|r^{(0)ab}$ (and with ς rather than ϵ).

We must now think about the best approach to solve the field equations when $\varkappa \neq 0$. Let us start by considering the case $\varsigma = 0$; it is easy to see from (5.34) that we can solve the equations exactly, so that $X = \tanh(u)$ (the kink solution) and h_{ab} is a constant. This means that, order by order in ς , we can solve the equations exactly to all orders in \varkappa . The calculations follow the same lines that we have shown already twice in this chapter: we compute the quantities h_{ab} , κ_{ab} and X at each order in \varkappa and use them to derive integrability constraints at the previous order. Let us just give here the results. [We write $Q^{(m,n)}$ for a quantity at order $\varsigma^m \varkappa^n$ and $Q^{(m,\cdot)}$ for the series (in \varkappa) at order ς^m .]

- To order ς^0 ,

$$\begin{aligned} h_{ab}^{(0,\cdot)} &= \underline{h}_{ab}^{(0,0)}, \\ \kappa_{ab}^{(0,\cdot)} &= \underline{\kappa}_{ab}^{(0,\cdot)} - \varkappa \underline{h}_{ab}^{(0,0)} f_0(u), \\ \kappa^{(0,\cdot)} &= \underline{\kappa}^{(0,\cdot)} - 3\varkappa f_0(u), \\ X^{(0,\cdot)} &= \tanh(u). \end{aligned} \tag{5.40}$$

- To order ς^1 ,

$$\begin{aligned} h_{ab}^{(1,\cdot)} &= \underline{h}_{ab}^{(1,\cdot)} + 2\underline{\kappa}_{ab}^{(0,0)} u - 2\varkappa \underline{h}_{ab}^{(0,0)} F_0(u), \\ \kappa_{ab}^{(1,\cdot)} &= \underline{\kappa}_{ab}^{(1,\cdot)} + \left(2\underline{\kappa}_{ac}^{(0,0)} \underline{\kappa}_b^{(0,0)c} - \|r_{ab}^{(0,\cdot)} \right) u \\ &\quad - \varkappa \left[\underline{h}_{ab}^{(0,1)} f_0(u) + \underline{\kappa}_{ab}^{(0,0)} (F_0 + 2f_1) + 4h_{ab}^{(0,0)} \tilde{G}_0(u) \right] \\ &\quad + \varkappa^2 \underline{h}_{ab}^{(0,0)} \tilde{G}_1(u), \\ \kappa^{(1,\cdot)} &= \underline{\kappa}^{(1,\cdot)} - \underline{\kappa}_{ab}^{(0,0)} 2u - 4\varkappa X^{(0,0)'} X^{(1,0)}, \\ X^{(1,\cdot)} &= -\frac{\varkappa}{6} [3u + \tanh(u)] \operatorname{sech}^2(u), \end{aligned} \tag{5.41}$$

and the equations for $X^{(1,\cdot)}$ implies $\underline{\kappa}^{(0,0)} = \underline{\kappa}^{(0,1)} = 0$, i.e. $\underline{\kappa}^{(0,\cdot)} = 0$.

- To order ς^2 , noting that the equation for $X^{(3,0)}$ reduces to

$$X^{(3,0)''} - 2(3X^{(0,0)2} - 1) X^{(3,0)} = -\kappa^{(2,0)} X^{(0,0)'}, \tag{5.42}$$

we see that if $\kappa^{(2,0)}$ contains even terms other than the constant $\underline{\kappa}^{(2,0)}$, then this is all we need to get the lowest-order corrections to the Nambu dynamics —

from the case $\epsilon > \varsigma$, we anticipate that this will indeed be the case. We find that

$$\kappa^{(2,0)} = \underline{\kappa}^{(2,0)} + \underline{\kappa}_{ab}^{(0,0)} \parallel_{r^{(0,0)ab}} u^2 + \text{plus terms odd in } u. \quad (5.43)$$

[In Eq. (5.41) we have not written all terms, but all that even ones are there.] The tilde functions are defined by

$$\begin{aligned} \tilde{G}_0(u) &\stackrel{\text{def}}{=} \int^u du \, 4 \tanh(u) \operatorname{sech}^2(u) X^{1,0}(u), \\ \tilde{G}_1(u) &\stackrel{\text{def}}{=} 2f_0(u)F_0(u) + \int^u du \, [4 \tanh(u) \operatorname{sech}^2(u) X^{(1,1)}(u) - 9f_0^2(u)]. \end{aligned} \quad (5.44)$$

From (5.43), we obtain that the first corrections to the Nambu–Gotō motion are given by:

$$\underline{\kappa} = -\frac{\varsigma^2}{2} \left(\frac{\pi^2}{6} - 1 \right) \underline{\kappa}_{ab}^{(0,0)} \parallel_{r^{(0,0)ab}} + \mathcal{O}(\varsigma^3, \varsigma^2 \varkappa). \quad (5.45)$$

5.5 An Example: Bending the Gravitating Wall

In the previous two sections, we have computed the lowest-order corrections to the Nambu dynamics of gravitating extended domain walls by the method of the integrability condition. In the two cases considered, $\epsilon > \varsigma$ and $\epsilon < \varsigma$, we have found that these corrections appear at quadratic order in the dominant parameter, and have the form

$$\underline{\kappa}^{(2)} = -\frac{1}{2} \left(\frac{\pi^2}{6} - 1 \right) \underline{\kappa}_{ab}^{(0)} \parallel_{r^{(0)ab}}. \quad (5.46)$$

In the case of the string, recall that we did not have any quadratic corrections to the Nambu motion because the term in the action which would have given such corrections was proportional to the Euler characteristic of the worldsheet; for the wall, the appearance of corrections at order ς^2 means that the equivalent term is not a topological invariant.

The problem now is that (except in flat spacetime) we do not know $\parallel_{r_{ab}^{(0)}}$, which is needed to understand the consequences of the corrected equations. Unfortunately, this is still work in progress and we do not yet have a general interpretation of (5.46), but we present below a case where we can estimate $\parallel_{r_{ab}^{(0)}}$ and obtain an equation of motion for the wall. We consider the gravitation-dominated case (5.31), and approximate the unknown $\parallel_{r_{ab}^{(0)}}$ by the $\parallel_{r_{ab}}$ obtained by bending a plane-symmetric

gravitating wall (see [46]), as shown in figure 5.1. The three-dimensional intrinsic metric (2.6) is given by

$$\gamma_{AB} = X^a{}_{,A} X_{a,B}, \quad (5.47)$$

where X^μ is the position of the wall in spacetime. We bend the wall by replacing

$$\begin{aligned} X^a &\rightarrow X'^a = X^a + \xi n^a, \\ n_a &\rightarrow n'_a = n_a + \xi_{,a}, \end{aligned} \quad (5.48)$$

where $\xi(t, x, y)$ is a scalar perturbation along n_a (defined only at $u = 0$) and the perturbation of n_a was determined by requiring that $X'^a{}_{,A} n'_a = 0$ (recall that $X'^a{}_{,A}$ is parallel to \mathcal{W}').

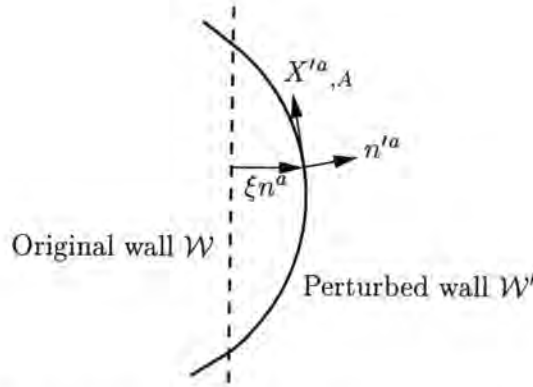


Figure 5.1: Bending the plane-symmetric wall.

We can use the general formula (3.35) to compute the variation of $\underline{\kappa}_{AB}$:

$$\underline{\kappa}_{AB} \rightarrow \underline{\kappa}'_{AB} = \underline{\kappa}_{AB} + \xi_{,AB} + \xi_{,C} X^C{}_{;AB} = \underline{\kappa}_{AB} + \xi_{,AB}. \quad (5.49)$$

[This could have been found from the definition (2.11) using $\delta \Gamma_{A^c B} n_c = 0$.] Therefore,

$$\underline{\kappa}' = \underline{\kappa}_{AB} \underline{h}^{AB} + \square \xi = \square \xi \quad (5.50)$$

since the unperturbed $\underline{\kappa}_{AB}$ corresponds to the flat wall and, at zeroth-order, obeys the Nambu dynamics $\underline{\kappa} = 0$. Here, \square is the background (i.e., unperturbed) three-dimensional d'Alembertian. The problematic quantity $\|_{\gamma'^{(0)} AB}$ can now be found as the (rescaled) Ricci tensor computed from the perturbed intrinsic metric γ'_{AB} ,

$$\gamma'_{AB} = \gamma_{AB} - \xi_{,A} \xi_{,B}. \quad (5.51)$$

Note that we want $\|_{\mathcal{T}_{AB}}^{(0)}$, and that therefore we can assume that γ_{AB} is the flat worldvolume (any corrections will presumably appear at higher orders $\|_{\mathcal{T}_{AB}}^{(n>0)}$); then,

$$\|_{\mathcal{T}'_{AB}} = -\frac{9}{4} (2 - \xi_{,c}^2) h_{AB} + \frac{9}{4} \xi_{,A} \xi_{,B} + \xi_{;AC} \xi_{;B}{}^{;C} \quad (5.52)$$

(where we have rescaled a factor ϵ^2). Finally, the equation of motion (5.31) is

$$\square \xi = -\frac{1}{2} \left(\frac{\pi^2}{6} - 1 \right) \left(\xi_{;AB} \xi^{;AC} \xi_{;C}{}^{;B} + \frac{9}{4} \xi_{;AB} \xi^{;A} + \xi^{;B} \right). \quad (5.53)$$

The worldvolume is to be totally geodesic if all solutions of the above equation (5.53) are such that $\square \xi = 0$; at first sight, this need not be the case.

Appendix A

An Exact Solution to the Perturbed Equations of Motion for the Helical Breather

In this appendix, we give (without deriving it), the general solution to the equation for the correction to the breather solution,

$$\begin{aligned} \delta\ddot{Z} + 2\frac{1-q^2}{\Omega}\sin(\tau)\cos(\tau)\delta\dot{Z} + \frac{q^2 - (1-q^2)\cos^2(\tau)}{\Omega}\delta Z \\ = -32\frac{\epsilon^4}{\mu}\sqrt{1-q^2}\cos(\tau)\Omega^{-3}(\beta_1 - \beta_2\Omega^{-1} + \beta_3\Omega^{-2} - \beta_4\Omega^{-3}). \end{aligned} \quad (\text{A.1})$$

This equation can be solved by varying the parameters of the zeroth order solution (3.69); this gives

$$\begin{aligned} \delta Z(\tau) = \frac{16}{\mu\Delta} \left[\left(\frac{\beta_1}{3} - \frac{\beta_2}{4} + \frac{\beta_3}{5} - \frac{\beta_4}{6} \right) (\cos(\tau) + \Delta^2\tau\sin(\tau)) \right. \\ \left. - \left(\frac{\beta_1}{3\Omega^3} - \frac{\beta_2}{4\Omega^4} + \frac{\beta_3}{5\Omega^5} - \frac{\beta_4}{6\Omega^6} \right) \cos(\tau) \right] \\ + \lambda_0 \sin(\tau) \tan^{-1}(q \tan(\tau)) + \sin^2(\tau) \cos(\tau) \sum_{n=1}^6 \lambda_n \Omega^{-n}. \end{aligned} \quad (\text{A.2})$$

Here, $\Omega(\tau)$ and the coefficients β_i are as defined in section 3.4.3 and the λ_i 's are

$$\begin{aligned} \lambda_0 = \frac{\Delta}{240q\mu} \left[640 \left(3 + \frac{1}{q^2} \right) \beta_1 - 360 \left(5 + \frac{2}{q^2} + \frac{1}{q^4} \right) \beta_2 + 48 \left(35 + \frac{15}{q^2} + \frac{9}{q^4} + \frac{5}{q^6} \right) \beta_3 \right. \\ \left. - 25 \left(63 + \frac{28}{q^2} + \frac{18}{q^4} + \frac{12}{q^6} + \frac{7}{q^8} \right) \beta_4 \right], \end{aligned} \quad (\text{A.3a})$$

$$\begin{aligned} \lambda_1 = \frac{\Delta}{720\mu} \left[1920 \left(3 - \frac{1}{q^2} \right) \beta_1 - 360 \left(15 - \frac{4}{q^2} - \frac{3}{q^4} \right) \beta_2 + 48 \left(105 - \frac{25}{q^2} - \frac{17}{q^4} \right. \right. \\ \left. \left. - \frac{15}{q^6} \right) \beta_3 - 5 \left(945 - \frac{210}{q^2} - \frac{136}{q^4} - \frac{110}{q^6} - \frac{105}{q^8} \right) \beta_4 \right], \end{aligned} \quad (\text{A.3b})$$

$$\lambda_2 = \frac{\Delta}{360\mu} \left[1920\beta_1 - 360 \left(5 - \frac{1}{q^2} \right) \beta_2 + 48 \left(35 - \frac{6}{q^2} - \frac{5}{q^4} \right) \beta_3 - 5 \left(315 - \frac{49}{q^2} - \frac{39}{q^4} - \frac{35}{q^6} \right) \beta_4 \right], \quad (\text{A.3c})$$

$$\lambda_3 = \frac{\Delta}{90\mu} \left[480\beta_1 - 360\beta_2 + 48 \left(7 - \frac{1}{q^2} \right) \beta_3 - 5 \left(63 - \frac{8}{q^2} - \frac{7}{q^4} \right) \beta_4 \right], \quad (\text{A.3d})$$

$$\lambda_4 = \frac{\Delta}{15\mu} \left[-60\beta_2 + 48\beta_3 - 5 \left(9 - \frac{1}{q^2} \right) \beta_4 \right], \quad (\text{A.3e})$$

$$\lambda_5 = \frac{8\Delta}{15\mu} [6\beta_3 - 5\beta_4], \quad (\text{A.3f})$$

$$\lambda_6 = -\frac{8\Delta}{3\mu} \beta_4. \quad (\text{A.3g})$$

We can use this solution to investigate the rigidity of the helicoidal trajectories in function of the parameters Δ and Σ , where $\Delta^2 = 1 - q^2$ and $\Sigma = \sin(\tau_0)$. We are going to observe how the Ricci curvature [given by the flat background case of the Gauß equation (2.15)]

$$\parallel_r = \underline{\kappa}_{\mu AB} \underline{\kappa}_{\mu}^{AB} - \underline{\kappa}_{\mu} \underline{\kappa}_{\mu} = -\frac{2q^2 \dot{Z}^2}{(q^2 + Z^2)^2 (1 - \dot{Z}^2)} - \frac{2Z \ddot{Z}}{(1 - \dot{Z}^2)^2 (q^2 + Z^2)} \quad (\text{A.4})$$

depends on the correction. We take $\beta = 1$ for simplicity, and note that for Z_0

$$\parallel_r = -\frac{2\Delta^2}{\Omega^3} [q^2 \sin^2(\tau) - \cos^2(\tau)]. \quad (\text{A.5})$$

Suppose we want to investigate the behaviour of \parallel_r near a general initial point τ_0 , where $\delta Z(\tau_0) = \delta \dot{Z}(\tau_0) = 0$. Then,

$$\delta \parallel_r \simeq -\frac{2\Delta \cos(\tau_0)}{\Omega^3(\tau_0)} \delta \ddot{Z}(\tau_0) = \frac{64\epsilon^4 \Delta^2 \cos^2(\tau_0)}{\mu \Omega^8(\tau_0)} (\beta_1 \Omega^2 - \beta_2 \Omega + \beta_3). \quad (\text{A.6})$$

[We have used (A.1) to evaluate $\delta \ddot{Z}$ and noticed that $\beta_4 = 0$ for $\beta = 1$.] The combination $\parallel_r \delta \parallel_r$ will be negative if the magnitude of the curvature is decreased, which corresponds to rigidity and positive if it is increased (antirigidity). From (A.5, A.6) we see that rigidity requires

$$[(2 - \Delta^2) \Sigma^2 - 1] [-\Delta^2 + 2\Delta^4 - 8\Delta^4 \Sigma^2 + 13\Delta^6 \Sigma^2 - 6\Delta^6 \Sigma^4] > 0. \quad (\text{A.7})$$

The sign of $\parallel_r \delta \parallel_r$ is shown in figure 3.8, and is positive in the shaded zones and negative in the white zone, showing respectively antirigidity and rigidity. With the exception of the loop $q = 0$, the string admits both rigid and antirigid behaviour for every value of q .

Appendix **B**

Numerical Tables

In this appendix, and in appendix C, we compile some of our numerical results from all chapters. The motivation for this is that, although figures provide a considerably more efficient (not to mention comfortable) way of analysing this numerical data, anyone trying to reproduce our results would appreciate some numbers with which to compare their own results. The tables below present only a (usually small) fraction of all the numerical data that we have collected.

B.1 Effective Motion of a Cosmic String

| β | $\mu/\pi\eta^2$ | $\alpha_1/\pi\eta^2$ | α_2/π | α_3/π |
|---------|-----------------|----------------------|----------------|----------------|
| 10.00 | 3.272 | 6.025 | 77.761 | -104.985 |
| 5.00 | 2.813 | 3.347 | 23.565 | -32.835 |
| 2.00 | 2.314 | 1.634 | 4.308 | -6.767 |
| 1.00 | 2.000 | 0.999 | 1.069 | -2.138 |
| 0.50 | 1.736 | 0.642 | 0.174 | -0.722 |
| 0.10 | 1.278 | 0.272 | -0.097 | -0.094 |
| 0.02 | 0.977 | 0.141 | -0.065 | -0.030 |
| 0.01 | 0.880 | 0.111 | -0.052 | -0.023 |

Table B.1: The numerical coefficients appearing in the action to fourth order for some values of the Bogomol'nyi parameter β . For $\beta = 1$, it can be analytically deduced from the equations of motion that $\mu/\pi\eta^2 = 2\alpha_1/\pi\eta^2 = 2$, and that $2\alpha_2 + \alpha_3 = 0$.

B.2 Gravitating Plane-Symmetric Domain Walls

| Λ | ϵ | z_h | X_h |
|-----------|------------|------------|----------|
| -0.3 | 0.640275 | No horizon | 1.000000 |
| | 1.000000 | 3.214 | 0.872038 |
| | 1.500000 | 2.422 | 0.468277 |
| | 1.980000 | 2.220 | 0.034594 |
| -0.2 | 0.495200 | >16.051 | 1.000000 |
| | 0.500000 | 10.885 | 1.000000 |
| | 1.000000 | 2.965 | 0.810156 |
| | 1.500000 | 2.344 | 0.376235 |
| | 1.698000 | 2.220 | 0.035201 |
| -0.1 | 0.325000 | No horizon | 1.000000 |
| | 0.500000 | 4.954 | 0.994331 |
| | 1.000000 | 2.784 | 0.743873 |
| | 1.598000 | 2.220 | 0.035841 |
| 0.0 | 0.000000 | ∞ | 1.000000 |
| | 0.500000 | 4.035 | 0.974744 |
| | 1.000000 | 2.643 | 0.672953 |
| | 1.498000 | 2.220 | 0.044748 |
| 0.1 | 0.000000 | 8.593 | 0.999996 |
| | 0.500000 | 3.548 | 0.943331 |
| | 1.000000 | 2.528 | 0.596269 |
| | 1.398000 | 2.220 | 0.037234 |
| 0.2 | 0.000000 | 6.076 | 0.999624 |
| | 0.500000 | 3.229 | 0.902233 |
| | 1.000000 | 2.433 | 0.511465 |
| | 1.298000 | 2.220 | 0.037234 |
| 0.3 | 0.000000 | 4.961 | 0.997155 |
| | 0.500000 | 2.996 | 0.852712 |
| | 1.000000 | 2.352 | 0.413619 |
| | 1.199000 | 2.219 | 0.027412 |

Table B.2: Proper distance to the horizon z_h and Higgs field at the horizon X_h for the Goldstone wall solutions, as functions of the cosmological constant Λ and the gravitational coupling ϵ .

| Λ | ϵ |
|-----------|------------|
| 0.0 | 0.0 |
| -0.1 | 0.3257 |
| -0.2 | 0.4951 |
| -0.3 | 0.6403 |
| -0.4 | 0.7736805 |
| -0.5 | 0.8999353 |
| -0.6 | 1.0213456 |
| -0.7 | 1.1392772 |
| -0.8 | 1.2545750 |
| -0.9 | 1.3678212 |
| -1.0 | 1.4794279 |

Table B.3: Value of ϵ at which the domain wall develops a horizon in anti-de Sitter case and for the Goldstone model.

| Λ | ϵ |
|-----------|------------|
| 0.0 | 0.0 |
| -0.010 | 0.034298 |
| -0.025 | 0.0598243 |
| -0.050 | 0.0934222 |
| -0.100 | 0.1540836 |
| -0.200 | 0.2632996 |
| -0.300 | 0.3679453 |
| -0.400 | 0.4708016 |
| -1.000 | 1.0773506 |

Table B.4: Value of ϵ at which the domain wall develops a horizon in anti-de Sitter case and for the sine-Gordon model.

Part III

Cosmic Strings and Black Holes

Abelian–Higgs Hair for Extreme Reissner–Nordstrøm Black Holes

6.1 Introduction and Chronology

For many years after their discovery, black holes have been believed to be rather simple physical systems, characterised only by a small number of parameters, or “charges”: M (the black hole’s mass), Q (its electric charge) and J (its angular momentum). (One should also allow for a magnetic charge obtained from Q by duality.) There even exist theorems that prove this conjecture, the so-called “no-hair theorems” (see for instance [13]). With time, however, some of these results were unduly extrapolated, and theorems made place to “folklore” in the non-specialist’s mind (see [34] for a review on this subject).

The classic no-hair theorems stipulate that “the only long range information that a black hole can support is its electromagnetic charge, its mass and its momentum.” No-hair folklore says that the only non-trivial field configurations an event horizon \mathcal{H} can carry are its massless spin-one and spin-two charges Q , M and J . In the past ten years, new, “hairy” black hole solutions have been found which either contradict the folklore or violate some assumption of the theorems:

- The theorems consider only “long-range fields,” whereas folklore seems to forbid even fields that live close to the black hole. For convenience, and following [1], we shall call *hair* a property of the black hole which can be measured at infinity, and *dressings* a short-ranged field living exclusively on the black hole’s horizon and its vicinity. Lee, Nair and Weinberg [68,67] have found a static

field configuration in $SU(2)$ gauge theory whose singular behaviour at the origin is hidden behind an event horizon. They have interpreted this solution as a small black hole inside a monopole; the $SU(2)$ fields then constitute dressing (but not hair) to the black hole, in clear contradiction with the folklore.

- No-hair theorems assume that the fields in question are stable; it is possible for a black hole to support hair (in the sense just defined) if the corresponding field solution is unstable. This is for instance the case of coloured black holes [11,90,14,65], which display Yang–Mills hair.
- It is also assumed by no-hair theorems that the topology of the spacetime outside the black hole’s horizon is trivial. This opens the possibility that topological defects might carry some field(s) from the black hole to infinity, thus constituting genuine hair. This is the case that we investigate in this chapter.

The present work is part of the effort started by the paper of Achúcarro, Gregory and Kuijken (AGK) [1] to determine whether or not a cosmic string can pierce a black hole and therefore constitute hair to this black hole.

In 1986, Aryal, Ford and Vilenkin (AFV) [7] wrote a metric which can be interpreted as an axisymmetric conical singularity centered on a Schwarzschild black hole (see figure 6.1), *i.e.* an infinitely thin cosmic string threading a black hole. The AFV metric is

$$ds^2 = \left(1 - \frac{2M}{r}\right) dt^2 - \frac{dr^2}{1 - \frac{2M}{r}} - r^2 d\theta^2 - r^2 (1 - 4G\mu)^2 \sin^2(\theta) d\phi^2. \quad (6.1)$$

Their work, however, did not resolve the question of the existence of abelian–Higgs hair growing on a black hole (this was not its purpose); indeed, not only did AFV not consider a thick string, there also remained the vital question of whether the fields would settle into a configuration corresponding to such a metric. The main concern would then be that the fields refuse to pierce the horizon. Recognising this fact, AGK [1] tackled numerically the problem of the abelian–Higgs field theory in a Schwarzschild background, and found that indeed, thin cosmic strings could thread a black hole; in fact, these strings seemed rather oblivious of the horizon (see figure 6.2 below). Thick strings, however, did react to the black hole’s presence by

exhibiting a pinching of the flux tubes close to the horizon's equator (figure 6.3). AGK then went on to include the string's backreaction in their calculations, and showed that their solutions were in fact smoothed versions of the AFV metric.

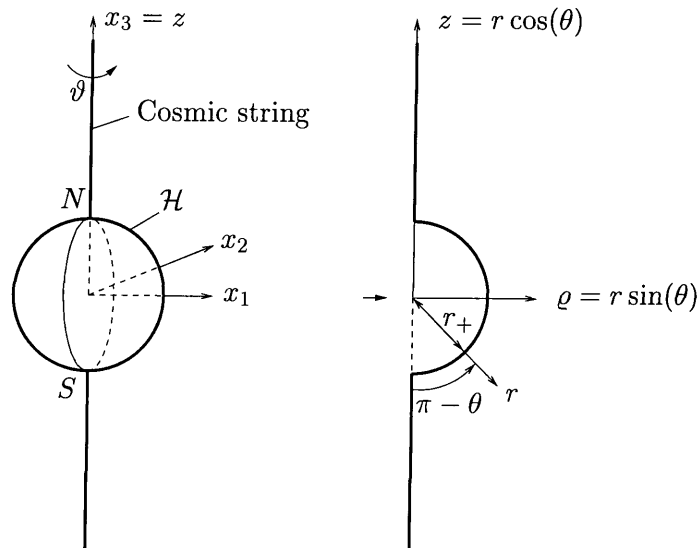


Figure 6.1: A cosmic string threading a black hole. N and S denote the “North” and “South” poles, at respectively $\theta = 0$ and $\theta = \pi$. (Note the difference between the angles θ and ϑ .)

Further work [54] showed that other conical singularities could also be smoothed out by the vortex. It had been known for some time (from the work of Gleiser and Pullin [48]) that a cosmic string modelled by a conical singularity can be split by an instanton, corresponding to the creation of a pair black hole/anti-black hole inside the “string.” Combining these two results, it was possible to find [38,57,39] an instanton to split smooth metrics as well; this provided a decay channel to extended (and thus more realistic) cosmic strings, which are otherwise stabilised by their topology. Unlike the original instanton, however, the one for smooth metrics contains two $U(1)$ gauge fields, the broken $U(1)$ (responsible for the creation of the vortex) and a new, unbroken, $U(1)$, which we shall call electromagnetism.

The extra $U(1)$ symmetry prompted naturally the question of what happened when the black hole itself was electromagnetically charged. This question was addressed by Chamblin *et al.* (CAES) using the numerical approach of AGK in [31,30]. They concluded that, while in nonextremal cases the picture remained the same as for a Schwarzschild black hole, in the extremal case a new phenomenon occurred as the string was always expelled, regardless of its thickness.

In this chapter, we are concerned with the extremal Reissner–Nordstrøm black hole. We shall see that things are not as simple as claimed by CAES, and that flux expulsion does not occur in all cases.

6.2 Abelian–Higgs Strings in a Reissner–Nordstrøm Background

We consider here the abelian–Higgs theory described in chapter 1, given by the Lagrangian density (1.16)

$$\mathcal{L} = (D_a \Phi)^\dagger (D^a \Phi) - \frac{1}{4} \tilde{F}_{ab} \tilde{F}^{ab} - \frac{\lambda}{4} (\Phi^\dagger \Phi - 1)^2, \quad (6.2)$$

where as usual Φ is the Higgs field and $D_a \stackrel{\text{def}}{=} \nabla_a + ieA_a$ is a gauge-covariant derivative describing the interaction between the gauge field A_a (with strength tensor \tilde{F}_{ab}) and Φ . As before, we make the conventional Ansatz

$$\begin{aligned} \Phi(x^a) &= \eta X(x^a) e^{i\chi(x^a)}, \\ A_a(x^a) &= \frac{1}{e} [P_a(x^a) - \nabla_a \chi(x^a)]. \end{aligned} \quad (6.3)$$

With this notation, we have seen that the equations of motion are (1.24):

$$\begin{aligned} \square X - P_a P^a X + \frac{1}{2w_H^2} X (X^2 - 1) &= 0, \\ \nabla_a F^{ab} + \frac{\beta}{w_H^2} X^2 P^b &= 0. \end{aligned} \quad (6.4)$$

To consider the existence of abelian–Higgs hair to the black hole, Ref. [1] solved the field equations in a Schwarzschild background, and Refs. [31,30] in a Reissner–Nordstrøm background. Since the Schwarzschild metric is the particular case $Q = 0$ of the Reissner–Nordstrøm one, we adopt the latter’s line element:

$$ds^2 = \left(\underbrace{1 - \frac{2Gm}{r} + \frac{q^2}{r^2}}_{\stackrel{\text{def}}{=} V(r)} \right) dt^2 - \frac{dr^2}{1 - \frac{2Gm}{r} + \frac{q^2}{r^2}} - r^2 d\Omega_{II}^2. \quad (6.5)$$

The equations can be (notationally) simplified by defining scaled quantities $(r, M, Q) \stackrel{\text{def}}{=} (r, Gm, q)/w_H$ and rescaling the radial variable by a factor of w_H as in section 1.3. Then, $V \rightarrow 1 - 2M/r + Q^2/r^2$ (with the new, rescaled, r) and

equations (6.4) become

$$-\frac{1}{r^2} [r^2 V(r) X']' - \frac{1}{r^2 \sin(\theta)} [\sin(\theta) \dot{X}]' + \frac{1}{2} X (X^2 - 1) + \frac{N^2 P^2 X}{r^2 \sin(\theta)^2} = 0, \quad (6.6)$$

$$[V(r) P']' + \frac{\sin(\theta)}{r^2} \left[\frac{\dot{P}}{\sin(\theta)} \right]' - \frac{X^2 P}{\beta} = 0.$$

Here we have assumed that the gauge field can be written $P_a = NP \nabla_a \vartheta$. The symmetry about ϑ ensures that X and P depend only in r and θ ; primes and dots therefore denote differentiation with respect to r and θ , respectively.

Notice that we are only left with two scales: r_+ (the radius of the black hole's outer horizon measured in units of the Higgs width of the string) and $\beta = w_g^2$ (the gauge width of the string, also in units of w_H , squared). Additionally, we can always thicken the string by increasing its winding N .

Eqs. (6.6) were solved in [1,31,30] for the range $[r_{\min}, r_m] \times [0, 2\pi]$, where r_{\min} is the radius of the black hole's outer horizon \mathcal{H} ,

$$r_{\min} = r_+ \stackrel{\text{def}}{=} M + \sqrt{M^2 - Q^2} \quad (6.7)$$

and r_m is some radius sufficiently larger than r_+ for the numerical results to make sense.

6.3 Numerical Method and Results

To solve numerically the equations (6.6), we have used the technique developed in [1], which consists in relaxing initial configurations of the fields X and P on the (rectangularly) discretized plane, $(r, \theta) \rightarrow (i, j) \stackrel{\text{notn}}{=} (r_i = r_+ + idr, \theta_j = jd\theta)$. We replace therefore the fields by their values on this grid, $X(r, \theta) \rightarrow X_{i,j} \stackrel{\text{notn}}{=} X(i, j)$ (and similarly for P), and the differential operators by suitably discretized versions. Adopting the notation of [1] and [30] (that is, $X_{00} \stackrel{\text{notn}}{=} X_{i,j}$, $X_{\pm 0} \stackrel{\text{notn}}{=} X_{i\pm 1, j}$ and $X_{0\pm} \stackrel{\text{notn}}{=} X_{i, j\pm 1}$), we find that the discretized version of (6.6) is $(X_{00}, P_{00}) \rightarrow (X_{00}^{\text{new}}, P_{00}^{\text{new}})$, with¹

$$X_{00}^{\text{new}} = \frac{\frac{2}{r} \left(1 - \frac{M}{r}\right) \frac{X_{+0} - X_{-0}}{2\Delta r} + \frac{\cot \theta}{r^2} \frac{X_{0+} - X_{0-}}{2\Delta \theta} + V \frac{X_{+0} + X_{-0}}{\Delta r^2} + \frac{X_{0+} + X_{0-}}{r^2 \Delta \theta^2}}{\frac{2V}{\Delta r^2} + \frac{2}{r^2 \Delta \theta^2} + \frac{1}{2} (X_{00}^2 - 1) + \left(\frac{NP_{00}}{r \sin \theta}\right)^2}, \quad (6.8a)$$

¹Two misprints crept into the corresponding equations (24a,b) of [20]: the terms divided by Δr^2 should be " $X_{+0} + X_{-0}$ " and " $P_{+0} + P_{-0}$ " — as above — instead " $X_{0+} + X_{0-}$ " and " $P_0 + P_{0-}$ ".

$$P_{00}^{\text{new}} = \frac{\frac{2}{r^2} \left(M - \frac{Q^2}{r} \right) \frac{P_{+0} - P_{-0}}{2\Delta r} - \cot \theta \frac{P_{0+} - P_{0-}}{2r^2 \Delta \theta^2} + V \frac{P_{+0} + P_{-0}}{\Delta r^2} + \frac{P_{0+} + P_{0-}}{r^2 \Delta \theta^2}}{\frac{2V}{\Delta r^2} + \frac{2}{r^2 \Delta \theta^2} + \frac{X_{00}}{\beta}}. \quad (6.8b)$$

There is, however, a subtlety in this process: relaxation methods usually require that the values of the fields be fixed at *all* the boundaries of the domain of integration. If indeed we know the asymptotic values of X and P at $r \rightarrow \infty$ (the vacuum) and at $\theta \rightarrow 0, \pi$ (the string core values), the solution at the horizon $r = r_+$ is not only unknown, it is the main result we expect from these numerical calculations. The solution imagined by AGK [1] to this problem was to also update the values of the fields at the horizon immediately after updating the interior of the grid. Replacing $r = r_+$ in (6.6), we obtain equations on the horizon:

$$\begin{aligned} V'(r_+) \left. \frac{\partial X}{\partial r} \right|_{r=r_+} &= -\frac{1}{r_+^2 \sin \theta} \left(\sin \theta \dot{X} \right)' + \frac{1}{2} X (X^2 - 1) + \frac{N^2 X P^2}{r_+^2 \sin^2 \theta}, \\ -V'(r_+) \left. \frac{\partial P}{\partial r} \right|_{r=r_+} &= \frac{\sin \theta}{r_+^2} \left(\frac{\dot{P}}{\sin \theta} \right)' - \frac{X^2 P}{\beta}. \end{aligned} \quad (6.9)$$

We discretize this in the same way that we discretized the equations on the interior of the grid, except that we must now take discretized differential operators that do not depend on X_{-0} or P_{-0} , since these points do not exist. The resulting equations are²

$$\begin{aligned} X_{00} \rightarrow X_{00}^{\text{new}} &= \frac{\sqrt{M^2 - Q^2} \frac{X_{+0}}{\Delta r} + \frac{X_{0+} + X_{0-}}{2\Delta \theta^2} + \cot \theta \frac{X_{0+} - X_{0-}}{4\Delta \theta}}{\frac{\sqrt{M^2 - Q^2}}{\Delta r} + \frac{1}{\Delta \theta^2} + \frac{r_+^2}{4} (X_{00}^2 - 1) + \frac{1}{2} \left(\frac{N P_{00}}{\sin \theta} \right)^2}, \\ P_{00} \rightarrow P_{00}^{\text{new}} &= \frac{\sqrt{M^2 - Q^2} \frac{P_{+0}}{\Delta r} + \frac{P_{0+} + P_{0-}}{2\Delta \theta^2} - \cot \theta \frac{P_{0+} - P_{0-}}{4\Delta \theta}}{\frac{\sqrt{M^2 - Q^2}}{\Delta r} + \frac{1}{\Delta \theta^2} + \frac{r_+^2}{2\beta} X_{00}^2}. \end{aligned} \quad (6.10)$$

The process of updating the interior of the grid and then the horizon at each iteration was carried on until the largest relative correction in absolute value on the grid became smaller than some ε :

$$\max_{i,j} \left| \frac{X_{i,j}^{\text{new}} - X_{i,j}^{\text{old}}}{X_{i,j}^{\text{old}}} \right|, \quad \max_{i,j} \left| \frac{P_{i,j}^{\text{new}} - P_{i,j}^{\text{old}}}{P_{i,j}^{\text{old}}} \right| < \varepsilon. \quad (6.11)$$

The evaluation of the maximum of the relative errors was carried out over the whole grid, including the horizon. (A value of $\varepsilon = 10^{-2}$ is usually enough for plots; for quantitative results, better accuracies must be considered.)

²Again, there were two misprints in equations (26a,b) of [20], where “ r_+ ” should read “ r_+^2 ” in both denominators.

We have first of all implemented the algorithm described above in the case of a Schwarzschild black hole. Figures 6.2 and 6.3 show the fields we obtained for thin and thick strings. In each case, our results compared well to the figures of [1]; in particular, we also found that the Nielsen–Olesen approximation is excellent for thin vortices, and is even reasonable for thicker vortices, which however tend to pinch slightly at the equator of \mathcal{H} .

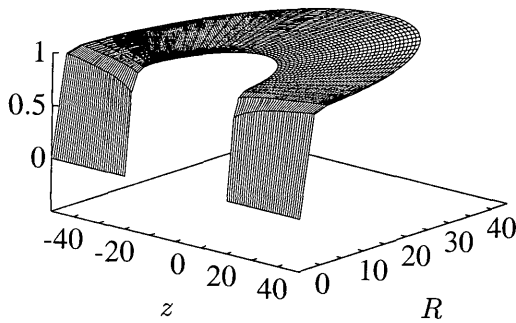
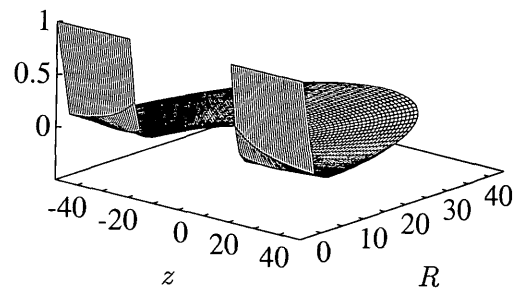
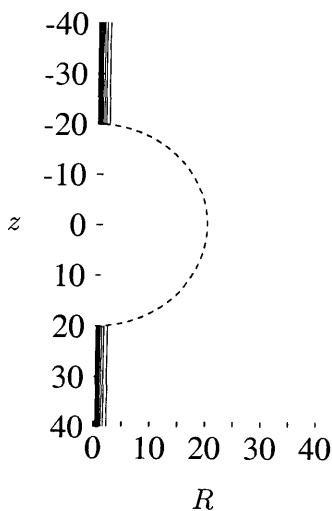
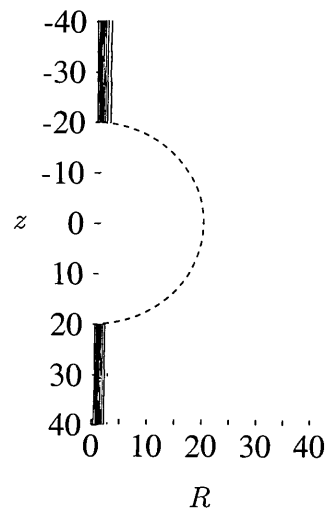
(a) Field X (b) Field P (c) X -contours(d) P -contours

Figure 6.2: A thin cosmic string threading a Schwarzschild black hole. Here, $M = 10$, $Q = 0$, $\beta = 1/2$, $N = 1$ and $r_m = 60$. For the sake of clarity, the grid in (a) and (b) was very coarse, $N_r = N_\theta = 50$; for (c) and (d) we used $N_r = N_\theta = 200$. $\varepsilon = 10^{-2}$ in all cases. The horizon is represented by the dashed line in (c) and (d).

We then turned our attention towards Reissner–Nordström black holes, comparing now our results with those of CAES. We found, as they did, that in the

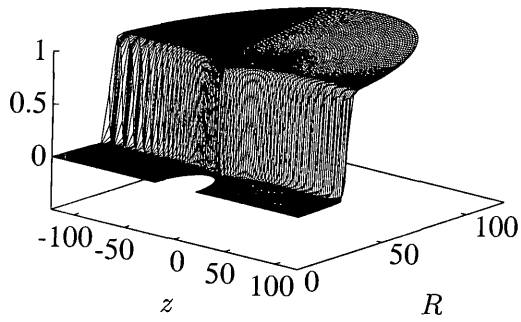
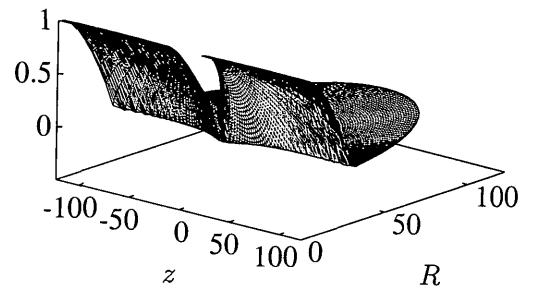
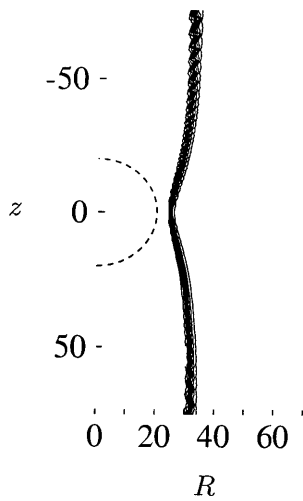
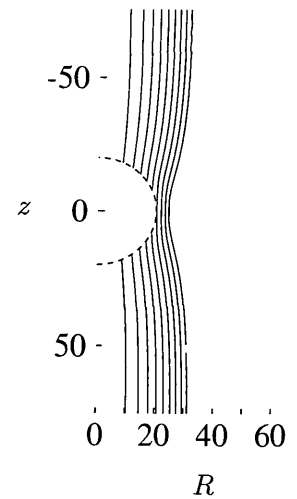
(a) Field X (b) Field P (c) X -contours(d) P -contours

Figure 6.3: A thick cosmic string threading a Schwarzschild black hole. This time $M = 10$, $Q = 0$, $\beta = 1/2$, $N = 400$ and $r_m = 150$. Here, $N_r = N_\theta = 100$ and $\varepsilon = 10^{-2}$.

nonextremal case the picture remains qualitatively the same as for Schwarzschild black holes. For extremal black holes, however, our results differ from their original claims; indeed, we find that the expulsion of the matter fields for thin strings in this limit is the result of a loophole in the numerical method (when applied to extremal black holes).

If we are to study piercing and expelled solutions numerically, we must first define those more precisely. We say that the string is expelled from the black hole if the solution on \mathcal{H} corresponds to a string core ($X = 0, P = 1$); otherwise, the string is considered to pierce the black hole.

Let us now see why our results differ from those of CAES. Because in the extremal case $V'(r_+) = 0$, it can be seen from (6.9 or 6.10) that *the extremal horizon decouples from the bulk of the grid*. This manifests itself in (6.9) by the fact that the terms containing derivatives of X or P with respect to r vanish, and in (6.10) by the disappearance of $X_{\pm 0}$ and $P_{\pm 0}$. Note that this leaves ODEs for $X(\theta)$ and $P(\theta)$ on \mathcal{H} , which are of course much simpler to solve than partial differential equations. Explicitly, these are

$$\begin{aligned} -\frac{1}{\sin\theta} \left(\sin\theta \dot{X} \right)' + \frac{N^2 P^2 X}{\sin^2\theta} + \frac{1}{2} M^2 X (X^2 - 1) &= 0, \\ \sin\theta \left(\frac{\dot{P}}{\sin\theta} \right)' - \frac{M^2 X^2 P}{\beta} &= 0. \end{aligned} \tag{6.12}$$

The consequence of this decoupling is that whatever happens inside the grid will have no influence on the horizon. In other words, before accepting a solution one must still check that it is continuous (better yet: smooth) as $r \rightarrow r_+$. This is not automatic; because of the nonlinearity of the equations to integrate, different initial guesses might lead to different solutions on the horizon.

Physically, the reason for this decoupling resides in the fact that the horizon lies at an infinite proper distance away from the rest of grid. Indeed, the (proper) distance between two points at constant t, θ and z , and at (coordinate) distances r_1 and $r_1 + \delta r$ from the singularity is

$$\Delta l \sim \int_{r_1}^{r_1 + \delta r} \frac{dr}{\sqrt{V(r)}} = \begin{cases} \int_{r_1}^{r_1 + \delta r} \frac{dr}{\sqrt{1 - \frac{2M}{r} + \frac{Q^2}{r^2}}} & M \neq Q, \\ \int_{r_1}^{r_1 + \delta r} \frac{dr}{1 - \frac{M}{r}} & M = Q. \end{cases} \tag{6.13}$$

In the extremal case, $\Delta l \sim r_1 + M \ln|r_1 - M|$ and the integral diverges as $r_1 \rightarrow r_+ = M$. In a numerical code, the first row of the grid ($i = 0$) lies at r_+ and the second lies at an infinite proper distance away from it.

By itself this would be harmless, because the program would still use Eq. (6.12) to update the horizon, albeit independently from the rest of the grid. We do, however, encounter a real problem if the initial guess on the horizon is a solution of (6.12), because clearly the program then never updates this guess. This is notably the case for a “core” guess ($X = 0, P = 1$), which was the one that CAES always used.³ If this guess is made on the horizon, the program will never be able to modify it, and whether or not it smoothly connects with the solution on the interior of the grid is left for the programmer to ensure. To turn around this problem, we have considered three different initial data sets:

- **Core:** $X = 0, P = 1$;
- **Vacuum:** $X = 1, P = 0$;
- **Sine:** $X = \sin \theta, P = 1$.

Note that although the vacuum solves Eqs. (6.12), it does not satisfy the boundary conditions on the poles, which are core.

Our results then show that (for a thin string) if we choose a core initial data set on the horizon (figures 6.4a, 6.5a), then we find that the string is expelled; however, if we use either of the vacuum or sine guess (figures 6.4b, 6.5b) we find that the string pierces the horizon. The solution on the interior of the grid is the same for all three initial data sets.

We have several physical and numerical reasons to believe that the piercing solution is to be preferred: firstly, the fields have lower energy in the piercing case (because of the X' and P' terms in the energy density); secondly, this solution is smooth at the horizon, unlike the expelled one (where, despite decreasing the stepsize Δr , it proved impossible to smooth the sharp jump from $X = 0$ on the horizon to $X \approx 1$ on the bulk of the grid); finally, it is numerically more robust, since it can be obtained by more general initial guesses.

³CAES’s paper [31] claims, just under Eq. (3.4) to have used a vacuum guess. From our results, this seems to have been a typo, however, and Andrew Sornborger confirmed to me that they have always used ($X = 0, P = 1$) (core) as the initial horizon guess.

Note that we consider the smoothness of the physical solution to be an important argument in favour of the piercing solution. Under the requirement that the solution should be continuous at $r = r_+$, it would be easy to simplify the numerical method described above by computing the values of the fields on the horizon simply by continuity from the bulk the grid. It is true that this method would be less accurate than relaxing equations (6.10),⁴ but it would have the advantage of always selecting smooth solutions.⁵

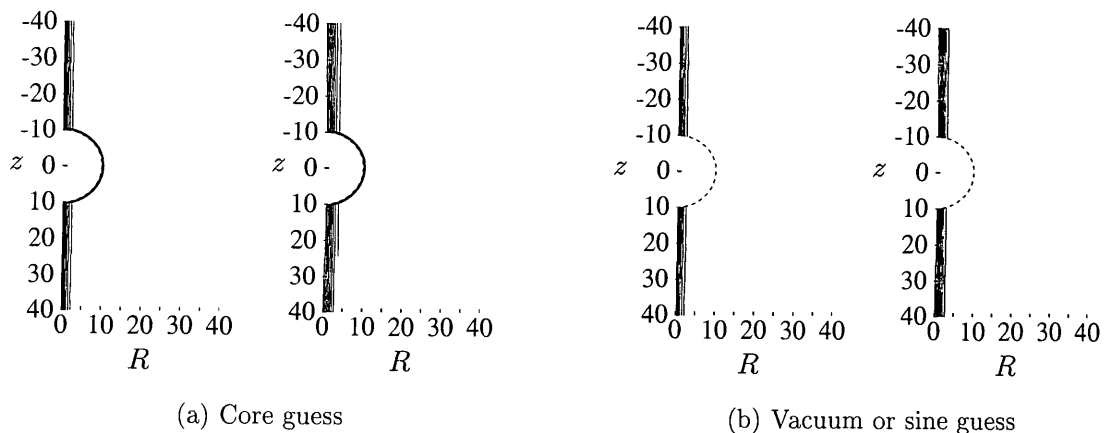


Figure 6.4: Contours of X and P for a core guess (left) and a vacuum (or sine) initial guess. The parameters are $M = Q = 10$, $\beta = N = 1$, $\varepsilon = 10^{-4}$, $N_r = N_\theta = 100$.

To determine how the transition from a piercing to a wrapping solution occurs as we thicken the string, we can take advantage of the fact that, on the horizon, we now have ODEs. This allows for much quicker and more accurate numerical methods. For the following calculations we have used the relaxation routine SOLVDE of [82, chapter 17].

The solutions we find all have the same shape on \mathcal{H} (figure 6.6): the Higgs field rises from the core value at the poles with a non-zero θ -derivative to some maximum value X_m at $\theta = \pi/2$, whereas the gauge field falls from the core value at the poles with vanishing θ -derivative to some minimum value P_m at $\theta = \pi/2$.

For massive black holes (or, equivalently, thin strings), the fields adopt a vacuum profile on most of the horizon (symmetrically around $\theta = \pi/2$) and interpolate

⁴Presumably, this was the reason for inventing this more complicated method in the first place.

⁵When we consider the case of a single string ending on a black hole in the next section, we will have to solve the equations on the boundary $\theta = \pi$; there, however, the discretized equations are unstable, and we will have to resort to this continuity method; see page 106.



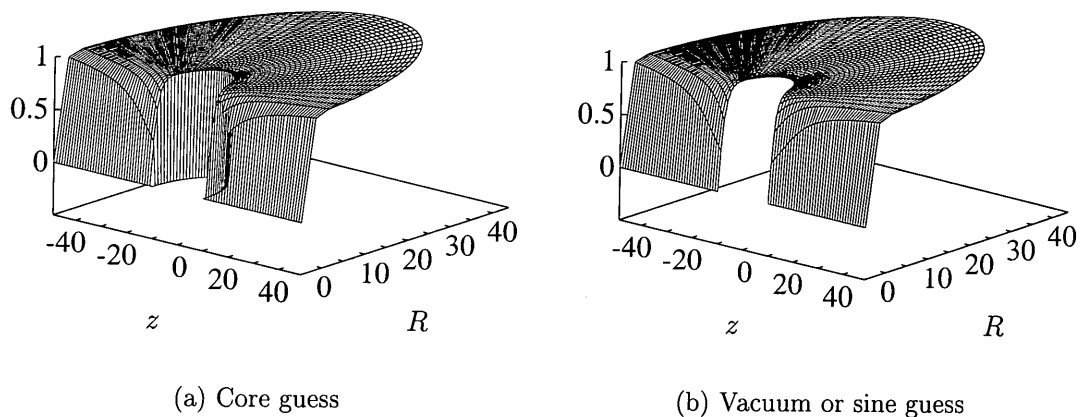


Figure 6.5: Field X relaxed from a core guess (left) and from a vacuum (or sine) initial guess. The parameters are $M = Q = 10, \beta = N = 1, \varepsilon = 10^{-4}, N_r = N_\theta = 50$.

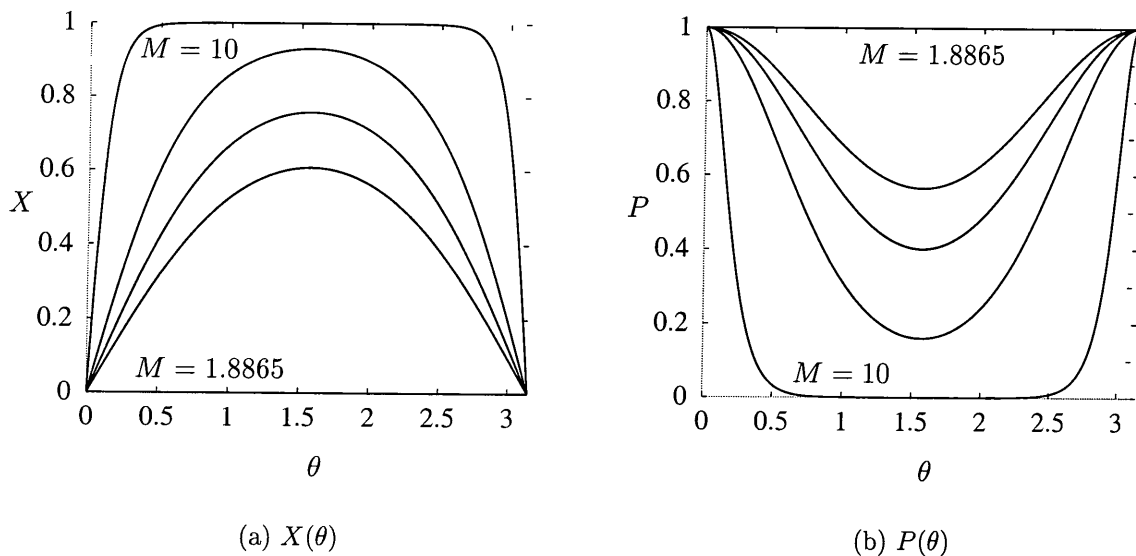


Figure 6.6: Functions $X(\theta)$ and $P(\theta)$ on the black hole's horizon for $\beta = N = 1$ and $M = 10, 2.5, 2, 1.9$ and 1.8865 .

smoothly to their fixed boundary values at the poles. As we decrease the black hole's mass (thicken the string), X_m and P_m move away from the vacuum values, i.e. X_m decreases and P_m increases. As figure 6.7 shows, for $\beta = N = 1$ this occurs gently at first, and accelerates suddenly, as if the string had crossed some critical width beyond which it cannot pierce the horizon any more; eventually, the fields are expelled from it (see figure 6.8 for an example of such a solution).

Figure 6.7 also shows the effect of varying the Bogomol'nyi parameter β on the curves $X_m(1/M)$ and $P_m(1/M)$. Increasing this parameter means thickening the gauge width of the string, and therefore we expect that the critical mass for the transition to occur will increase, which is precisely what happens. However, there seems to be a limit value of $M = 1/2$, that is, for $N = 1$ and regardless of the value of β , all strings whose width w_H is smaller than $r_+/2$ must pierce the horizon, and therefore constitute hair to the extremal black hole.

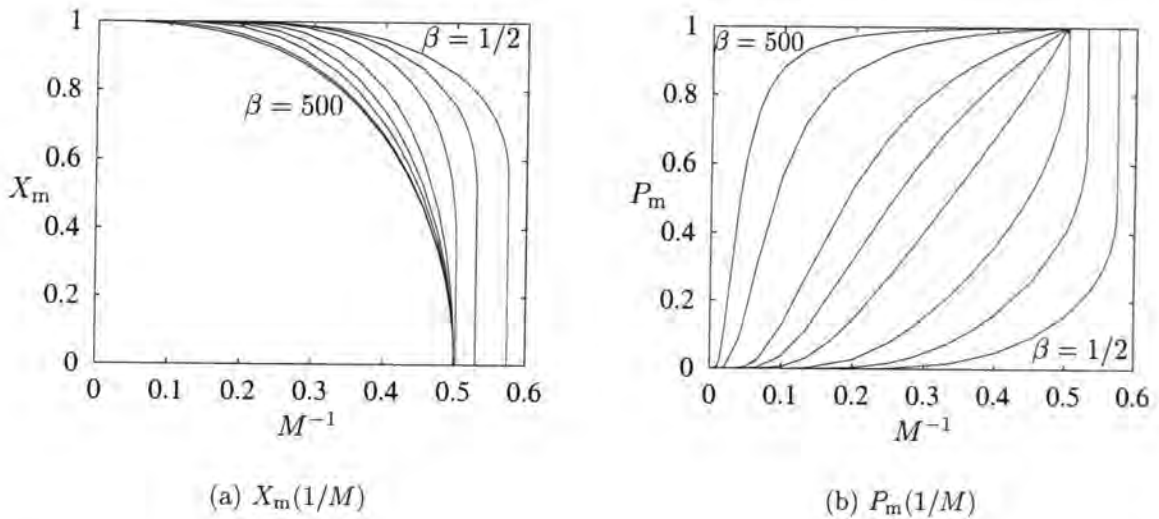


Figure 6.7: Evolution of $X_m(1/M)$ and $P_m(1/M)$ for $N = 1$ and $\beta = 1/2, 1, 2, 5, 10, 20, 100$ and 500 .

This can also be inferred from figure 6.9, which shows the evolution of M_c (defined as the critical mass below which the only possible solution is the expelled one) as a function of β and N . This figure also shows that increasing N has that same effect of increasing M_c , which had also been anticipated from the fact that it also thickens the string. This time, however, we observed that increasing N actually shifted the curves $X_m(1/M)$ and $P_m(1/M)$ to the left, without changing their shape. This is in

contrast to figure 6.7, where clearly the shape of $P_m(1/M)$ changes as β increases. (This is probably due to the fact that varying β changes the gauge width of the string, but not the Higgs width.) Beyond $N = 8$, the numerical results started becoming somewhat unreliable; unfortunately, that is not enough to obtain evidence for the existence (or otherwise) of a limit value of M , as when we varied β at fixed $N = 1$.

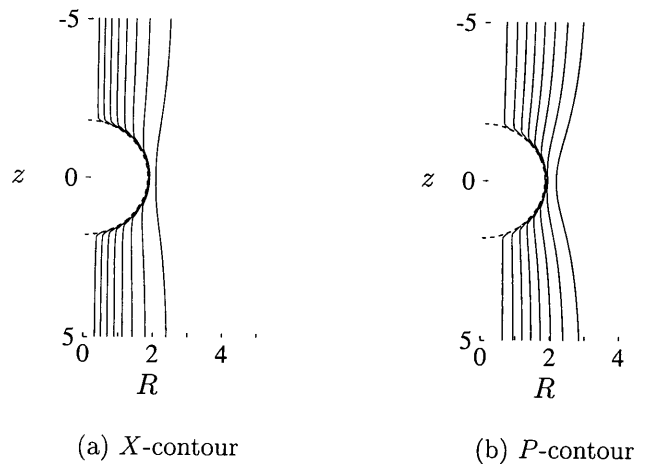


Figure 6.8: An example of expelled solution. Here, $M = Q = 1.8$ (just below the critical value $M = 1.8865$ shown on figures 6.6 and 6.7); also, $\beta = N = 1$, $\varepsilon = 10^{-3}$ and $N_r = N_\theta = 100$.

6.4 String Ending on a Black Hole

We now turn to the important case of a string ending on a black hole. The existence of such a configuration is necessary to check that a pair black hole/anti-black hole can be created inside the string, which might then be split and decay. We have seen that in the Schwarzschild case, AGK [1] have proved that these configurations are quite possible; we now investigate the case of Reissner–Nordström black holes, and show that not only these configurations always exist, they also exhibit in the extremal case a phenomenon analogous to the flux expulsion of the previous section.

On the horizon, and for numerical purposes, the single-string case differs from the one we considered previously only by the boundary conditions on the poles. At $\theta = 0$ we still require a string, but at $\theta = \pi$ nothing actually forces the fields to take a vacuum configuration. Indeed, we found that the only smooth solutions were such that the Higgs field X had a vanishing derivative at the South Pole (see figure 6.10).

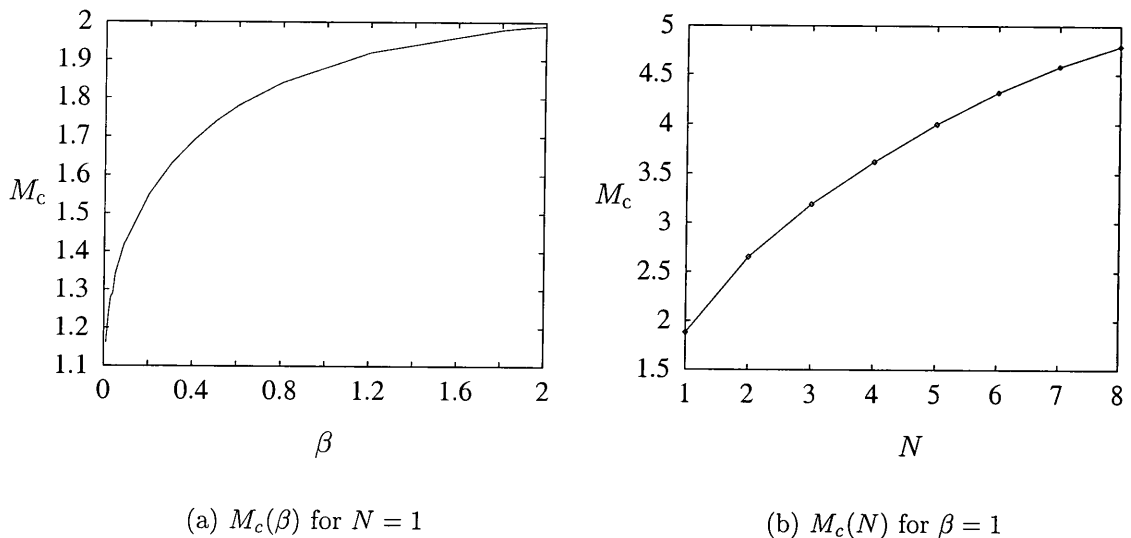


Figure 6.9: Critical mass M_c as a function of the Bogomol'nyi parameter β (for $N = 1$) and of N (for $\beta = 1$). On figure (a), the curve asymptotes at 2; on figure (b) we cannot tell, more points would be required. [In (b) we have joined the points to guide the eye.]

Clearly the value of $X_m = X(\pi)$ depends on the black hole's mass; therefore, if we want to tackle this problem on the whole grid (and following the method that worked so well on the horizon), we need to also update the $\theta = \pi$ boundary. We can find the equations of motion on this line by assuming that $P/\sin\theta \rightarrow 0$ and that $X_\theta \rightarrow 0$ there, but unfortunately the resulting numerical scheme was unstable (i.e., numerical roundoff errors propagated uncontrollably) and the replacement of the discrete differential operators by more sophisticated ones, accurate to order $O(\Delta r^4, \Delta\theta^4)$ or higher, failed to stabilize the code. This problem was solved by decomposing the method in three steps:

1. **Solve the problem on the horizon alone and fix the value of the fields at the South Pole S .** The initial guess for X on \mathcal{H} was $X = \sin(\theta/2)$, which is 1 at S , and as the program updated it, $X(S)$ decreased. Without fixing the value of $X(S)$, the program of step 2 “missed” the real solution and updated X until it vanished identically on the horizon.
2. **Solve inside the grid and on the horizon as before.** Also (and only for the first 100 iterations or so) couple the horizon to the grid interior, so that the solution on the horizon will drive that on the whole spacetime outside it.

3. Update the $\theta = \pi$ boundary by continuity, assuming $X_{,\theta} = P_{,\theta} = 0$ there.

An example of a configuration found by this program is presented on figure 6.11.

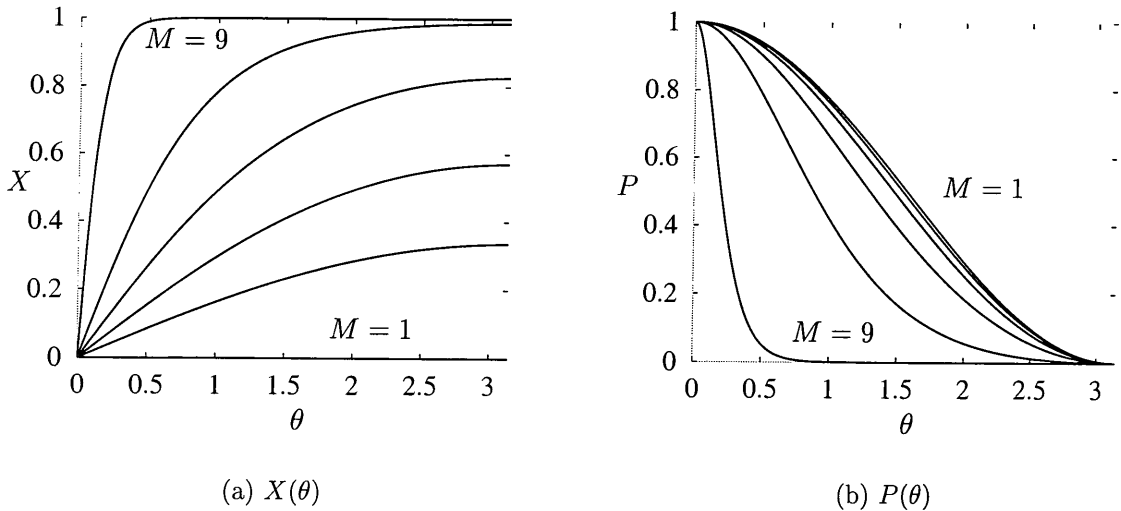


Figure 6.10: Solution on the horizon for a single string ending on the extremal black hole for $\beta = N = 1$ and $M = 9, 2, 1.3, 1.1, 1.03$ and 1. (At this scale, the X -profile for $M = 1$ lies on the axis.)

Returning to figure 6.10, we see that as we thicken the string, the X field is again expelled from the horizon (completely so for $M \approx 1$, i.e. for a string of width comparable to the black hole’s outer radius), whereas the P field quickly adopts the “monopole” form:

$$P_{\text{mon}} \stackrel{\text{def}}{=} \frac{1 + \cos(\theta)}{2}.$$

This configuration is illustrated on figure 6.12.

6.5 Analytical Considerations

In this section, we shall try to extract analytically some information from equations (6.6). We will show in particular that both penetration and flux expulsion must occur (respectively for thin and thick strings), and place bounds on each behaviour. We shall see that these bounds will be somewhat weak, but in agreement with the numerical values previously found.

We can first of all argue that thin strings must penetrate the black hole’s horizon. Following [1], we postulate that such a string would look very much like a Nielsen–

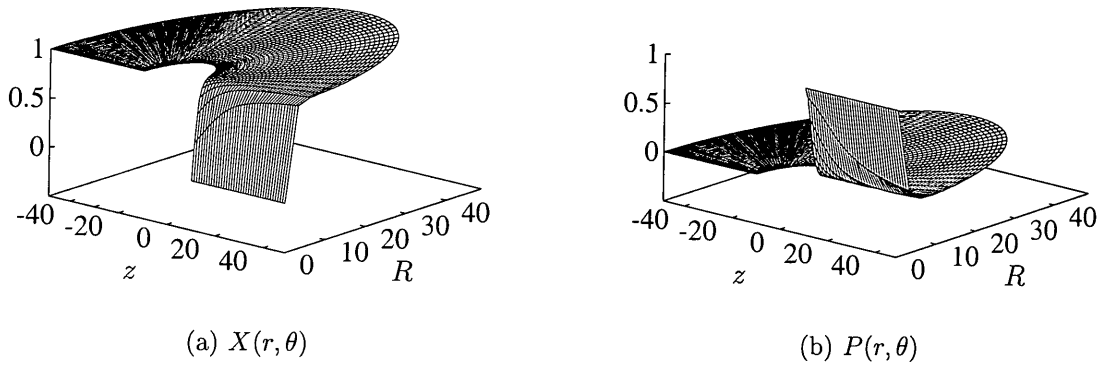


Figure 6.11: Solution for a single string ending on the extremal black hole for $M = Q = 10$, $\beta = N = 1$ and $\varepsilon = 10^{-3}$, $N_r = N_\theta = 50$.

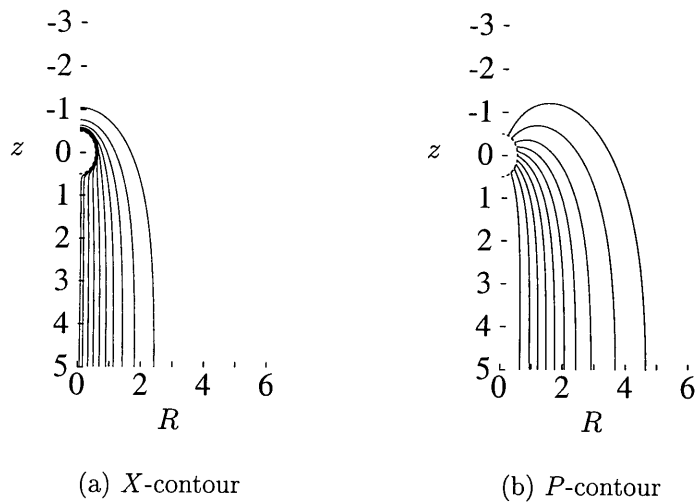


Figure 6.12: Contours of X and P for a single string ending on the black hole, and $M = Q = 1/2$, $\beta = N = 1$, $N_r = N_\theta = 100$, $r_m = 10$.

Olesen vortex, and therefore take the shape $X = X(\varrho)$, $P = P(\varrho)$, where ϱ is still the distance from the z -axis, $\varrho = r \sin \theta$. Then, the equations of motion (6.6) become

$$\begin{aligned} -X'' - \frac{X'}{\varrho} + \frac{N^2 X P^2}{\varrho^2} + \frac{1}{2} X (X^2 - 1) &= \frac{\varrho^2}{r^2} \left(\frac{2M}{r} - \frac{Q^2}{r^2} \right) \left(X'' + \frac{X'}{\varrho} \right), \\ -P'' + \frac{P'}{\varrho} + \frac{X^2 P}{\beta} &= \frac{\varrho^2}{r^2} \left[\frac{Q^2}{r^2} \left(P'' - 2 \frac{P'}{\varrho} \right) - \right. \\ &\quad \left. \frac{2M}{r} \left(P'' - \frac{P'}{\varrho} \right) \right]. \end{aligned} \quad (6.14)$$

On the right-hand side we have terms of the order ϱ^2/r^2 times terms of order unity. Near the core, $\varrho \sim O(M^{-2})$; for thin strings, $M \gg \sqrt{N} \geq 1$ and therefore this is negligible. Then, since the left-hand side of the equations are precisely the Nielsen–Olesen equations, we find that the Nielsen–Olesen solution satisfies the equations of motion near the core. These solutions tending exponentially fast to their asymptotic values (1.27), by the time the premultiplying factor ϱ^2/r^2 becomes significant, the terms in X' , P' , X'' and P'' are themselves negligible, and the solution should still be Nielsen–Olesen. In brief, the Nielsen–Olesen solution (which penetrates the horizon) should be an excellent approximation to the real solution for thin strings. Notice that this argument does not make any assumption on Q , and that therefore its conclusion should be valid for extremal black holes too.

However, it was shown in [31] that for high-winding (and hence thick) strings the flux must be expelled. Indeed, if the black hole is deep inside the string core, we can neglect the $X^2 P$ -term in the equation for P (6.6), which is then solved by

$$P \approx 1 - p (r^2 - Q^2) \sin^2 \theta, \quad (6.15)$$

where p is some constant. Clearly, $P = 1$ on the horizon if $M = Q = r_+$. Moreover, the flux across the horizon is $G_{\theta\theta} = \dot{P}$ and vanishes. Finally, the corresponding solution for X is given by $X = [b(r) \sin \theta]^N$; near the horizon, [31] found that

$$d(\ln b) \propto \frac{dr}{\sqrt{(r - r_+)(r - r_-)}}. \quad (6.16)$$

For extremal black holes, $b \sim r - r_+$ and X vanishes at the horizon.

6.5.1 Proof of Flux Expulsion for Thick Strings

First of all, recall that in the extremal case, the horizon decouples from the rest of the spacetime, and that flux expulsion is always a solution on the horizon. Hence,

all we need to do to prove that expulsion must happen is to show that for some range of $M > M_c$ a piercing solution cannot exist.⁶ We are going therefore to assume that a piercing solution exists on the horizon, and use (6.9) to deduce some properties of this solution. Whenever these properties are found to be inconsistent, the solution must correspond to flux expulsion.

Assume therefore that a nontrivial solution $(X(\theta), P(\theta))$ exists on the horizon. This solution must be symmetric about $\theta = \pi/2$, and thus X and P have respectively a maximum X_m and a minimum P_m there. By expanding the equations at $\theta = 0, \pi$ it can be seen that $|\dot{X}| > \dot{P} = 0$ at the poles; therefore, there exists a point θ_0 such that $\ddot{P} = 0$ and $\dot{P} < 0$ at $\theta = \theta_0$.

Consider equation (6.9) at $\theta = \pi/2$; since $X_{,\theta\theta} < 0$, it implies

$$P_m^2 < \frac{1}{2} \frac{M^2}{N^2} (1 - X_m^2) < \frac{1}{2} \frac{M^2}{N^2}.$$

Hence,

$$\ddot{P}(\pi/2) = \frac{M^2}{\beta} X_m^2 P_m < \frac{M^3}{\sqrt{2}\beta N} X_m^2 \sqrt{1 - X_m^2} < \frac{\sqrt{2}}{3\sqrt{3}} \frac{M^3}{\beta N} \quad (6.17)$$

(where we have maximized over X_m in the last step). This gives us an upper bound on $\ddot{P}(\pi/2)$. We will now obtain a lower bound on the same quantity, and the consistency of these two bounds will provide the maximum range of the parameter M over which a piercing solution can exist.

The lower bound on $\ddot{P}(\pi/2)$ can be estimated by noting that P_m must be larger than it would be if P decreased linearly from the pole to $\pi/2$ with the highest possible slope, which is $\dot{P}(\theta_0)$:

$$P_m > 1 - \frac{\pi}{2} |\dot{P}(\theta_0)|. \quad (6.18)$$

Now, this slope is

$$|\dot{P}(\theta_0)| = \frac{M^2}{\beta} X^2 P \tan \theta_0 < \frac{M^2}{\beta} \tan \theta_0 \quad (6.19)$$

and therefore (using the bound previously found on P_m)

$$|\dot{P}(\theta_0)| > \frac{2}{\pi} \left(1 - \frac{M}{\sqrt{2}N} \right). \quad (6.20)$$

Assuming that $M < \sqrt{2}N$, this gives

$$\frac{\pi}{2} - \theta_0 < \cot \theta_0 < \frac{\pi M^2}{2\beta \left(1 - \frac{M}{\sqrt{2}N} \right)}. \quad (6.21)$$

⁶We consider only smooth solutions.

For $M^2 X_m^2 < 2\beta$, one can show that \ddot{P} has a maximum at $\pi/2$, and hence

$$\ddot{P}(\pi/2) \geq \frac{\dot{P}(\pi/2) - \dot{P}(\theta_0)}{\pi/2 - \theta_0} > \left(\frac{2}{\pi}\right)^2 \frac{\beta}{M^2} \left(1 - \frac{M}{\sqrt{2}N}\right)^2. \quad (6.22)$$

The compatibility between (6.17) and (6.17) implies

$$\sqrt{2}\pi^2 M^5 > 12\sqrt{3}\beta^2 N \left(1 - \frac{M}{\sqrt{2}N}\right)^2. \quad (6.23)$$

If this inequality is violated, then the vortex flux must be expelled. Writing $\mathcal{M} = M/\sqrt{2}N$, this is the case for

$$\frac{\mathcal{M}^5}{(1 - \mathcal{M})^2} < \frac{3\sqrt{3}\beta^2}{2\pi^2 N^4} \simeq \frac{\beta^2}{4N^4}. \quad (6.24)$$

For $\beta = N = 1$, this gives $M < 0.7$, which is a weak bound: as we have seen, our numerical work puts this bound at $M \approx 1.8865$ (figure 6.6).

6.5.2 Proof of Penetration for Thin Strings

Now we are going to employ the same kind of argument to show that thin strings must penetrate the horizon. That is, we are going to show that expelled solutions cannot exist for big enough black hole masses. Since expulsion is always permitted on the horizon (and therefore can only be excluded by continuity with the rest of the grid), we need to consider the general equations (6.6) close to (but not only at) the horizon.

Assume that a solution is expelled. Then at $r = r_+$, $X = 0$ and $P = 1$; for $r \gtrsim M$ therefore, $M^2 X^2 \ll 1$ and $[(r - M)^2 X']' > 0$. Then, for $r > M$

$$\frac{1}{2}M^2 X \sin^2 \theta + \sin \theta \partial_\theta (\sin \theta \partial_\theta X) < X N^2 P^2 < X N^2. \quad (6.25)$$

We know that X is symmetric around $\pi/2$, where it reaches a maximum value X_m , and that $\sin \theta \dot{X}$ vanishes at $\theta = 0, \pi/2$ and π . Let θ_0 be the value at which $(\sin \theta \dot{X})' = 0$; it must satisfy $\frac{1}{2}M^2 \sin^2 \theta_0 < N^2$. For $M < \sqrt{2}N$, this is trivial, so let us now assume that $M > \sqrt{2}N$. Let $\alpha > \theta_0$ be defined by $M^2 \sin^2 \alpha = 2N^2$.

Integrating (6.25) on the range $(\theta, \pi/2)$ for $\theta > \alpha$ gives

$$\dot{X}(\theta) > X(\theta) \left[\frac{1}{2}M^2 \cot \theta + N^2 \csc \theta \ln \tan \theta/2 \right]. \quad (6.26)$$

But since $\ddot{X} < 0$ in $(\alpha, \pi/2)$, we can deduce that

$$\dot{X} < \frac{X(\theta) - X(\theta_0)}{\theta - \theta_0} < \frac{X(\theta)}{\theta - \alpha}. \quad (6.27)$$

Consistency of this with (6.26) therefore requires that

$$\frac{1}{N^2} > (\theta - \alpha) [\csc^2 \alpha \cot \theta + \csc \theta \ln \tan \theta/2] \quad (6.28)$$

holds for all $\theta \in (\alpha, \pi/2)$. The lowest value of M for which this inequality is violated gives the bound for the existence of an expelled solution. For $N = 1$, we find $M^2 = 8.5$, i.e. $1/M \approx 0.343$.

6.5.3 String Ending on a Black Hole

Our aim in this paragraph is to show analytically that the phenomenon of X -flux expulsion observed numerically for strings ending on a black hole must indeed occur.

Consider the equations on the horizon (6.9); as we mentioned in the previous section, they will have the boundary values $X = 0, P = 1$ at the North Pole $\theta = 0$ and $X = X_m, P = 0$ at the South Pole $\theta = \pi$. By integrating the equation for P , we obtain

$$\underbrace{\left(1 - \frac{M^2 X_m^2}{\beta}\right)}_{\stackrel{\text{def}}{=} \lambda} (1 + \cos \theta) < 2P < (1 + \cos \theta). \quad (6.29)$$

Therefore, as $M^2/\beta \rightarrow 0$, P approaches P_{mon} . Let us assume that this is the case, and find the behaviour of X . As in the case of the string threading the black hole, note that $X = 0, P = P_{\text{mon}}$ is always a solution on the horizon.

Assume that there exists a piercing solution. Then $X(\pi) = X_m > 0$ is a local maximum value of the Higgs field. Let θ_0 be defined by $(\sin \theta_0 \dot{X})' = 0$. Then, at θ_0 we have

$$P_0^2 = \frac{M^2}{2N^2} \sin^2 \theta_0 (1 - X_0^2).$$

Since $M \ll N$, θ_0 will be close to π ; using the bounds on P , we can see that

$$\frac{2}{\pi} (\pi - \theta_0) < \sin \theta_0 < \frac{4M}{\sqrt{2}N\lambda}. \quad (6.30)$$

Integrating the equation for X (6.9) between 0 and π gives

$$\int_{\theta_0}^{\pi} d\theta X \left[\frac{M^2}{2N^2} \sin \theta (1 - X^2) - \frac{P^2}{\sin \theta} \right] = \int_0^{\theta_0} X \left[\frac{P^2}{\sin \theta} - \frac{M^2}{2N^2} \sin \theta (1 - X^2) \right]. \quad (6.31)$$

The first integral can be bounded above by $4M^2X_m/N^4\lambda^2$. The second one can be also bounded by noting that \ddot{X} is positive on $[\pi/2, \theta_0]$, but negative at π . Therefore, we have a bound for \dot{X} in $[\pi/2, \pi]$ in

$$\dot{X} < X_m N^2 \sin^3 \theta_0. \quad (6.32)$$

Hence, X can be bounded below in this interval by

$$X > X_m \left[1 - \frac{4\pi M^3}{N\lambda^3} \right]. \quad (6.33)$$

Finally,

$$\begin{aligned} \int_0^{\theta_0} X \left[\frac{P^2}{\sin \theta} - \frac{M^2}{2N^2} \sin \theta (1 - X^2) \right] &> \int_{\pi/2}^{\theta_0} X \left[\frac{P^2}{\sin \theta} - \frac{M^2 \sin \theta}{2N^2} \right] \\ &> \frac{\lambda^2}{16} X_m \left(1 - \frac{4\pi M^3}{N\lambda^3} \right) \left(1 - \frac{8M^2}{N^2\lambda^2} \right)^2. \end{aligned} \quad (6.34)$$

Inserting these bounds in (6.31), we find that the piercing solution cannot exist if

$$M^4 < \frac{N^4\lambda^4}{64} \left(1 - \frac{4\pi M^3}{N\lambda^3} \right) \left(1 - \frac{8M^2}{N^2\lambda^2} \right)^2 \quad (6.35)$$

For $N = 1$, this gives $M < 0.3$.

6.6 Discussion and Outlook

The most prominent results of this chapter are the proof that thin strings always pierce a Reissner–Nordström horizon (and therefore may be seen as hair to the black hole), and the existence of the phase transition separating the piercing and the wrapping solutions (and illustrated in figure 6.7). This phase transition is somewhat reminiscent of that separating wall and vacuum-de Sitter solutions in Chapter 4, where (recall the discussion from pages 68ff) we concluded that the compactness of the spatial section of the wall and de Sitter spacetimes was responsible for the phenomenon.

We can similarly trace the existence of wrapping solutions (and therefore of the phase transition) to the topology of the space where the fields X and P live. From the literature [30,31] and from our own results, we know that flux expulsion occurs only when the Reissner–Nordström black hole is extremal, which — according to (6.13) — corresponds to the black hole’s horizon decoupling from the rest of

spacetime. In the discussion attached to that equation, we have recognised this fact as the cause of the numerical problems which invalidated some of the results of [30,31]; now we are also in a position to argue that this particularity of the extremal black hole is at the source of the phase transition.

Indeed, for a nonextremal Reissner–Nordström black hole the spatial section of spacetime where the fields live is three-dimensional, and only its boundary (the horizon) is a compact manifold. However, if \mathcal{H} decouples from the rest of the spacetime exterior to it, we must consider the fields separately on the horizon and on the space exterior to it (with some proper joining condition in the coordinate distance r). The fields on the horizon then truly live on a compact spatial section of spacetime, namely \mathbb{S}^2 , and our discussion of section 4.7 applies.

We can compare this result with an interesting extension of our work and that of AGK and CAES. Moderski & Rogatko [73,74] and (in a more general case) Santos & Gregory [85] have studied the same problem of a cosmic string piercing a Reissner–Nordström black hole, but in dilatonic gravity. After our papers [21,20] outlining the subtlety in the numerical treatment of the horizon, Moderski & Rogatko [74] re-examined their previous claims of flux expulsion for extremal black holes, and confirmed — in contrast to the results of this chapter — that flux expulsion occurred in all cases.

In our notation, the metric of the case that they have considered is

$$ds^2 = \left(1 - \frac{M}{r}\right) dt^2 - \frac{dr^2}{1 - \frac{M}{r}} - r \left(r - \frac{Q^2}{M}\right) d\Omega_{II}^2 \quad (6.36)$$

and the extremal case is given by $r_+ = M = Q$. The key point is to notice that a term $r(r - Q^2/M)$ replaces r^2 in $g_{\theta\theta}$. This term vanishes for the extremal horizon, which implies that the field equation for P reduces to

$$\ddot{P} - \cot(\theta)\dot{P} = 0, \quad (6.37)$$

and we conclude from the boundary conditions that the only solution is $P(r_+, \theta) \equiv 1$. Moderski & Rogatko then confirmed this result numerically by using the three initial guesses that were introduced earlier in this chapter.

Apart from considering dilatonic gravity (or other generalizations of Einstein's theory of gravity), there are several ways to continue the work of this chapter.

The most obvious way would be to consider more general black hole and/or string solutions, such as rotating black holes or superconducting strings. But one could also decide to go all the way in the numerical direction and investigate dynamical and/or less symmetric interactions of strings and black holes; this would be necessary, for instance, to verify the stability of the solutions discussed in this chapter, or how they can form (*e.g.*, is the string captured by the black hole?).

Looking back at the beginning of this chapter, we recall that the work on this topic started with the study by AGK [1] of a Nielsen–Olesen string piercing a Schwarzschild black hole. Then CAES introduced a second $U(1)_{\text{EM}}$ group corresponding to electromagnetism by replacing the Schwarzschild black hole by a Reissner–Nordström one [31,30]. Therefore, it would now seem logical to analyze the case where this $U(1)_{\text{EM}}$ interacts not only with the black hole but also with the string; this implies replacing the Nielsen–Olesen string by a superconducting one. Let us then consider the bosonic Lagrangian density (1.31)

$$\begin{aligned} \mathcal{L} = & (D_a \Phi) (D^a \Phi)^\dagger - \frac{1}{4} \tilde{F}_{ab} \tilde{F}^{ab} + \\ & (D_a \sigma) (D^a \sigma)^\dagger - \frac{1}{4} \tilde{G}_{ab} \tilde{G}^{ab} - V(\Phi, \sigma), \end{aligned} \quad (6.38a)$$

$$V(\Phi, \sigma) = \frac{\lambda}{4} (|\Phi|^2 - \eta^2)^2 + \frac{\tilde{\lambda}}{4} |\sigma|^4 - m^2 |\sigma|^2 + f |\Phi|^2 |\sigma|^2. \quad (6.38b)$$

We make the same Ansatz for the fields as (1.32), but in this chapter we consider the string in a Reissner–Nordström background and therefore (refer to figure 6.1)

$$\begin{aligned} X &= X(r, \theta), \\ P_a &= P(r, \theta) \nabla_a \vartheta, \\ s &= s(r, \theta), \\ C_a &= C_r(r, \theta) \nabla_a r + C_\theta(r, \theta) \nabla_a \theta. \end{aligned} \quad (6.39)$$

According to (1.35), this form for C_a allows for an electromagnetic current j_a in the r and θ directions, *i.e.* around \mathcal{H} .

The equations of motion derived from the Lagrangian (1.33) are

$$\square X - P_a P^a X + \frac{1}{2} X (X^2 - 1) + \alpha_2 s^2 X = 0, \quad (6.40a)$$

$$\square S - C_a C^a s + 2 \frac{\alpha_3}{\alpha_1} s (s^2 - 1) + \frac{\alpha_2}{\alpha_1} X^2 s = 0, \quad (6.40b)$$

$$\nabla_a F^{ab} + \frac{1}{\beta} X^2 P^b = 0, \quad (6.40c)$$

$$\nabla_a G^{ab} + \frac{\alpha_1}{\beta} s^2 C^b = 0. \quad (6.40d)$$

In the Reissner–Nordström background

$$ds^2 = V(r)dt^2 - V^{-1}(r)dr^2 - r^2 d\Omega_{II}^2, \quad (6.41)$$

these become

$$-\frac{1}{r^2} [r^2 V(r) X']' - \frac{1}{r^2 \sin(\theta)} [\sin(\theta) \dot{X}]' + \frac{1}{2} X (X^2 - 1) + \frac{N^2 X P^2}{r^2 \sin(\theta)^2} = 0, \quad (6.42a)$$

$$-\frac{1}{r^2} [r^2 V(r) s']' - \frac{1}{r^2 \sin(\theta)} [\sin(\theta) \dot{s}]' + \left[V(r) C_r^2 + \frac{C_\theta^2}{r^2} \right] + 2 \frac{\alpha_3}{\alpha_1} s (s^2 - 1) + \frac{\alpha_2}{\alpha_1} X^2 s = 0, \quad (6.42b)$$

$$[V(r) P']' + \frac{\sin(\theta)}{r^2} \left(\frac{\dot{P}}{\sin(\theta)} \right)' - \frac{X^2 P}{\beta} = 0, \quad (6.42c)$$

$$-\frac{1}{r^2 \sin(\theta)} [\sin(\theta) (\dot{C}_r - C'_\theta)]' + \frac{\alpha_1}{\beta} s^2 C_r = 0, \quad (6.42d)$$

$$- [V(r) (\dot{C}_r - C'_\theta)]' - \frac{\alpha_1}{\beta} s^2 C_\theta = 0 \quad (6.42e)$$

on the bulk of the grid, and

$$(r_+ - M) X' + \frac{1}{2} \ddot{X} + \frac{1}{2} \cot(\theta) \dot{X} - \frac{r_+^2}{2} X (X^2 - 1) - \frac{1}{2} \frac{N^2 P^2 X}{\sin^2(\theta)} = 0, \quad (6.43a)$$

$$(r_+ - M) s' + \frac{1}{2} \ddot{s} + \frac{1}{2} \cot(\theta) \dot{s} - \frac{1}{2} C_\theta^2 - \frac{\alpha_3}{\alpha_1} r_+^2 s (s^2 - 1) - \frac{r_+^2}{2} \frac{\alpha_2}{\alpha_1} X^2 s = 0, \quad (6.43b)$$

$$(r_+ - M) P' + \frac{1}{2} \ddot{P} - \frac{1}{2} \cot(\theta) \dot{P} - \frac{r_+^2}{2} \frac{X^2 P}{\beta} = 0, \quad (6.43c)$$

$$\ddot{C}_r - \dot{C}'_\theta + \cot(\theta) (\dot{C}_r - C'_\theta) - \frac{\alpha_1}{\beta} r_+^2 s^2 C_r = 0, \quad (6.43d)$$

$$(r_+ - M) (\dot{C}_r - C'_\theta) + \frac{\alpha_1}{\beta} r_+^2 s^2 C_\theta = 0 \quad (6.43e)$$

on the horizon. These equations are currently being studied, but sadly we lacked the time to make some real progress towards understanding the behaviour of this system. We can see, however, that the equation for C_r on the horizon, (6.43d), does not reduce to an ODE at extremality, and the analysis might well prove more difficult than in the case of the abelian–Higgs vortex.

Numerical Tables

This Appendix contains the numerical tables corresponding to Part III. As in Appendix B, only a small subset of our numerical results are given below.

| N | β | M | $1/M$ | $X(\pi/2)$ | $P(\pi/2)$ |
|-----|---------|-------|----------|------------|-------------|
| 1 | 0.1 | 5.0 | 0.200 | 0.999610 | 1.04910e-09 |
| | | 3.0 | 0.333 | 0.987626 | 1.82632e-05 |
| | | 1.5 | 0.667 | 0.683601 | 0.0646497 |
| | 1.0 | 5.0 | 0.200 | 0.999210 | 0.00390753 |
| | | 3.0 | 0.333 | 0.974058 | 0.0748739 |
| | | 1.9 | 0.526 | 0.607430 | 0.564400 |
| | 10.0 | 5.0 | 0.200 | 0.992768 | 0.323259 |
| | | 3.0 | 0.333 | 0.886321 | 0.704002 |
| | | 2.1 | 0.476 | 0.389957 | 0.967027 |
| | 100.0 | 5.0 | 0.200 | 0.963488 | 0.872222 |
| | | 3.0 | 0.333 | 0.818832 | 0.967984 |
| | | 2.1 | 0.476 | 0.344228 | 0.997370 |
| 2 | 1.0 | 5.0 | 0.200 | 0.997470 | 0.00625655 |
| | | 3.0 | 0.333 | 0.901614 | 0.138023 |
| 4 | 5.0 | 5.0 | 0.200 | 0.988423 | 0.0142843 |
| | | 4.0 | 0.250 | 0.924558 | 0.0724505 |
| 6 | 5.0 | 0.200 | 0.962400 | 0.0307028 | |
| 8 | 5.0 | 0.200 | 0.870635 | 0.0767509 | |

Table C.1: Value of $X(\pi/2)$ and $P(\pi/2)$ on the horizon of the extremal Reissner–Nordström black hole as function of N , β and M (or $1/M$). See figure 6.7.

| M | $X(\pi)$ |
|-----|----------|
| 2.0 | 0.98625 |
| 1.8 | 0.97278 |
| 1.6 | 0.94513 |
| 1.4 | 0.88336 |
| 1.2 | 0.73490 |
| 1.0 | 0.06253 |

Table C.2: Value of $X(\pi)$ on the horizon for a single string ending on a black hole (see figure 6.10).

Part IV
Conclusion

Conclusion

In this thesis, we have studied some properties of extended topological defects in a cosmological setting. More precisely, we have studied the effective dynamics of cosmic strings and gravitating domain walls, the spacetimes of domain walls, and the static solutions of the system consisting of an abelian–Higgs cosmic string and an extremal Reissner–Nordström black hole. All these topics — although related — do not form a logical ensemble, and we chose to present our conclusions at the end of each corresponding chapter. We therefore only summarize these conclusions here.

Our efforts to understand the dynamics of cosmic strings yielded an effective equation of motion for the strings in terms of either its extrinsic curvatures $\underline{\kappa}_\mu$ [Eq. (3.49)] or the spacetime coordinates of its core X^a [Eq. (3.45)]. We investigated the corrected dynamics of three different trajectories (a circular loop, a travelling wave and a helical breather) and compared them with their Nambu–Goto counterparts. With the help of these results, and a more general argument valid for any trajectory, we found that the corrected trajectory was generically antirigid.

We then investigated the spacetimes of plane-symmetric domain walls, and found that, depending on the strength ϵ of the Higgs’s gravitational interaction, they could be of two distinct kinds. The first corresponds to a wall solution, and in the second the scalar field sits at the top of the potential (false vacuum) while the spacetime is exactly de Sitter. These two types of solution are separated by a second-order phase transition (see figure 4.5). The existence of the vacuum-de Sitter solutions can be linked to the topology of the domain wall and the de Sitter spacetimes. We then specialized our investigations to the particular cases of a Goldstone and a sine-Gordon walls, which allowed us to perform some numerical simulations to confirm

and refine our analytical predictions.

Our analysis of the dynamics of topological defects continued with the case of gravitating domain walls. After identifying the two qualitatively different cases to consider, we determined the lowest-order corrections to the Nambu–Goto equation of motion in both cases [Eq. (5.46)]. This chapter describes work still in progress, and sadly some more work is necessary to determine whether this equation forces the wall to be totally geodesic or not; preliminary findings suggest that it does not.

Finally, we also discussed the interactions between abelian–Higgs cosmic strings and extremal Reissner–Nordström black holes in the case where the string’s axis passes through the center of the black hole. In particular, we addressed the question of flux expulsion, a phenomenon which had been analytically established for high-winding strings, but only numerically observed for thin vortices. Using a mix of analytical and numerical methods, we showed that in fact thin strings must penetrate the horizon \mathcal{H} (and therefore count as hair) and that thick strings are expelled from \mathcal{H} . These two types of solution are separated by a second-order phase transition (see figure 6.7a) reminiscent of the one which we observed in the spacetime of domain walls, which occurs when the string has a thickness comparable to that of the black hole. In this case too, the existence of expelled solutions can be traced to the topology of the space where the fields live.

Bibliography

- [1] A. Achúcarro, R. Gregory & K. Kuijken, ‘Abelian Higgs hair for black holes.’ *Phys. Rev.*, **D52** (1995) 5729–5742. gr-qc/9505039.
- [2] A. Albrecht, R. A. Battye & J. Robinson, ‘The case against scaling defect models of cosmic structure formation.’ *Phys. Rev. Lett.*, **79** (1997) 4736–4739. astro-ph/9707129.
- [3] M. Anderson, ‘Leading-order corrections to the Nambu action.’ *Phys. Rev.*, **D51** (1995) 2863–2871.
- [4] M. Anderson, F. Bonjour, R. Gregory & J. Stewart, ‘Effective action and motion of a cosmic string.’ *Phys. Rev.*, **D56** (1997) 8014–8028. hep-ph/9707324.
- [5] H. Arodź, ‘Expansion in the width: the case of vortices.’ *Nucl. Phys.*, **B450** (1995) 189–208. hep-th/9503001.
- [6] —, ‘On expansion in the width for domain walls.’ *Nucl. Phys.*, **B450** (1995) 174–188. hep-th/9502018.
- [7] M. Aryal, L. H. Ford & A. Vilenkin, ‘Cosmic strings and black holes.’ *Phys. Rev.*, **D34** (1986) 2263–2266.
- [8] S. J. Avis & C. J. Isham, ‘Vacuum solutions for a twisted scalar field.’ *Proc. R. Soc. A*, **363** (1978) 581–596.
- [9] A. Babul, T. Piran & D. N. Spergel, ‘Bosonic superconducting cosmic strings. I. Classical field theory solutions.’ *Nucl. Phys.*, **B202** (1988) 307–314.

- [10] A. J. Banday, S. Zaroubi & K. M. Górski, ‘On the non-Gaussianity observed in the COBE-DMR sky maps.’ (1999). astro-ph/9908070.
- [11] R. Bartnick & J. McKinnon, ‘Particlelike solutions of the Einstein-Yang-Mills equations.’ *Phys. Rev. Lett.*, **61** (1988) 141–144.
- [12] R. Basu & A. Vilenkin, ‘Nucleation of thick topological defects during inflation.’ *Phys. Rev.*, **D46** (1992) 2345–2354.
- [13] J. D. Bekenstein, ‘Black holes: classical properties, thermodynamics and heuristic quantization.’ gr-qc/9808028. Talk given at the 9th Brazilian School of Cosmology and Gravitation (BSCG 98), Rio de Janeiro, Brazil, 27 July–7 August 1998.
- [14] P. Bizon, ‘Colored black holes.’ *Phys. Rev. Lett.*, **64** (1990) 2844–2847.
- [15] E. B. Bogomol’nyi, ‘The stability of classical solutions.’ *Yad. Fiz.*, **24** (1976) 861. English translation: *Sov. J. Nucl. Phys.*, **24** (1976) 449–454.
- [16] B. Boisseau, C. Charmousis & B. linet, ‘Dynamics of a self-gravitating cosmic string.’ *Phys. Rev.*, **D55** (1997) 616–622. gr-qc/9607029.
- [17] F. Bonjour, *Cosmic strings and their dynamics*. Master’s thesis, Department of Mathematical Sciences, University of Durham (September 1996).
- [18] F. Bonjour, C. Charmousis & R. Gregory, ‘Thick domain wall universes.’ *Class. Quantum Grav.*, **16** (1999) 2427–2445. gr-qc/9902081.
- [19] —, ‘Thick self-gravitating plane-symmetric domain walls.’ (1999). gr-qc/9903059. Talk given by at the Les Houches Winter School on topological defects (TOPDEF 99), Les Houches, France, 16–26 February 1999.
- [20] F. Bonjour, R. Emparan & R. Gregory, ‘Vortices and extreme black holes: The question of flux expulsion.’ *Phys. Rev.*, **D59** (1999) 084022. gr-qc/9810061.
- [21] F. Bonjour & R. Gregory, ‘Comment on “Absence of abelian Higgs hair for extreme black holes”.’ *Phys. Rev. Lett.*, **81** (1998) 5034. hep-th/9809029 (as ‘Comment on “Abelian Higgs hair for extremal black holes and selection rules for snapping strings”’ in version 1).

- [22] B. C. Bromley & M. Tegmark, 'Is the cosmic microwave background really non-Gaussian?' (1999). astro-ph/9904254.
- [23] C. Burden, 'Gravitational radiation from a particular class of cosmic strings.' *Phys. Lett.*, **164B** (1985) 277–281.
- [24] B. Carter, 'Brane dynamics for treatment of cosmic strings and vortons.' Lectures given at the 2nd Mexican School on Gravitation and Mathematical Physics, Tlaxcala, Mexico, 1-7 Dec 1996. hep-th/9705172.
- [25] —, 'Basic brane theory.' *Class. Quantum Grav.*, **9** (1992) S19–S33.
- [26] —, 'Outer curvature and conformal geometry of an imbedding.' *J. Geom. Phys.*, **8** (1992) 53–88.
- [27] —, 'Dynamics of cosmic strings and other brane models.' In *Cambridge 1994, Formation and Interactions of Topological Defects* (A.-C. Davis & R. Brandenberger, editors) (1995). hep-th/9611054. Talk given at the NATO ASI Conference on Formation and Interactions of Topological Defects, Cambridge, England, 22 August–2 September 1995.
- [28] —, 'Amalgamated Codazzi–Raychaudhuri identity for foliation.' *Contemp. Math*, **203** (1997) 207–219. hep-th/9705083. Presented at the Conference on Geometric Issues in Foundation of Science in honor of Sir Roger Penrose's 65th Birthday, Oxford, England, 25–29 June 1996 and at the Conference on New Trends in Geometrical and Topological Methods (in Memory of William Kingdon Clifford), Funchal, Madeiro, 30 July–5 August 1995.
- [29] B. Carter & R. Gregory, 'Curvature corrections to dynamics of domain walls.' *Phys. Rev.*, **D51** (1995) 5839–5846. hep-th/9410095.
- [30] A. Chamblin, J. M. Ashbourn-Chamblin, R. Emparan & A. Sornborger, 'Absence of abelian Higgs hair for extreme black holes.' *Phys. Rev. Lett.*, **80** (1998) 4378–4381. gr-qc/9706032. Talk given at the 8th Marcel Grossmann Meeting on Recent Developments in Theoretical and Experimental General Relativity, Gravitation and Relativistic Field Theories (MG 8), Jerusalem, Israel, 22–27 June 1997.

- [31] —, ‘Can extreme black holes have (long) Abelian Higgs hair?’ *Phys. Rev.*, **D58** (1998) 124014. gr-qc/9706004.
- [32] C. Charmousis, *Dynamique des cordes cosmiques autogravitantes*. Ph.D. thesis, Université François Rabelais, Tours, France (1998).
- [33] C. Charmousis, B. Boisseau & B. Linet, ‘Dynamics of a self-gravitating global string with large Higgs boson mass.’ *Phys. Rev.*, **D57** (1998) 5150–5157. gr-qc/9708001.
- [34] P. T. Chruściel, ‘“No hair” theorems: Folklore, conjectures, results.’ gr-qc/9402032.
- [35] M. Cvetič, S. Griffies & H. H. Soleng, ‘Local and global gravitational aspects of domain wall space-times.’ *Phys. Rev.*, **D48** (1993) 2613–2634. gr-qc/9306005.
- [36] M. Cvetič & H. H. Soleng, ‘Supergravity domain walls.’ *Phys. Rep.*, **282** (1997) 159–223. hep-th/9604090.
- [37] R. Davis, ‘Goldstone bosons in string models of the galaxy.’ *Phys. Rev.*, **D32** (1985) 3172–3177.
- [38] D. M. Eardley, G. T. Horowitz, D. A. Kastor & J. Traschen, ‘Breaking cosmic strings without monopoles.’ *Phys. Rev. Lett.*, **75** (1995) 3390–3393. gr-qc/9506041.
- [39] R. Emparan, ‘Pair creation of black holes joined by cosmic strings.’ *Phys. Rev. Lett.*, **75** (1995) 3386–3389. gr-qc/9506025.
- [40] J. A. Espichán Carrillo, A. Maia Jr. & V. M. Mostepanenko, ‘Jacobi elliptic solutions of $\lambda\phi^4$ theory in a finite domain.’ (1999). hep-th/9905151.
- [41] P. G. Ferreira, J. a. Magueijo & K. M. Gorski, ‘Evidence for non-gaussianity in the DMR four year sky maps.’ *Ap. J.*, **503** (1998) L1–L4. astro-ph/9803256.
- [42] D. Förster, ‘Dynamics of relativistic vortex lines and their relation to dual theory.’ *Nucl. Phys.*, **B81** (1974) 84–92.

- [43] D. Garfinkle & R. Gregory, ‘Corrections to the thin-wall approximation in general relativity.’ *Phys. Rev.*, **D41** (1990) 1889–1894.
- [44] D. Garfinkle & T. Vachaspati, ‘Radiation from kinky, cusplless cosmic loops.’ *Phys. Rev.*, **D36** (1987) 2229–2241.
- [45] —, ‘Cosmic string travelling waves.’ *Phys. Rev.*, **D42** (1990) 1960–1963.
- [46] J. Garriga & A. Vilenkin, ‘Perturbations on domain walls and strings: a covariant theory.’ *Phys. Rev.*, **D44** (1991) 1007–1014.
- [47] R. Gass & M. Mukherjee, ‘Domain wall space-times and particle motion.’ gr-qc/9903012.
- [48] R. Gleiser & J. Pullin, ‘Are cosmic strings gravitationally stable topological defects?’ *Class. Quantum Grav.*, **6** (1989) L141–L144.
- [49] J. Goldstone, ‘Field theories with “superconductor” solutions.’ *Nuovo Cim.*, **XIX** (1961) 154–164.
- [50] G. Götz, ‘The gravitational field of plane-symmetric thick domain walls.’ *J. Math. Phys.*, **31** (1990) 2683–2687.
- [51] R. Gregory, ‘Effective action for a cosmic string.’ *Phys. Lett.*, **206B** (1988) 199–204.
- [52] —, ‘Effective actions for bosonic topological defects.’ *Phys. Rev.*, **D43** (1991) 520–525.
- [53] R. Gregory, D. Haws & D. Garfinkle, ‘Dynamics of domain walls and strings.’ *Phys. Rev.*, **D42** (1990) 343–348.
- [54] R. Gregory & M. Hindmarsh, ‘Smooth metrics for snapping strings.’ *Phys. Rev.*, **D52** (1995) 5598–5604. gr-qc/9506054.
- [55] C. Hawes, M. Hindmarsh & N. Turok, ‘Superconducting strings or springs?’ *Phys. Lett.*, **209B** (1988) 255–261.
- [56] S. W. Hawking & G. Ellis, *The large-scale structure of space-time*. Cambridge University Press, Cambridge (1973).

- [57] S. W. Hawking & S. F. Ross, 'Pair production of black holes on cosmic strings.' *Phys. Rev. Lett.*, **75** (1995) 3382–3385. gr-qc/9506020.
- [58] C. T. Hill, D. N. Schramm & J. N. Fry, 'Cosmological structure formation from soft topological defects.' *Comments Nucl. Part. Phys.*, **19** (1989) 25–39.
- [59] M. Hindmarsh & T. Kibble, 'Cosmic strings.' *Rep. Progr. Phys.*, **58** (1995) 477–562. hep-ph/9411342.
- [60] J. R. Ipser & P. Sikivie, 'The gravitationally repulsive domain wall.' *Phys. Rev.*, **D30** (1984) 712–719.
- [61] W. Israel, 'Singular hypersurfaces and thin shells in general relativity.' *Nuovo Cim.*, **44B**(Serie 10) (1966) 1–14. Erratum: *ibid.*, **48B** 463 (1967).
- [62] A. H. Jaffe, A. Stebbins & J. A. Friedman, 'Minimal microwave anisotropy from perturbations induced at late times.' *Ap. J.*, **420** (1994) 9–25. astro-ph/9301011.
- [63] T. Kibble, 'Topology of cosmic domains and strings.' *J. Phys.*, **A9** (1976) 1387–1398.
- [64] T. Kibble & N. Turok, 'Selfintersection of cosmic strings.' *Phys. Lett.*, **116B** (1982) 141–143.
- [65] H. P. Künzle & A. K. M. Masood-ul-Alam, 'Spherically symmetric $SU(2)$ Einstein–Yang–Mills fields.' *J. Math. Phys.*, **31** (1990) 928–935.
- [66] C. R. Lawrence, D. Scott & M. White, 'What have we already learned from the CMB?' *Publ. Astron. Soc. Pac.*, **111** (1999) 525. astro-ph/9810446.
- [67] K. Lee, V. P. Nair & E. J. Weinberg, 'Black holes in magnetic monopoles.' *Phys. Rev.*, **D45** (1992) 2751–2761. hep-th/9112008.
- [68] —, 'A classical instability of Reissner–Nordström solutions and the fate of magnetically charged black holes.' *Phys. Rev. Lett.*, **68** (1992) 1100–1103. hep-th/9111045.

- [69] A. Linde, ‘Monopoles as big as a universe.’ *Phys. Lett.*, **B237** (1994) 208–213. astro-ph/9402031.
- [70] A. Linde & L. Dmitri, ‘Topological defects as seeds for eternal inflation.’ *Phys. Rev.*, **D50** (1994) 2456–2468. hep-th/9402115.
- [71] K.-i. Maeda & N. Turok, ‘Finite-width corrections to the Nambu action for the Nielsen–Olesen string.’ *Phys. Lett.*, **202B** (1988) 376–380.
- [72] D. Maison & S. Liebling, ‘Some remarks on gravitational monopoles.’ (1999). Gr-qc/9908038.
- [73] R. Moderski & M. Rogatko, ‘Abelian Higgs hair for electrically charged dilaton black holes.’ *Phys. Rev.*, **58** (1998) 124016. hep-th/9808110.
- [74] —, ‘The question of Abelian Higgs hair expulsion from extremal dilaton black holes.’ (1999). hep-th/9907025.
- [75] M. Mukherjee, ‘Gravitational fields of cosmic membranes.’ *Class. Quantum Grav.*, **10** (1993) 131–146.
- [76] H. B. Nielsen & P. Olesen, ‘Vortex-line models for dual strings.’ *Nucl. Phys.*, **B61** (1973) 45–61.
- [77] D. Novikov, H. A. Feldman & S. F. Shandarin, ‘Minkowski functionals and cluster analysis for CMB maps.’ *Int. J. Mod. Phys.*, **D8** (1999) 291–306. astro-ph/9809238.
- [78] J. Pando, D. Valls-Gabaud & L.-Z. Fang, ‘Evidence for scale-scale correlations in the cosmic microwave background radiation.’ *Phys. Rev. Lett.*, **81** (1998) 4568–4571. astro-ph/9810165.
- [79] U.-L. Pen, U. Seljak & N. Turok, ‘Power spectra in global defect theories of cosmic structure formation.’ *Phys. Rev. Lett.*, **79** (1997) 1611–1614. astro-ph/9704165.
- [80] L. Perivolaropoulos, ‘Asymptotics of Nielsen–Olesen vortices.’ *Phys. Rev.*, **D48** (1993) 5961–5962. hep-ph/9310264.

- [81] A. Polyakov, 'Fine structure of strings.' *Nucl. Phys.*, **B268** (1986) 406–412.
- [82] W. H. Press, S. A. Teukolsky, W. T. Vetterling & B. P. Flannery, *Numerical Recipes in C: The Art of Scientific Computing*. Cambridge University Press, Cambridge, second edition (1992).
- [83] M. Sakellariadou, 'Gravitational waves emitted from infinite strings.' *Phys. Rev.*, **D42** (1990) 354–360. Erratum: *ibid.*, **D43** (1990) 4150.
- [84] D. S. Salopek, 'Generating non-Gaussian adiabatic fluctuations from inflation.' (1999). astro-ph/9903327.
- [85] C. Santos & R. Gregory, 'Vortices and black holes in dilaton gravity.' (1999). gr-qc/9906107.
- [86] M. Spivak, *A comprehensive introduction to differential geometry*. Publish or Perish, Boston (1970–1975). Five volumes.
- [87] A. Vilenkin, 'Gravitational field of vacuum domain walls.' *Phys. Lett.*, **133B** (1984) 177–179.
- [88] —, 'Topological inflation.' *Phys. Rev. Lett.*, **72** (1994) 3137–3140. hep-th/9402085.
- [89] A. Vilenkin & E. P. S. Shellard, *Cosmic strings and other topological defects*. Cambridge University Press, Cambridge (1994).
- [90] M. S. Volkov & D. V. Gal'tsov, 'Black holes in Einstein-Yang-Mills theory.' *Sov. J. Nucl. Phys.*, **51** (1990) 747–753. *Yad. Fiz.* **51** (1990) 1171–1181.
- [91] L. M. Widrow, 'Dynamics of thick domain walls.' *Phys. Rev.*, **D40** (1989) 1002–1010.
- [92] —, 'General-relativistic domain walls.' *Phys. Rev.*, **D39** (1989) 3571–3575.
- [93] E. Witten, 'Superconducting strings.' *Nucl. Phys.*, **B249** (1985) 557–592.

